Large-Scale Hydrogen Liquefaction

Process Modelling, Viability and Techno-economic Analysis

Energy, Flow and Process Technology MSc Thesis

P. B. Tamarona

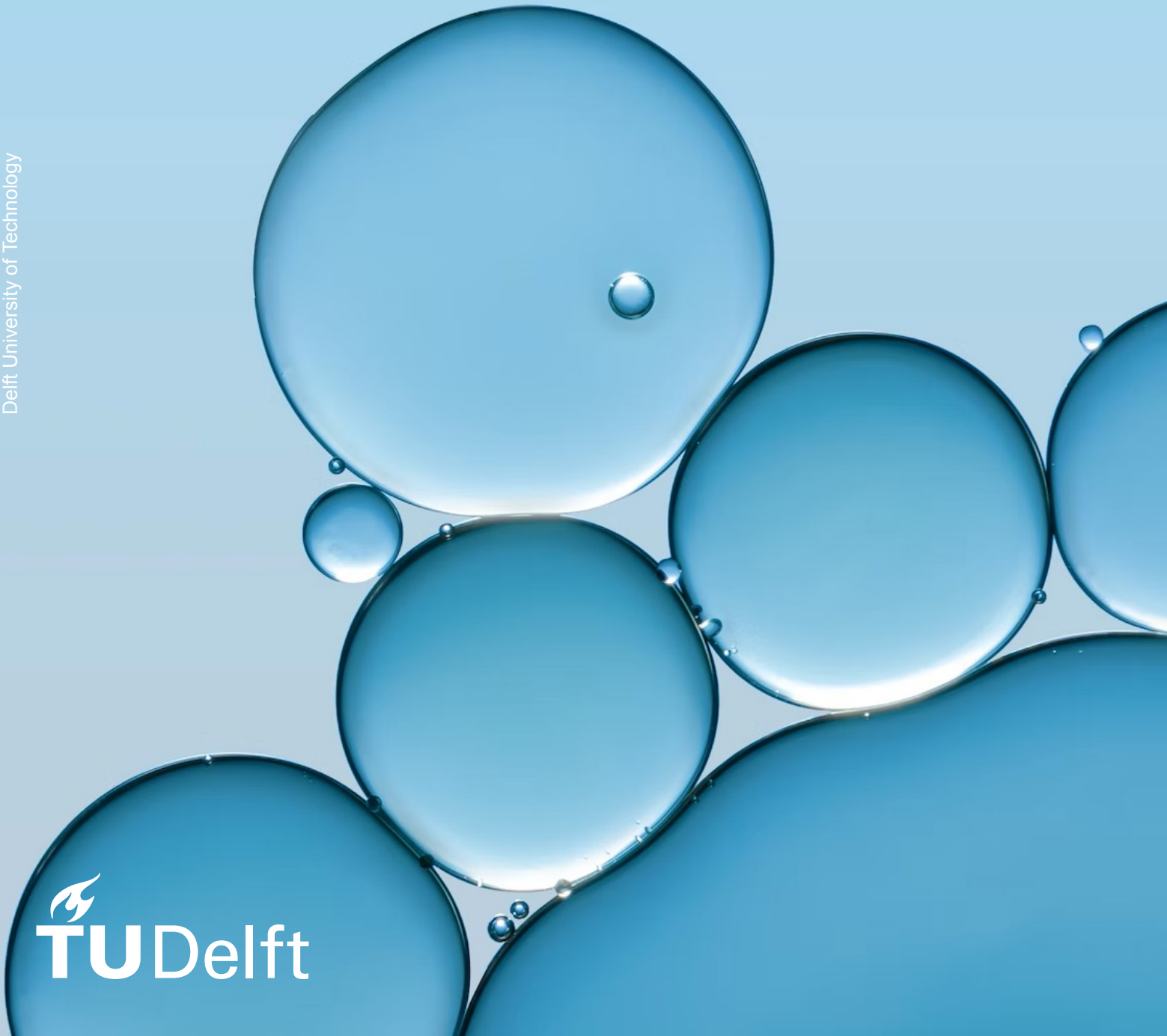

Delft University of Technology

TU Delft

Large-Scale Hydrogen Liquefaction

Process Modelling, Viability and Techno-economic Analysis

by

P. B. Tamarona

to obtain the degree of Master of Science
at the Delft University of Technology,
to be defended publicly on Monday, September 25 2023 at 01:00 PM.

Student Name	Student Number
Panji B. Tamarona	5427509

Faculty:	Faculty of Mechanical, Maritime and Materials Engineering	
Project Duration:	December 1, 2022 – September 25, 2023	
Thesis committee:	Dr.ir. M. Ramdin,	TU Delft, thesis supervisor
	Prof.dr.ir. R. Pecnik,	TU Delft, thesis supervisor
	Dr.ir. L. van Biert,	TU Delft
	Prof.dr.ir. T.J.H. Vlugt,	TU Delft

Cover:	Taken from International Energy Agency Hydrogen Fuels and Technologies webpage (modified)
Style:	TU Delft Report Style, with modifications by Daan Zwaneveld

TU Delft

Acknowledgement

I would like to express my sincere gratitude to the following individuals who have been instrumental in the successful completion of my master's thesis:

Mahinder and Rene: I want to express my heartfelt gratitude to my thesis supervisors, Mahinder and Rene, for the exceptional support and dedication during the past 9 months. Your commitment to my academic journey has been truly commendable. Thank you for the time you make for our weekly meetings, where you have provided me with insightful feedbacks and guidance. I am especially thankful for their unwavering enthusiasm for my thesis work, which has motivated me to push the boundaries of my research. I hope to have the opportunity to collaborate with you again in the future.

LPDP—The Ministry of Finance of Republik Indonesia: I would like to express my sincere gratitude to LPDP for their generous scholarship support. This financial assistance has played a crucial role in enabling me to focus on my master's program and complete this thesis. I am committed to utilizing the knowledge and skills I've acquired during my master's program to contribute to the sustainable development of Indonesia.

P&E Flex Room Friends: I want to express my heartfelt appreciation to my friends in the P&E Flex Room—Fathaah, Thomas, Ankit, Akhilesh, Mayank, Vignesh, and Daniel. We have shared countless moments of laughter and scientific discussion over the past 9 months. Your friendship and support have made this academic journey even more memorable.

Delft/Indonesian Friends: Riki, Kanya, Sasa, Poci, Helmi, Dewo, and Kiki, you guys have been an essential part of my life during my studies. We've hung out together, played (a lot of) tennis, travelled across Europe, and created unforgettable memories. Your companionship and the adventures we've shared have added a unique dimension to my master study in Delft.

Long-Time Best Friends: My dear friends, Fasya, Naomi, Rangga, Anya, Jesse, Ifan, Galih, Arfan, Ario, Icas, Amadea, Candrika, Taqia, Syela, Novinda, Yusnur, Haekal, Raihan, Engine, and others, our friendships spanning over a decade has been a constant source of joy and strength in my life. Your steadfast support, constructive criticism and all the fun memories we've created together have enriched my life journey in profound ways. Thank you for being a significant part of my life.

Close Families: I would like to extend my heartfelt appreciation to my extended family. Your encouragement have been a source of warmth and strength throughout my academic journey. Your presence in my life is deeply cherished, and I am grateful for the bonds that connect us.

Dhika dan Genta: I want to extend my appreciation to my two amazing little brothers, Dhika and Genta. Our adventures, fights, jokes, and all of our shared moments have added immeasurable joy to my life. You both continue to make me a proud brother every day.

Ayah dan Bunda: I would like to express my profound and heartfelt gratitude to my Ayah dan Bunda, for your unwavering support, love, unfaltering guidance, constant prayers and the knowledge and experience you have shared throughout my transformative journey. Your countless sacrifices, continuous encouragement, and steadfast belief in me have been the persistent driving force behind my academic and personal achievements. I am deeply and sincerely thankful for everything you have done.

Anggita Gatra: I want to express my deepest gratitude to my *belahan jiwa*, Anggita. Your unwavering support, constructive criticism, constant prayers, and unceasing encouragement in the pursuit of my goals and dreams have been truly invaluable. Your love, patience, and understanding have been my anchor during the challenges and uncertainties of this academic pursuit. Thank you for always being there for me. The anticipation of our upcoming marriage has given me the strength to persevere and finally finished this thesis.

Lastly, I am grateful to all those whose names I may have unintentionally omitted but who have nonetheless played a role in my academic journey. Your contributions, however small, have not gone unnoticed.

This thesis is a culmination of the collective efforts and support of these individuals and institutions. Any errors or shortcomings in this work are entirely my own. Thank you all for being an integral part of my academic pursuit.

Thank you.

Panji Baskara Tamarona
Delft, 11 September 2023

"Somewhere in our DNA must lie the key mutation (or, more probably, mutations) that set us apart—the mutations that make us the sort of creature that could wipe out its nearest relative, then dig up its bones and reassemble its genome."

-Elizabeth Kolbert, The Sixth Extinction: An Unnatural History

Abstract

The competitiveness of hydrogen as a sustainable energy carrier depends greatly on the cost associated with its transportation and storage. Transporting and storing hydrogen in liquid form offers several advantages, such as purity, versatility and higher volumetric density. However, current industrial hydrogen liquefaction processes face challenges in terms of efficiency and expense, with a second-law efficiency below 25% and costs ranging from 2.5-3.0 US$/kg$_{LH_2}$. Moreover, these processes have been limited to small-scale applications. Recent studies suggest that increasing plant capacity may reduce liquefaction costs, but existing models often overlook the possible capital and operating expenses of the conceptual plants, as well as the technical feasibility of scaling up the components. These considerations are crucial for the realisation of efficient large-scale hydrogen liquefaction facilities.

Most reported liquefaction costs rely on "ballpark" estimation, making it difficult to compare economic aspects across various processes. Additionally, industry-sponsored studies often use confidential data, limiting accessibility for researchers. This thesis aims to develop a general and comprehensive framework for modelling large-scale liquefaction processes and assessing their technical and economic feasibility. In the demonstration of the framework, it provides a preliminary feasibility study of a *high-pressure hydrogen Claude-cycle liquefier concept*.

The technical analysis focuses on the preliminary design of main process equipment for large-scale liquefiers, including compressors, turboexpanders, and heat exchangers, ensuring compatibility with current technology constraints. Based on the preliminary equipment designs, along with the process simulation model, a techno-economic analysis is conducted. For this analysis, the Aspen Process Economic Analyzer (APEA) is employed to estimate the capital and operating expenditure. In the base scenario, which assumes an electricity price of 0.1 €/kWh, the 125 tonnes per day (TPD) Claude-cycle concept yielded specific liquefaction costs (SLC) of 1.55 €/kg$_{LH_2}$. Sensitivity analyses reveal that the economic performance of the plant is highly sensitive to electricity prices. Additionally, according to the methodology of this thesis, the implementation of high-speed centrifugal compressors in hydrogen liquefiers has the potential to reduce the SLC by 5.42% and even more significantly in instances of low electricity prices.

Furthermore, scaling up the 125 TPD concept showed potential cost improvements, with a 7.80% SLC reduction at 250 TPD and a 9.45% reduction at 500 TPD under a base electricity price of 0.1 €/kWh. Future projections, cost reevaluations with lower design allowances and contingencies, suggest a potential 12.6% reduction in SLC as the Claude cycle becomes a *proven* industrial concept. In the best-case scenario, where financial incentives and low-cost renewable electricity are available, liquefaction costs could range from 0.87 to 1.09 €/kg$_{LH_2}$.

Finally, a *cost-scaling curve* for hydrogen liquefaction plants are estimated based on the cost results from this study. The curve is comparable to existing cost curves reported by industrial and government joint research projects, providing validation of the methodologies developed in this thesis. Moreover, an *experience curve* is also predicted using cost data from this study and data found in the literature, assuming the global establishment of these plants. This analysis suggests that with each doubling of the installed global liquefaction capacity, the price of hydrogen liquefiers is expected to decrease by an average of approximately 17%.

In summary, hydrogen's economic viability depends on efficient liquefaction processes. This thesis provides a comprehensive framework and analysis, highlighting the sensitivity to electricity prices and the potential for cost reduction as technology advances and capacities increase.

Nomenclature

The most commonly used symbols in this thesis are listed here. Symbols used but not listed here are clarified in their respective contexts.

Symbols

Roman	Description	Unit
A	Area	m^2
a	Constant in van der Waals EOS; first rate constant	$Pa \cdot m^6/kg^2$
a	Constant (process economics)	\$ or €
a_s	Specific heat transfer surface area	$m^2\,m^{-3}$
b	Constant in van der Waals EOS; second rate constant	$m^3\,kg^{-1}$
b	Learning coefficient (process economics)	
b	Blade height (turbomachinery)	m
C	Capital cost	US\$ or €
C_1	Capital cost of plant with capacity S_1	\$ or €
C_2	Capital cost of plant with capacity S_2	\$ or €
c	Specific heat	$J\,kg^{-1}\,K^{-1}$
c	Absolute velocity (turbomachinery)	$m\,s^{-1}$
c	Specific cost or unit cost (process economics)	*
D	Diameter	m
D_s	Specific diameter	m
E_a	Activation energy	$J\,mol^{-1}$
F	Force	N
h	Specific enthalpy	$J\,kg^{-1}$
I	Interest rate	
k	Kinetic rate constant	1/s
LR	Learning rate (process economics)	
Ma	Mach number	
$\dot{m}$	Mass flow rate	$kg\,s^{-1}$
n	Rotation per minute	RPM
n	Capital cost exponent (process economics)	
PR	Compression ratio	
PR	Progress ratio (process economics)	
p	Pressure	Pa
$\dot{Q}$	Heat transferred per unit time	W
q	Cummulative capacity or output	*
R	Universal gas constant, 8.314	$J\,mol^{-1}\,K^{-1}$
R	Degree of reaction (turbomachinery)	$J\,mol^{-1}\,K^{-1}$
Re	Reynold's number	
$\dot{r}$	Conversion rate	$mol\,m^{-3}\,s^{-1}$
S	Plant or equipment capacity	*
S_1	Capacity of plant 1	*

*Dimensions are dependent on the type of equipment or process.

(Symbols continued)

S_2	Capacity of plant 2	*
s	Specific entropy	$\mathrm{J\,kg^{-1}\,K^{-1}}$
T	Temperature	K
t	Time	s
tp	Payment period	year
U	Overall heat-transfer coefficient	$\mathrm{W\,m^{-2}\,K^{-1}}$
U	Plant utilization rate (process economics)	
u	Impeller wheel tip velocity	$\mathrm{m\,s^{-1}}$
V	Volume	$\mathrm{m^3}$
$\dot{V}$	Volumetric flow rate	$\mathrm{m^3\,s^{-1}}$
v	Specific volume	$\mathrm{m^3\,kg^{-1}}$
$\dot{W}$	Work per unit time	W
w	Specific energy consumption	$\mathrm{J\,kg^{-1}}$
w	Relative velocity (turbomachinery)	$\mathrm{m\,s^{-1}}$
x	Mole fraction	
y	Liquid yield	
z	Number of stages or components	

Greek	**Description**	**Unit**
a	Absolute flow angle	°
β	Relative flow angle	°
γ	Heat capacity ratio (isentropic expansion factor)	
Δ	Difference	
δ_h	Rotor hub diameter ratio	
δ_t	Rotor tip diameter ratio	
η	Efficiency	
μ_JT	Joule-Thomson coefficient	$\mathrm{Pa \cdot K}$
ν_s	Isentropic velocity ratio	
ξ	Rotor meridional velocity ratio	
π	3.14159265359	
ρ	Density	$\mathrm{kg\,m^{-3}}$
φ	Flow coefficient	
ψ	Work coefficient	
ω	Speed of rotation	rad/sec
ω_s	Specific speed	

Sub- and Superscripts

0	Reference condition or initial state
0	Nozzle inlet (turbomachinery)
1,2,..	At point 1, 2,..; at time 1, 2,..
1	Rotor inlet (turbomachinery)
2	Rotor outlet (turbomachinery)
3	Diffuser outlet (turbomachinery)
a	Annual
base	Baseline scenario
base	Base year of costs pricing
cat	Catalyst
comp	Compressor
dis	Discharge

eq	Equilibrium
f	Fluid
fix	Fixed
hx	Heat Exchanger
i	Ideal
in	Inlet
inv	Inversion
ic	Intercoolers
is	Isentropic
m	Mean
m	Meridional
max	Maximum
min	Minimum
mol	Molar based property
out	Outlet
p	Polytropic
p	Constant pressure
para	Parahydrogen
R	Stator
recov	Baseline scenario with power-recovery
sim	Simulation
stg	Turbomachinery stage
S	Stator
suc	Suction
t	At time t
ts	*Total-to-static*
turb	Turbine

Abbreviations

Short	Description
AACE	Association for the Advancement of Cost Estimating
ACCE	Aspen Capital Cost Estimator
ALPEMA	Aluminium Plate-Fin Heat Exchanger Manufacturer's Association
APEA	Aspen Process Economic Analyzer
APERC	Asia Pacific Energy Research Centre
ASPEN	Advanced System for Process Engineering
ASU	Air Separation Unit
CAPEX	Capital Expenses
CEPCI	Chemical Engineering Plant Cost Index
CCOP	Cash Cost of Production
CH_4	Methane
CO_x	Oxocarbon
DOE	Department of Energy
EDR	Exchanger Design and Rating
EOS	Equation of State
EPC	Engineering, Procurement and Construction
e-H_2	Equilibrium-hydrogen
EU	European Union
EUR	Euro
FOM	Figure of Merit (Exergy Efficiency)

(Abbreviations continued)

Short	Description
GRAPE	Global and Long-Term Intertemporal Optimization Energy Model
H_2	Hydrogen
H_2S	Hydrogen Sulfide
HDSAM	Hydrogen Delivery Scenario Analysis Model
He	Helium
HPC	High-pressure Compressor
HX	Heat Exchangers
IDEALHY	Integrated Design for Efficient Advanced Liquefaction of Hydrogen
IEA	International Energy Agency
ISBL	Inside Battery Limits
JB	Joule-Brayton
JT	Joule-Thompson
KHI	Kawasaki Heavy Industries
LH_2	Liquid Hydrogen
LN_2	Liquid Nitrogen
LNG	Liquified Natural Gas
LPC	Low-pressure Compressor
MR	Mixed Refrigerant
MRC	Mixed Refrigerant Compressor
MLI	Multilayer Superinsulation
N_2	Nitrogen
n-H_2	Normal-hydrogen
Ne	Neon
NIST	National Institute of Standards and Technology
NTNU	Norwegian University of Science and Technology
OM	Operation and Maintenance
o-H_2	Ortho-hydrogen
OPEX	Operating Expenses
OSBL	Outside Battery Limits
p-H_2	Para-hydrogen
PFHX	Plate-fin Heat Exchangers
REFPROP	Reference Fluid Properties
ROI	Return On Investment
rnd	Research and Development
SDS	Sustainable Development Scenario
SEC	Specific Energy Consumptions
SINTEF	Stiftelsen for Industriell og Teknisk Forskning
SLC	Specific Liquefaction Cost
SMR	Steam-Methane Reforming
TEA	Techno-economic Analysis
TPD	Tonnes per Day
TSA	Temperature-Swing Adsorbers
TU Delft	Technische Universiteit Delft
WE-Net	World Energy Network

Contents

List of Figures

List of Tables

1

Introduction

1.1. Background

Hydrogen (H_2), as an energy carrier, has the potential to become a key player in a sustainable energy future.[1] However, there are still many challenges preventing the widespread use of hydrogen. Transport and storage costs are critical to the competitiveness of hydrogen, as they can significantly increase the final price of hydrogen fuels.[1] Due to its low energy density, gaseous H_2 from the production stage would require an additional physical or chemical conversion process before storing and transporting the fuel over long time scales and distances.[2] One of the viable process options for this is hydrogen liquefaction. The storage and transport of hydrogen as a liquid has several advantages, such as purity, versatility for end use, and high volumetric hydrogen density compared to other possible hydrogen vectors.[2] It can be particularly cost effective for long-distance delivery with moderate demands by using cryogenic liquid trucks.[3] Nonetheless, the current production and logistic processes associated with liquid hydrogen (LH_2) have several limitations that hinder its global use, including economics and scale limitations.

Most commercial hydrogen liquefaction plants have a capacity of less than 20 tons per day (TPD), while the largest one can liquefy up to 32 TPD.[2] The specific energy consumptions (SEC) of these liquefiers are between 10 and 20 kWh/kg_{LH_2},[4] which makes a significant contribution to the current specific liquefaction cost (SLC) range of 2.5-3 $US\$/kg_{LH_2}$.[2,5] In contrast, the theoretical energy to liquefy hydrogen from ambient (300 K, 1.01 bar) conditions is 3.9 kWh/kg_{LH_2}, including the necessary conversion of ortho to para-H_2,[6] indicating that there is ample room for improvement. Recent studies have shown that liquefaction costs typically decrease with increasing plant capacity, with some estimates suggesting that the liquefaction cost could drop to less than 1 $US\$/kg_{LH_2}$.[7–14] The Asia Pacific Energy Research Centre (APERC) even estimated that a liquefaction plant with a capacity of 800 TPD would have cost as less as 0.53-0.78 $US\$/kg_{LH_2}$.[15] In addition to reducing the cost of hydrogen liquefaction, the requirement for larger plants is further strengthened by the expected increase in global hydrogen demand.

Ishimoto et al.[16] evaluated the global hydrogen deployment and found that the demand in 2050, according to the GRAPE (see abbreviation) model used, is 217 Mt, increasing almost threefold from the current market. The International Energy Agency (IEA), in their Sustainable Development Scenario (SDS), projected global demand to increase to 520 Mt by 2070.[17] Hydrogen Council expects that by 2050, about 10% of the hydrogen demand, just under 60,000 TPD, could be transported by sea.[7] If this amount were to be transported in a liquid state, the world would require a significant increase from the current global liquefaction capacity of 350 TPD.[2] For

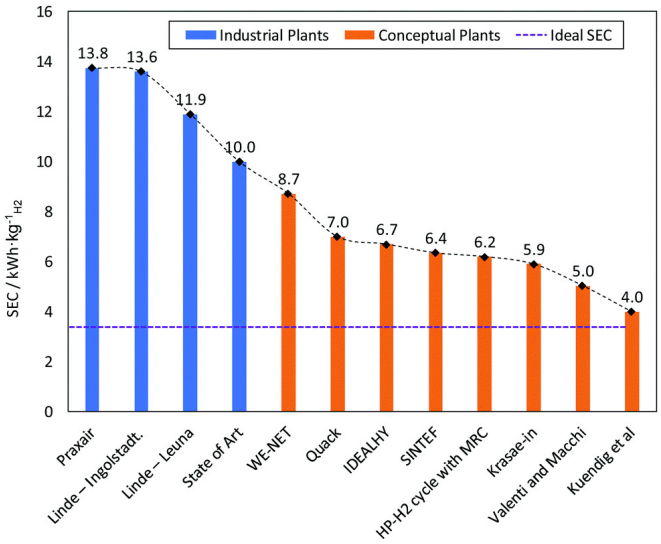

Figure 1.1: Efficiency performance of industrial and conceptual hydrogen liquefiers[a]

comparison, the current global liquefaction capacity of natural gas is approximately 800,000 TPD.[18]

Numerous conceptual designs of large-scale hydrogen liquefaction plants have been developed,[19–26] with the aim of optimising the efficiency of the liquefaction process and thus decreasing the overall SEC of the plant, as demonstrated in Figure 1.1. These concepts have shown that an SEC target ranging between 6 and 8 kWh/kg_{LH_2} should be achievable for large-scale liquefiers without the need for groundbreaking technologies.[2] However, insufficient attention has been paid to the capital and operating expenses of the plant, which are essential to estimate the costs of liquefaction, as well as the technical feasibility of scaling up the components to meet the required unit operations. Considering these factors is crucial, as practical and economically viable methods are essential for the realisation of large and efficient H_2 liquefaction facilities.

Most of the hydrogen liquefaction costs reported in the literature were estimated by projecting the overall capital costs of the process plant using scaling factors that were derived based on limited historical data.[8–13,27,28] While this approach is useful for providing a ballpark estimate of the project cost, it is not ideal for carrying out costs assessment of various plant configurations, especially when the capacities are similar. Feasibility studies sponsored by industries and governments often rely on confidential equipment cost correlations and recent quotations from companies to estimate capital costs, leading to the most accurate cost evaluation.[14,19] However, this approach is not feasible for the majority of academics and researchers in this field of study.

Based on the circumstances mentioned above, this thesis aims to develop a robust framework for modelling a large-scale hydrogen liquefaction process and evaluating the economic feasibility of the plant while carefully considering the existing technical limitations. The study commences by focussing on the modelling of a highly promising conceptual high-capacity H_2 liquefaction plant using a commercial process simulation tool. Subsequently, a systematic procedure is developed for the preliminary designs of the main equipment as part of the technical evaluation of the process plant. The results from the equipment designs are then integrated back into the liquefier simulation model. Building upon the model and preliminary designs, the plant's capital and operating costs are estimated using a general cost estimation tool based on the procedure developed in this study, followed by a comprehensive economic evaluation. Furthermore, sensitivity and scale-up analyses are conducted to assess the impact of various operational parameters and increased capacity on the overall efficiency and economics of the plant. Finally, the study

[a]Reproduced from Hydrogen Liquefaction: A Review of the Fundamental Physics, Engineering Practice and Future Opportunities[2] with permission from the Royal Society of Chemistry.

predicts possible learning/scaling curves of the hydrogen liquefaction plant, based on the cost results from this research and cost projections from other relevant literature.

In summary, **the main objective of this thesis is to provide a comprehensive assessment of the technical and economic viability of a conceptual large-scale hydrogen liquefaction process while developing modelling and cost estimation frameworks that incorporate technical considerations.** Following this objective, the main research question of this master thesis is:

How to model a conceptual large-scale hydrogen liquefaction process, considering technical feasibilities, and effectively evaluate the economic viability of the plant?"

Sub-research questions and search plans of this thesis are discussed in the following sub-chapters.

The frameworks formulated in this thesis are intended to offer a universal methodology for fellow researchers and plant designers to develop large-scale hydrogen liquefaction processes that focus not only on maximising the efficiency but also on the technical aspects and economic evaluation of the plant. The frameworks could serve as a foundation for establishing a general cost-optimisation procedure for designing hydrogen liquefaction plants. The study's results and analyses improve understanding of technical limitations in hydrogen liquefaction technology and identify key factors for enhancing its competitiveness. Additionally, it offers valuable insights to policymakers and regulators in developing strategies and policies related to integration of hydrogen as a clean energy carrier in various sectors.

1.2. Sub-research Questions

In order to completely answer the main research question, the following sub-research questions are formulated:

1. How can a conceptual high-capacity H_2 liquefaction plant be accurately modeled using a commercial process simulation tool?
2. What is the technical evaluation procedure for the preliminary designs of the main equipment in a large-scale hydrogen liquefaction process, and how can the findings from these preliminary designs be incorporated into the overall plant design?
3. How to effectively estimate the capital and operating costs of a conceptual hydrogen liquefier based on process simulation model and equipment preliminary designs, and what are the key factors influencing the plant's economic feasibility?

1.3. Search Plan

The search plan for the literature research in this thesis is based on the *snowball method* and *citation searching*. Key publications that initiate the literature search are as follows:

1. Al Ghafri, S. Z. et al. Hydrogen liquefaction: a review of the fundamental physics, engineering practice and future opportunities, Energy & Environmental Science, 2022.
2. Cardella, U. F. Large-scale hydrogen liquefaction under the aspect of economic viability, Doktor-Ingenieurs, Universität München, 2018.
3. Aasadnia, M. & Mehrpooya, M. Large-scale liquid hydrogen production methods and approaches: A review, Applied Energy 212, 2018.

2

Literature Review

2.1. Theoretical Background

2.1.1. Thermodynamic Principles

Hydrogen liquefaction, in general, can be accomplished through two types of thermodynamic systems: a liquefier system and a refrigeration system for liquefaction. Figure 2.1 compares the thermodynamic structure of the refrigerator, liquefier, and refrigerator for liquefaction. The working principle of a refrigerator is based on the refrigeration cycle, which is considered a closed cycle, where the process fluid absorbs heat at a temperature below that of the environment and rejects it to ambient.[29–31] In a refrigerator for the liquefaction application, the thermal load of the refrigerator is spread over the feed stream from gas at ambient temperature to liquid at cryogenic temperature.[31] In contrast, a gas liquefier system is considered an open system process, where the liquid product accumulates and is withdrawn at cryogenic temperature.[29,30] In liquefier systems, the feed gas is also the working fluid that is being compressed and expanded in the system.

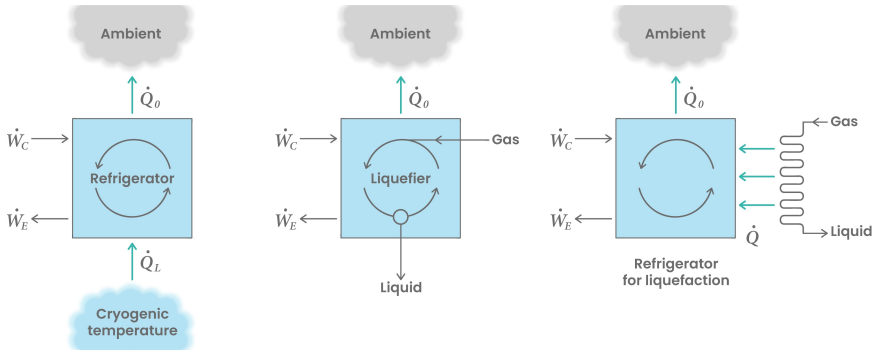

Figure 2.1: Thermodynamic structure of (from left to right) refrigerator, liquefier and refrigerator for liquefaction

Like any thermodynamic process, liquefaction performance is limited by the thermodynamically ideal liquefaction system for both the liquefier and refrigerator for liquefaction systems. The perfect liquefaction system consists of two ideal processes from the Carnot cycle; reversible isothermal compression followed by a reversible isentropic expansion,[29,32] as shown in Figure 2.2 Based on the energy and entropy balance of this cycle, the work per unit mass of the liquefied gas is given by:

$$-\dot{W}_i/\dot{m}_f = T_0(s_1 - s_f) - (h_1 - h_f). \tag{2.1}$$

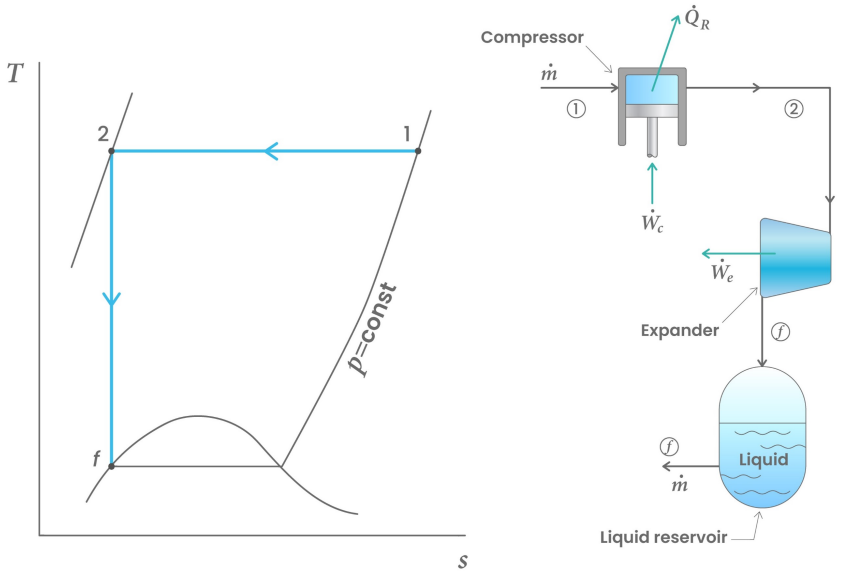

Figure 2.2: T-s diagram and schematic of ideal liquefaction process

Ideal work requirements reported in the literature for the liquefaction of common gases from an initial condition of 300 K and 1.013 bar, along with their standard boiling points, are shown in Table 2.1. As the table shows, hydrogen liquefaction has a work requirement significantly higher than other commonly liquefied gases, including helium, which has a lower boiling point than hydrogen.

Table 2.1: Ideal work requirements for the liquefaction of several gases initially at 300 K and 1.013 bar[32]

Gas	Normal Boiling Point [K]	$-\dot{W}_i/\dot{m}_f$ [kJ/kg]
Helium-3	3.19	8,178
Helium-4	4.21	6,819
Hydrogen	20.27	12,019
Neon	27.09	1,335
Nitrogen	77.36	768.1
Air	78.80	738.9
Carbon monoxide	81.60	768.6
Oxygen	90.18	635.6
Methane	111.7	1,091
Ethane	184.5	353.1
Propane	231.1	140.4
Ammonia	239.8	359.1

The ideal power requirements in Table 2.1 are physical limitations of the liquefaction process. They are used as a reference system to compare the efficiencies of actual gas liquefaction systems.[33] For liquefier, the figure of merit (FOM), also termed as exergy efficiency, compares the theoretical ideal specific work with the actual specific work required by the liquefier system[29,31–33]:

$$\text{FOM} = \frac{\dot{W}_i/\dot{m}_f}{\dot{W}/\dot{m}_f}, \tag{2.2}$$

where $\dot{W}$ is the net work requirement defined as the difference between the total power consumption and the recovered power (from turbines) in the liquefaction cycle. A FOM value close to one implies that the liquefier is approaching ideal performance. In addition, the actual work

per unit mass of gas liquefied (specific work) from Equation (2.2) is also termed as the specific energy consumption (SEC)[2,34]:

$$w = \frac{\dot{W}}{\dot{m}_\mathrm{f}}. \tag{2.3}$$

FOM and SEC both system performance parameters or payoff functions for indicating the performance of a given liquefaction system. Another payoff function that are commonly used in literature[32–34] is the liquid yield, which is defined as the fraction of the total flow of gas that is liquefied:

$$y = \frac{\dot{m}_\mathrm{f}}{\dot{m}}. \tag{2.4}$$

Joule-Thomson Effect

In real applications, most gas liquefaction systems employ Joule-Thomson (JT) effect to enable temperature reduction through isenthalpic expansion of the fluid by using an expansion valve (JT valve).[29] Although the flow within an actual expansion valve is irreversible and nonisenthalpic, the inlet and outlet conditions can be considered to have the same total enthalpy since there is no work done on or by the fluid and because external heat transfers to or from the equipment are minimal.[29,33] The change in fluid temperature due to an isenthalpic change in pressure is represented by the Joule-Thomson coefficient, defined as:

$$\mu_\mathrm{JT} = \left(\frac{\partial T}{\partial p}\right)_h. \tag{2.5}$$

The JT coefficient is equivalent to the isenthalpic lines on a fluid's pressure-temperature diagram. Figure 2.3 shows a general pressure-temperature diagram of a real gas. The region where μ_JT is less than 0 indicates that isenthalpic expansion will increase temperature. In contrast, in the region where μ_JT is higher than 0, the respective expansion will decrease temperature.[33] The inversion curve is the curve that separates the two regions, and this is where the slope of the isenthalpic lines, thus the JT coefficient, is equal to zero. Figure 2.4 displays JT inversion curves for several fluids in the $p-T$ plane, shown with a linear and a logarithmic scale of T.

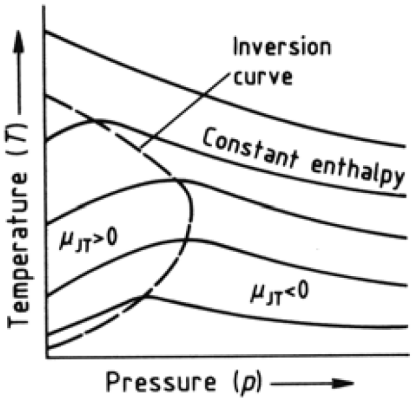

Figure 2.3: General pressure-temperature diagram of a real gas[a]

[a]Reproduced with permission of John Wiley & Sons - Books, from Cryogenic Technology In: Ullmann's Encyclopedia of Industrial Chemistry,[33] Windmeier, Christoph & Barron, Randall F., Volume 22, 2013; permission conveyed through Copyright Clearance Center, Inc.

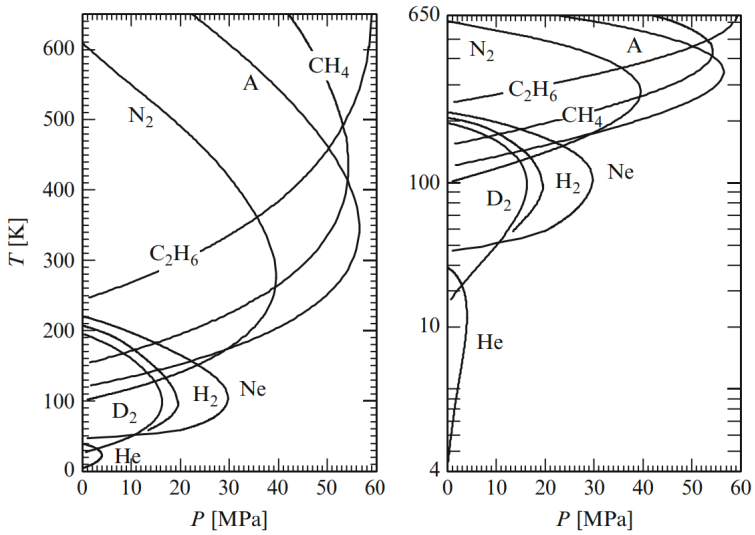

Figure 2.4: JT inversion curves for several gases in the plane of pressure and temperature[b]

The source of this phenomenon lies within the existence of intermolecular attraction and repulsion in the non-ideal fluid.[33] Thus, the JT coefficient can be evaluated using an equation of state (EOS) for real gases. The expression of JT coefficient evaluated using the simplest EOS for real gases, the van der Waals EOS, is given as:[33]

$$\mu_{\mathrm{JT}} = \frac{(2a/RT)(1-b/v)^2 - b}{c_p[1-(2/vRT)(1-b/v)^2]}. \tag{2.6}$$

The inversion temperature, T_{inv} (temperature points where $\mu_{\mathrm{JT}} = 0$), can be derived from above equation and is given as:

$$T_{\mathrm{inv}} = \left(\frac{2a}{bR}\right)(1-b/v)^2. \tag{2.7}$$

The maximum inversion temperature for van der Waals fluid occurs when the term $b/v = 0$; hence $T_{\mathrm{inv,max}} = 2a/bR$. The maximum inversion temperature for several gases is given in Table 2.2. For gases with maximum inversion temperature below ambient temperatures, such as helium, hydrogen and neon, JT expansion alone is insufficient to liquefy these gases: other means of process or equipment must be introduced into the liquefaction systems to achieve this.

Other Thermodynamic Processes

In addition to the Joule-Thomson effect, several other fundamental thermodynamic processes play a crucial role in the gas liquefaction processes. These processes include heat transfer, gas compression, and gas expansion with work (turbine expansion).

Heat transfer is the process of energy exchange between two substances due to a temperature difference between them. In the context of thermodynamic refrigeration and gas liquefaction processes, the exchange of energy is between fluid streams that are at different temperatures and is facilitated by heat exchangers. The energy balance equation for a steady-state heat exchanger involves equating the energy entering the system to the energy leaving the system. The energy

[b]Reproduced with permission from Springer Nature, from The Joule-Thomson Effect, Its Inversion and Other Expansions. 2 In: Miniature Joule-Thomson Cryocooling : Principles and Practice[35] Pfotenhauer, John M. & Maytal, Ben-Zion, 2013; permission conveyed through Copyright Clearance Center, Inc

balance equation for a steady-state counterflow heat exchanger can be expressed in terms of the difference in enthalpy between the two fluids.[36] Assuming no heat loss to the surroundings as well as neglecting the changes in the kinetic and potential energy, the equation is:[36]

$$\dot{m}_1 \cdot (h_{1,\text{out}} - h_{1,\text{in}}) = \dot{m}_2 \cdot (h_{2,\text{in}} - h_{2,\text{out}}). \tag{2.8}$$

The enthalpy values should be determined at the specified conditions of pressure and temperature for each fluid. Also, the equation above assumes that the fluids do not undergo phase changes (e.g., boiling or condensation) within the heat exchanger.

Gas compression is a process in which the volume of a gas is reduced by increasing its pressure. This is achieved by using mechanical devices called compressors. Compressors take in a gas at a certain pressure and volume, and then use a specific volume reduction mechanism, which varies according to the compressor type, to decrease the gas's volume and elevate its pressure. The power required by a compressor can be calculated using thermodynamic principles, specifically based on the work done on the gas during compression. The ideal power of a reversible adiabatic compressor, with negligible kinetic and potential energy variations, can be calculated using the following equation:[36]

$$\dot{W}_{\text{comp,is}} = \dot{m} \cdot (h_{\text{in}} - h_{\text{out,is}}). \tag{2.9}$$

To calculate the actual compressor power, the isentropic efficiency of the compressor needs to be determined. The compressor's isentropic efficiency is defined as:[36]

$$\eta_{\text{is}} = \frac{h_{\text{in}} - h_{\text{out,is}}}{h_{\text{in}} - h_{\text{out}}}. \tag{2.10}$$

Thus, the actual compressor power requirement can be determined as follows:[36]

$$\dot{W}_{\text{comp}} = \frac{\dot{m} \cdot (h_{\text{in}} - h_{\text{out,is}})}{\eta_{\text{is}}}. \tag{2.11}$$

Expansion with work, in this context referring to turbine expansion, is the process in which a high-pressure fluid (in this context, gas) undergoes a controlled decrease in pressure while performing mechanical work on the turbine. The ideal power output of a turbine is calculated on the basis of the change in enthalpy of the fluid as it expands isentropically (reversibly and adiabatically) through the turbine.[36] The equation is given by:[36]

$$\dot{W}_{\text{turb,is}} = \dot{m} \cdot (h_{\text{in}} - h_{\text{out,is}}). \tag{2.12}$$

To calculate the actual turbine output, the isentropic efficiency of the turbine needs to be deter-

Table 2.2: Maximum inversion temperature for several gases[33]

Gas	$T_{inv,max}$ [K]
Helium	45
Carbon Monoxide	652
Hydrogen	205
Neon	250
Argon	794
Air	603
Oxygen	761
Nitrogen	621
Methane	939

mined. The turbine's isentropic efficiency is defined as:[36]

$$\eta_{is} = \frac{h_{in} - h_{out}}{h_{in} - h_{out,is}}. \tag{2.13}$$

Thus the actual turbine power output can be determined as follows:[36]

$$\dot{W}_{turb} = \eta_{is} \cdot \dot{m} \cdot (h_{in} - h_{out,is}). \tag{2.14}$$

2.1.2. Fundamental Liquefaction Systems

Throughout the literature[2,29–34,37] on hydrogen liquefaction and cryogenic technology, there are three fundamental liquefaction systems or cycles are commonly associated with hydrogen liquefaction application: 1.) Linde-Hampson system (Joule-Thomson expansion cycle); 2.) Claude Liquifier system; 3.) Joule-Brayton refrigeration cycle.

Linde-Hampson System

The Linde-Hampson system, sometimes called the Joule-Thomson cycle when used as a refrigerator,[34] is considered as the simplest liquefaction system[32]. The schematic of a basic Linde-Hampson system is shown in Figure 2.5a. Here, the working gas is first compressed to a pressure of ca. 20 MPa and then passed to a recuperative heat exchanger, where the returning stream of the cold gas cools the warm high-pressure working gas. At point (3), the cold high-pressure gas will be expanded through JT valve. The stream will be in the gas and liquid phase at (4) near ambient pressure. The liquefied gas can be withdrawn (f), while the saturated vapour could be recycled to cool down the incoming gas (g).

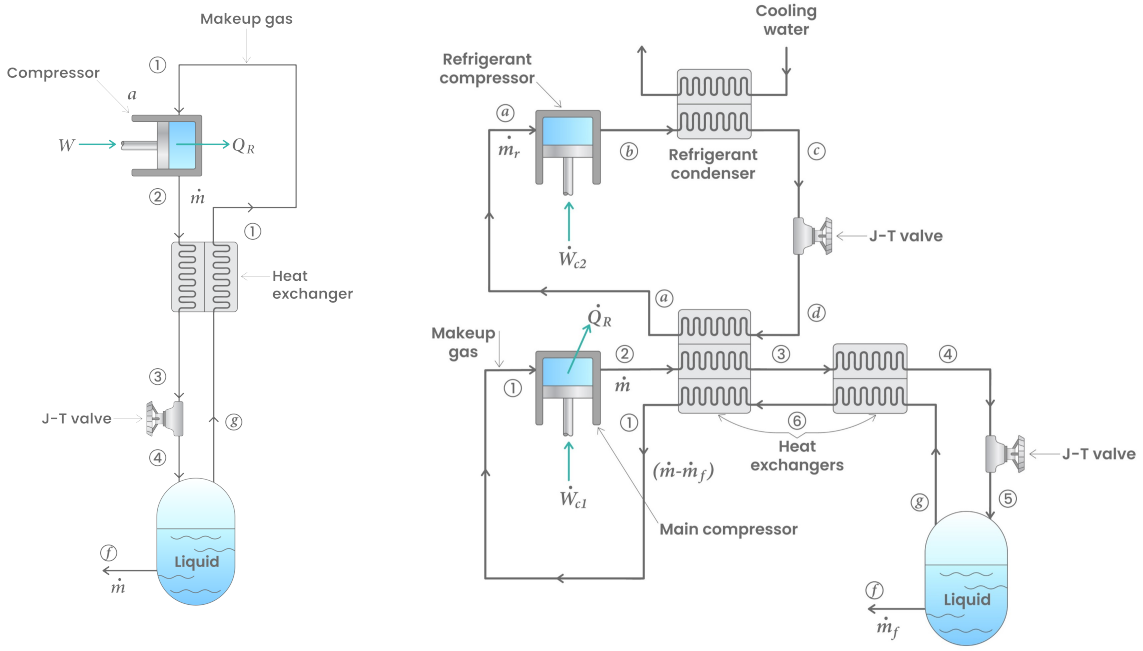

(a) Simple Linde-Hampson liquefier

(b) Precooled Linde-Hampson liquefier

Figure 2.5: Schematic of Linde-Hampson refrigeration and liquefaction systems

For hydrogen application, the simple Linde-Hampson system is not applicable for liquefying hydrogen from ambient conditions because its maximum inversion temperature is lower than the

standard ambient temperature.[33] The system could not start from the warm condition since the hydrogen gas would only experience an increase in temperature during the isenthalpic expansion in the JT valve. In order to make use of the Linde-Hampson principle, hydrogen needs to be precooled below ca. 205 K. This can be achieved via Precooled Linde-Hampson liquefaction system, shown in Figure 2.5b.

Precooled Linde-Hampson systems use separate refrigeration systems, using various refrigeration fluids, to precool the main gas stream, in this case, hydrogen, such that the hydrogen enters the original (two-stream) heat exchanger at a temperature significantly lower than ambient[33]. Further modification of the Linde-Hampson systems applicable for hydrogen liquefaction is the precooled dual-pressure Linde Hampson system,[34] which could reduce the total work required though somewhat reducing the liquid yield of the system.[32]

Claude Liquefier

As explained in the literature, the Linde-Hampson system is characterized by low efficiency and is usually only considered for small-scale hydrogen liquefaction applications (less than two TPD).[2,31,34] The Claude system is considered more appropriate for large systems; therefore, many industrial hydrogen liquefiers are based on this principle.[2,31–34] The Claude system improves the performance of the previous Linde-Hampson cycle by incorporating energy removal through an expander performing work (turbine)[33]. Figure 2.6 illustrates the original Claude liquefier system from 1902.

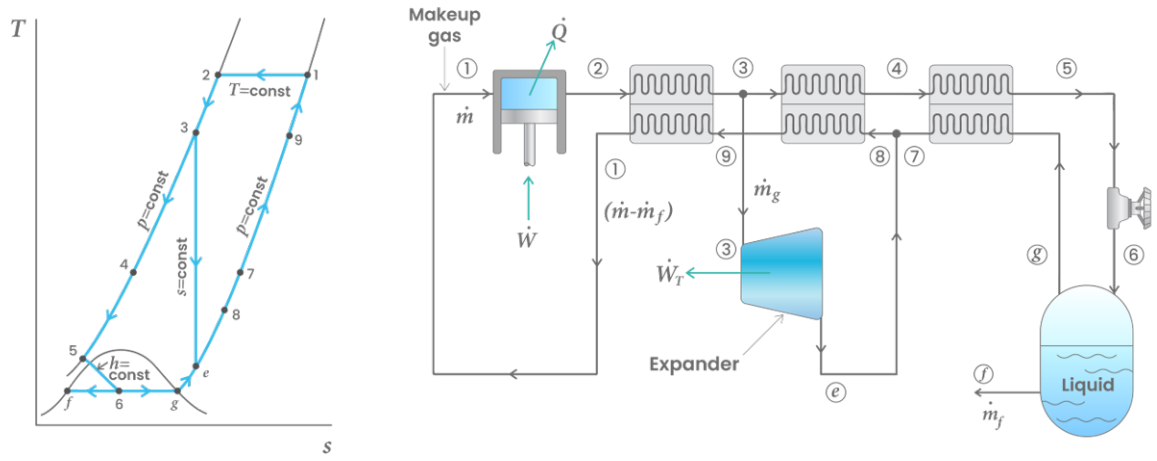

Figure 2.6: The Claude liquefaction system

In the original Claude system, the feed gas is first compressed to pressure on the order of 40 bar.[32] After passing the first heat exchanger, at point (3), about 60 to 80 per cent of the fluid is diverted from the mainstream to be expanded through an expansion engine or turbine and reunited with the returning stream entering the second heat exchanger (stream (*e*), (7) and (8) in Figure 2.6). The main gas stream continues to experience temperature reduction through the second and third heat exchangers and is finally expanded through the JT valve. The stream will be in multiphase at point (6), and the liquid form is collected from the liquid receiver, stream (*f*), while the cold vapour is returned to the heat exchangers to cool the incoming gas streams. Note that the JT expansion valve is still necessary for Claude liquefier because real turbine expanders, in practice, cannot tolerate the formation of substantial liquid without damaging its blades.[32]

Compared to the basic Linde-Hampson system, the Claude system has the advantage of being able to be used for hydrogen liquefaction applications without an additional precooling system. According to Barron,[33] the FOM of a Claude liquefier is considerably higher than all Linde-

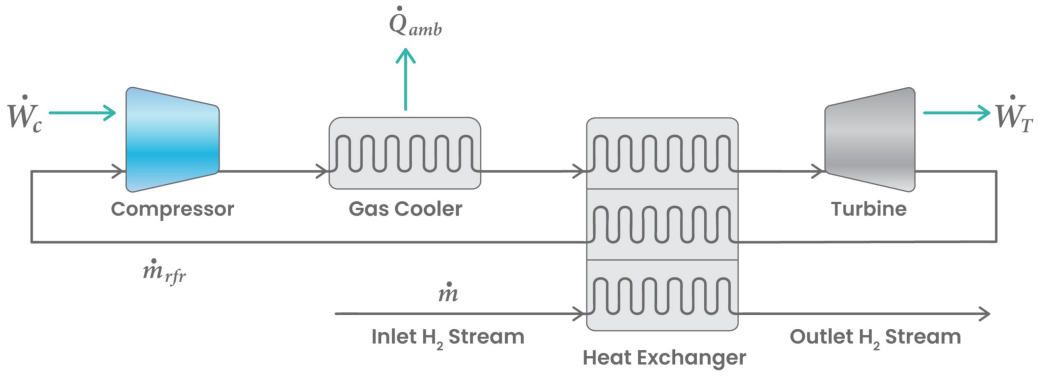

Figure 2.7: Schematic of a simplified J-B refrigeration cycle for hydrogen liquefaction

Hampson cycles due to several phenomena: 1.) Removal of enthalpy in the expander delivers refrigeration effect directly at low temperatures; 2.) Entropy production is reduced during the isenthalpic JT expansion due to the sub-cooling of the flow at the valve's inlet; 3.) Direct bypass of mass flow through the expander effectively reduced the temperature difference between the two streams in the intermediate heat exchanger. In many practical cases, the Claude system is considered a very effective liquefaction system.[32]

Several variations to the simple Claude system are applicable for hydrogen liquefaction, including Kapitza, dual pressure Claude, precooled simple Claude, precooled dual pressure Claude, and helium-precooled Claude systems.[34] The performance of a Claude liquefier can be dramatically improved by increasing the number of the heat exchanger or by adding a precooling process such as a liquid-nitrogen (LN_2) precooling bath.[2,32–34] Due to the high capital expense (CAPEX) for adding turbine energy recovery system, in current H_2 liquefaction practices, the mechanical energy output from the expansion engine is usually dissipated through a braking system or an external wind blower.[22] This does not affect the liquid yield of the system; however, it does reduce the system's overall efficiency performance.

Joule-Brayton Refrigeration Cycle

The Joule-Brayton (JB) refrigeration cycle (also called reverse Joule-Brayton cycle) utilizes an expansion engine (turbine) to expand the flow of working fluid as if replacing the throttle of the Linde-Hampson refrigeration cycle.[38] This system employs a closed refrigeration cycle containing a pure or mixed refrigerant (MR) as the working fluid to cool the stream of the fluid to be liquefied.[2,39] The schematic of a simplified JB refrigeration cycle for hydrogen liquefaction is shown in Figure 2.7.

Theoretically, the minimum operating temperature of a JB refrigerator is limited by the refrigerant's freezing temperature. However, the more practical limit would be at the condensing point of the refrigerant since multiphase flow in turbines is technically challenging and often avoided.[22] This determines whether the JB system would be capable to liquefy hydrogen by itself. However, the cycle can be useful as a precooler system for Linde-Hampson and Claude liquefaction systems.[31] Chang et al.[40] reported that using two turboexpanders in series or parallel could enhance the thermodynamic efficiency of a conventional JB refrigeration cycle. Numerous gas liquefaction system designs have incorporated the JB refrigeration cycle throughout the conceptual and real applications. Traditionally, reverse Joule-Brayton cycle has only been considered for small-scale hydrogen liquefaction plants, but lately, there has been growing interest in its application in high-capacity systems.[5,22,31,34]

2.1.3. Fundamental Properties of Hydrogen

Scientists estimate that hydrogen makes up a significant portion of the material world, accounting for 90% of the total atoms or 75% of the total matter in the universe, surpassing helium, the second most common element.[39,41] Hydrogen is present primarily in atomic and ionic states in space, with some existence in molecular form. On Earth, however, hydrogen is mainly bonded with other atoms in chemical compounds, including water and hydrocarbons.[39]

Hydrogen's natural occurring isotopes, protium, deuterium, and tritium, can combine and form diatomic molecules. However, since tritium is unstable and radioactive, and deuterium is incredibly scarce compared to protium (which has an abundance of more than 99.98%), only the properties of hydrogen molecules comprising protium are considered for industrial applications.[39] In this work, the term "Hydrogen (H_2)" refers only to protium-based hydrogen molecules. This section discusses hydrogen's fundamental characteristics as a molecule, emphasising its peculiar thermodynamic properties in low temperatures, significantly impacting the development of the hydrogen liquefaction cycle.

Spin Isomers of Hydrogen

Molecular hydrogen exists in two isomeric variations, ortho- and para-hydrogen, distinguished by the nuclear spin state of the protons in each hydrogen atom.[2] Ortho-hydrogen (o-H_2) is when the two proton nuclear spins of the hydrogen molecule is aligned in parallel, while para-hydrogen (p-H_2) is when the nuclear spins are in the opposite direction.[32,39] Figure 2.8 shows a schematic representation of these two nuclear spin isomers.

Figure 2.8: Ortho- and para-hydrogen spin isomers; p-proton and e-electron, while the arrow correspond to the spin direction of the nucleus

The ratio of the average number of all hydrogen molecules in the p-H_2 form and that in the o-H_2 form at equilibrium conditions varies with temperature. The equilibrium mixture at a given temperature is called the equilibrium-hydrogen (e-H_2)[32]. Table 2.3 and Figure 2.9 show the fraction of para-hydrogen at equilibrium as a function of temperature. The impact of pressure on hydrogen equilibrium concentrations is considered insignificant.[34,42] The ratio between the ortho-para isomers affects the overall magnetic, optical, volumetric and thermal properties of the hydrogen.[34] At ambient temperatures and above, a pseudo-pure substance commonly known as normal hydrogen (n-H_2) consisting of 75% o-H_2 and 25% p-H_2 provides an excellent representation for estimating hydrogen properties.[2]

Table 2.3 and Figure 2.9 implies that if hydrogen at room temperature is cooled to a temperature close to its normal boiling point (≈20.27 K), there is a conversion from ortho- to para-hydrogen as the temperature of hydrogen decreases. During the transition, the original o-H_2 molecules drop to a lower molecular-energy level, thus, releasing a quantity of energy (an exothermic reaction) called the heat of conversion.[32] The reaction enthalpy of this conversion process is plotted as a function of temperature in Figure 2.9. At the normal boiling point of hydrogen, the conversion heat is 703.3 kJ/kg, which is significantly higher than its latent heat of vaporization, which is 443 kJ/kg.

Unfortunately, in the absence of a catalyst, the process of converting ortho- to para-hydrogen happens very slowly.[30] Consequently, when normal-hydrogen is liquefied, the liquid hydrogen has essentially room-temperature compositions (of o-H_2 and p-H_2) unless extra measures are being taken to accelerate the conversion process.[32] Finally, the unconverted normal liquid hydrogen (the unconverted o-H_2 fraction) will slowly convert to p-H2, releasing sufficient heat to vaporize a substantial amount of the liquid.[30] For LH_2 with n-H_2 initial composition, the evaporation rate, namely *boil-off*, is about 1 percent of the stored liquid per hour.[32] Timmerhaus and Flynn[29] demonstrate how the boil-off of LH_2 varies over time as a result of the initial ortho-hydrogen concentration, as shown in Figure 2.10.

Table 2.3: Equilibrium concentration of para-hydrogen in equilibrium hydrogen[32]

Temperature [K]	Mole fraction of p-H_2
20.27	0.9980
30	0.9702
40	0.8873
50	0.7796
60	0.6681
70	0.5588
80	0.4988
100	0.3947
120	0.3296
140	0.2980
160	0.2796
200	0.2597
250	0.2526
300	0.2507

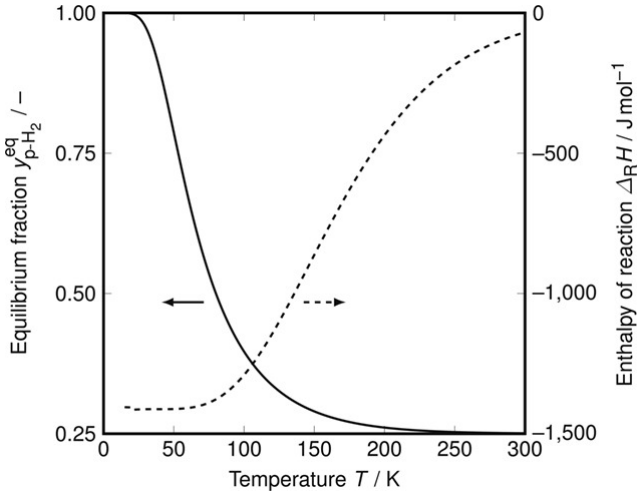

Figure 2.9: Equilibrium composition & enthalpy of reaction of ortho- & para-hydrogen mixtures[c]

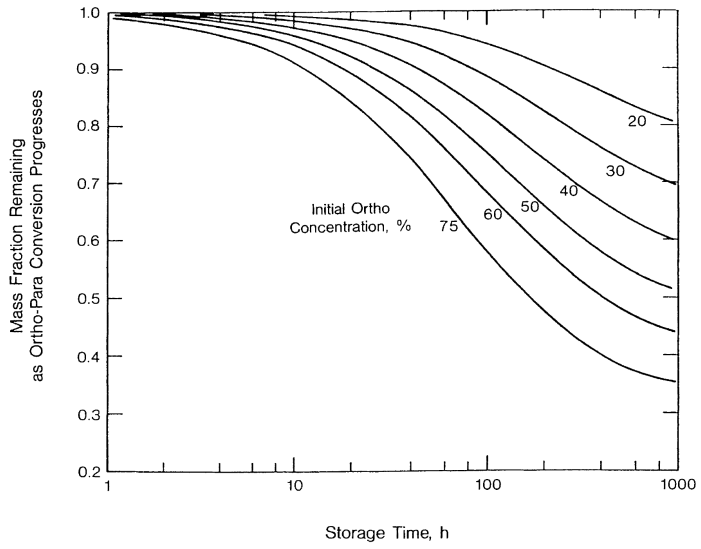

Figure 2.10: Fraction of liquid hydrogen evaporated due to ortho-para conversion as a function of time[d]

[c]Used with permission of John Wiley and Sons, from Kinetics and Heat Exchanger Design for Catalytic OrthoPara Hydrogen Conversion during Liquefaction In: Chemical Engineering & Technology,[43] Harald Klein, Lutz Decker, Umberto Cardella, et al, 2019; permission conveyed through Copyright Clearance Center, Inc

[d]Reproduced with permission from Springer Nature, from Properties of Cryogenic Fluids In: Cryogenic Process Engineering, Klaus D. Timmerhaus and Thomas M. Flynn, 1989; permission conveyed through Copyright Clearance Center, Inc.

Figure 2.10 illustrated that to bring the boil-off losses inside the cryogenics tanks or vessels to a minimum, the conversion process must occur during the liquefaction process before the LH_2 is stored. Thus, catalyst materials are often integrated into the liquefaction system to speed up the conversion process and allow the released heat to be absorbed by the liquefier.[2,32] According to Valenti,[39] The catalytic conversion process can be achieved in two modes: batch and continuous mode. Batch mode is executed via reactors which can be either adiabatic or isothermal. In continuous mode, the catalyst is packed inside the heat exchangers of the liquefier system. Since the enthalpy of the reaction is lower at higher temperatures, and heat removals are thermodynamically more efficient (as described by the Carnot refrigeration cycle), it is preferable to perform the ortho- to para-hydrogen conversion in a continuous process along the equilibrium hydrogen curves.[22,44] Although, in actual kinetic reactors, the catalytic conversion never actually reach the theoretical equilibrium compositions of ortho- and para-hydrogen fractions.[22]

Catalytic Conversion of Ortho-Para H_2

Comprehension of the reaction kinetics involved in catalytic conversion of o-H_2 to p-H_2 is important as it influences the thermodynamic efficiency and economic feasibility of hydrogen liquefaction process design.[22] In general, the kinetics of catalyzed conversion of ortho-para H_2 can be sufficiently described by the first-order kinetic model equation[2,22,43]:

$$\dot{r} = k\rho_{\text{mol}}\left(x_{\text{para}}^{\text{eq}} - x_{\text{para}}\right), \tag{2.15}$$

where k is the rate contant given as[45]:

$$k = \frac{\exp\left(-\frac{E_a}{RT}\right)}{x_{\text{p}}^{\text{eq}}(a\rho_{\text{mol}} + b)}. \tag{2.16}$$

The activation energy, E_a, and the rate constant parameters, a and b, are all assumed to be constant and do not vary with temperature, pressure and concentration. Curve fitting of three sets of experimental data[46–48] has determined that the average values of E_a, a and b are 336.45 J/mol, 2.2 × 10⁻3 m^3_{cat}·s/mol and -35.11 × 10⁻3 m^3_{cat}·s/$m^3_{H_2}$, respectively.[43,45] The Langmuir-Hinshelwood approach was also used to incorporate the effects of adsorption and desorption on the catalyst surface to the first-order equation mentioned above.[43] However, this modification did not result in any notable enhancement in agreement with the experimental conversion data.

Solid catalysts are used in hydrogen liquefaction to convert hydrogen spin-isomers through two mechanisms: spin-conversion at magnetically ordered surfaces or spin-conversion at paramagnetic surfaces.[2] According to Barron,[32] catalysts proven effective for ortho-para conversion are 1.) Hydrous ferric oxide; 2.) Chromic oxide on alumina particles; 3.) Charcoal and silica gel; and 4.) Nickel-based catalyst. Among all these materials, the hydrous ferric oxide-based catalyst is reported to be the most active catalyst for this application.[32] Additionally, due to the low production cost of hydrous ferric oxide, it is widely used in the hydrogen liquefaction industry.[22] Solid catalysts are very sensitive to certain impurities such as N_2, CH_4, CO_x, H_2S, et cetera, which can act as temporary poisons or cause permanent damage to the activity performance of the catalyst.[2,32] For this reason, because they might solidify and cause blockage, such impurities are normally removed early in the liquefaction system through adsorption.

Thermodynamic Property of Molecular H_2

Adequate knowledge of hydrogen thermodynamics properties is paramount in hydrogen liquefaction. Leachman et al.[49] developed the state-of-the-art Helmholtz free energy-explicit fundamental EOS for ortho-, para-, and normal-hydrogen, valid from the triple point of the temperature of each fluid (≈ 14 K) to 1,000 K for pressures up to 20,000 bar. The critical point and

triple conditions used by Leachman et al. in developing the reference EOS of hydrogen are shown in Table 2.4. According to the paper[49], Leachman EOS for para- and normal-hydrogen

Table 2.4: Critical- and triple-point properties used by Leachman et al.[49] state-of-the-art para-, ortho- and normal- hydrogen EOS

	Temperature [K]	Pressure [bar]	Density [mol·dm^{-3}]
		Para-hydrogen	
Critical point	32.938	12.858	15.538
Triple point	13.8033	0.07041	38.185
		Normal-hydrogen	
Critical point	33.145	12.964	15.508
Triple point	13.957	0.0736	38.2
		Ortho-hydrogen	
Critical point	33.22	13.1065	15.445
Triple point	14.008	0.07461	38.2

have relatively small uncertainties, with the uncertainties in densities of 0.1% at pressures up to 400 bar and temperature up to 250 K, except near the critical point where an uncertainty of 0.2% in pressure is observed. At temperatures between 250-450 K and pressures up to 3,000 bar, the uncertainty in density is even lower, at 0.04%. The uncertainties of the heat capacities are estimated to be at 1.0% for both para- and normal-hydrogen below 1,000 bar. Minor deviations are also seen in other properties, such as the speed of sound, vapour pressures and saturated liquid densities. It is anticipated that the differences in the ortho-hydrogen EOS will be comparable to those found in the formulations of para- and normal-hydrogen. However, no direct comparisons have been made due to a lack of experimental data for o-H_2. These minor uncertainties make Leachman EOS more than sufficient for developing and improving hydrogen liquefaction processes, provided that the ortho-parahydrogen ratio is appropriately monitored or managed at every stage.

Most commercial process simulation software packages utilize cubic EOS, such as the Peng-Robinson EOS, to calculate thermodynamic properties for pure fluids and their mixtures. However, the cubic-type methodology is usually unreliable for predicting properties of fluids such as hydrogen, helium and neon, where quantum effects play a significant role in determining their critical properties. REFPROP[50] (ver. nine and above), a low-cost software developed by the U.S. National Institute of Standards and Technology (known as NIST), employs the Leachman EOS as the main reference for calculating ortho-, para- and normal-hydrogen properties; hence, they are currently regarded as the most accurate computational tool for the thermodynamic and transport properties of hydrogen.[39]

In 2012, Valenti et al.[51] reported that the choice for the heat capacity model in the ideal gas state of hydrogen pure forms (o-H_2 and p-H_2) and their mixtures (e-H_2 and n-H_2) is paramount for accurate and robust hydrogen liquefaction simulation. Valenti et al. modelled the equilibrium-hydrogen ideal gas heat capacity based on Le Roy et al.[52] works in 1990. The volumetric behaviour of the equilibrium-hydrogen in low-temperature regions is approximated by pure para-hydrogen since equilibrium-hydrogen is mainly composed of para-hydrogen in cryogenic conditions. The paper[39,51] concluded that the choice of EOS is of lesser importance compared to the ideal gas heat capacity model in the overall hydrogen liquefaction simulation; however, it plays a vital role in sizing a plant's operational units which are strongly affected by volume flows (accurate density estimation).

[e]Reprinted from Fluid Phase Equilibria, 504, Silvia Lasala, Romain Privat, Philippe Arpentinier, Jean-Noël Jaubert, Note on the inconsistent definition assigned in the literature to the heat capacity of the so-called equilibrium hydrogen mixture,[53] 112325, Copyright 2020, with permission from Elsevier

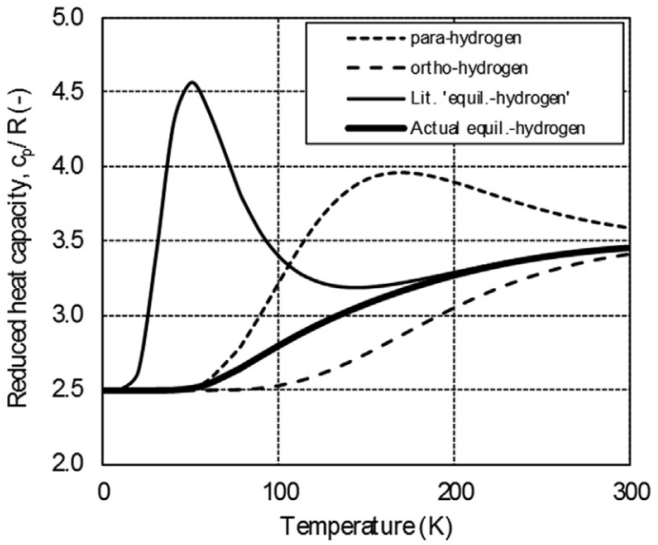

Figure 2.11: Comparison of reduced specific heat capacity of p-H_2, o-H_2, literature 'equilibrium'-H_2 and and actual equilibrium-H_2[e]

Le Roy et al.[52] and Valenti et al.[51] reported the ideal gas heat capacity values of equilibrium hydrogen as a function of temperature in their publications. However, the term "equilibrium hydrogen heat capacity" in these cases is misleading, as the reported heat capacity values are equivalent to a fictive pure component with the same enthalpy as a reacting mixture of para- and ortho-hydrogen at chemical equilibrium. This inconsistent definition in the literature is exposed and explained relatively recently by Lasala et al.[53]. Using the fundamental definition of heat capacity and perfect gas mixture, Lasala et al.[53] shows that the published ideal gas-specific heat capacity values of the binary mixture of ortho- and para-hydrogen at equilibrium (e-H_2) contradicts the underlying theory as they do not lie in the intermediate values between specific heat capacity of the ortho- and para-hydrogen components which form the equilibrium mixture. Comparison between the reduced gas heat capacities of e-H_2 reported in past literature[51,52], and the actual reduced heat capacities of e-H_2 based on the equilibrium hydrogen compositions, as functions of temperature, is shown in Figure 2.11.

However, the model in the past literature of the pseudo-pure component having the same enthalpy as the reacting mixture of p-H_2 and o-H_2 at chemical equilibrium gives practical advantages for process simulation of hydrogen liquefaction. With this approach, the cooling duty of continuous catalytic heat exchangers in liquefier systems can be calculated using a simple heat exchanger model in the process simulation. The pseudo-component heat capacity aggregates sensible heat effects and thermal effects due to compositional change. Henceforth in this work, the pseudomodel of "equilibrium hydrogen" by Le Roy et al.[52] and Valenti et al.[39,51] will be referred to as "pseudo equilibrium hydrogen" or "pseudo-e-H_2".

2.2. Existing and Conceptual Hydrogen Liquefaction

2.2.1. Industrial Liquid Hydrogen Production

According to a recent review article[2], the existing hydrogen liquefaction plant SEC ranges from 10-15 kWh/kg_{LH_2}, with FOM ranging from 20-30%. This high energy consumption is in part because the scale of the existing liquefiers is relatively small (less than 32 TPD per liquefaction system), leading to designs that focus on lower CAPEX instead of high efficiency. As mentioned in the Introduction, the high SEC values of LH_2 production will add to the cost and carbon

footprint of end-use hydrogen. The most recent hydrogen liquefiers are based on Claude cycle modifications and employ a catalyst-packed heat exchanger to continuously convert ortho- to para-hydrogen continuously.[2] In general, industrial hydrogen liquefaction systems are designed to produce LH_2 with a para-hydrogen concentration exceeding 95%.[39]

The history of the establishment of hydrogen liquefaction plants has been described in the literature.[2,34,54] However, detailed performance reports of existing hydrogen liquefiers are quite scarce in the literature. Thus, this section will briefly discuss only two built liquefaction systems: 1.) Linde-Leuna; and 2.) Praxair. Other major gas liquefaction companies, such as Air Products and Air Liquide, have also constructed hydrogen liquefaction plants around the world; however, there is no publicly available information about how these plants are performing. Recently, Chart Industries and Kawasaki Heavy Industries (KHI) have also successfully demonstrated their hydrogen liquefaction solutions.[55,56] In 2022, Air Products announced their plan to start construction of a second hydrogen liquefaction plant in Rotterdam, which will double Europes current liquid hydrogen capacity on opening in 2025.[57,58]

Linde-Leuna

Linde Kryotechnik AG has designed multiple hydrogen liquefaction facilities of various sizes in different parts of the globe.[59] Linde's H_2 liquefaction plant in Leuna, Germany, works based on a modified precooled hydrogen Claude cycle where LN_2 is used in the precooling system and H_2 recycle stream for cryogenic cooling.[2,59] The significant improvements from Linde's previous, now decommissioned, Ingolstadt liquefaction plant are the implementation of dynamic gas bearing turbines, ejector to reliquefy boiling gas and flash gas, and packing of $Fe_2(OH)_3$ catalyst to promote continuous ortho-para conversion.[2,59]

The simplified process flow diagram of the Leuna liquefier is shown in Figure 2.12. The reported SEC and exergy efficiency values for the Leuna plant are 11.9 kWh/kg_{LH_2} and 23.6%, respectively. The plant was originally built in 2007, with a capacity of 5 TPD.[59] According to a recent report,[2,60] the capacity of the plant doubled to 10 TPD in 2021.

Praxair

Praxair has five hydrogen liquefaction plants in the USA, with capacities ranging between 18-36 TPD. Its largest plant is a double-train liquefier.[2,54,59] These plants operate based on a modified precooled Claude cycle that includes three heat exchangers and continuous ortho-para conversion. This system utilizes nitrogen gas and refrigerant from an external cycle as the primary coolant in the first heat exchanger. The main cooling agents in the second heat exchanger are liquid nitrogen and the hydrogen recycle stream, while the third exchanger uses the hydrogen stream alone.[2,54] The typical SEC of Praxair's plants are between 12.5-15 kWh/kg_{LH_2} while the exergy efficiency (FOM) is between 19.3-24%.[2,54,59] In 2018 Praxair merged with Linde AG to form Linde plc and the name Praxair was discontinued in 2020 in the US.

2.2.2. Conceptual Hydrogen Liquefaction System

Over the last 30 years, many conceptual hydrogen liquefaction processes have been published in the literature.[2,34,61] Unlike in most existing hydrogen liquefiers, where the design's primary focus is to reduce CAPEX, conceptual models are developed to demonstrate how the efficiency of the hydrogen liquefaction process can be improved. The SEC of these conceptual models ranges from 4-14 kWh/kg of LH_2, with a capacity of between 50 and 864 TPD.[2,34,61] Most conceptual studies have primarily focused on "pure" simulations[18] using commercial process simulation

[f] Reproduced from Hydrogen Liquefaction: A Review of the Fundamental Physics, Engineering Practice and Future Opportunities[2] with permission from the Royal Society of Chemistry.

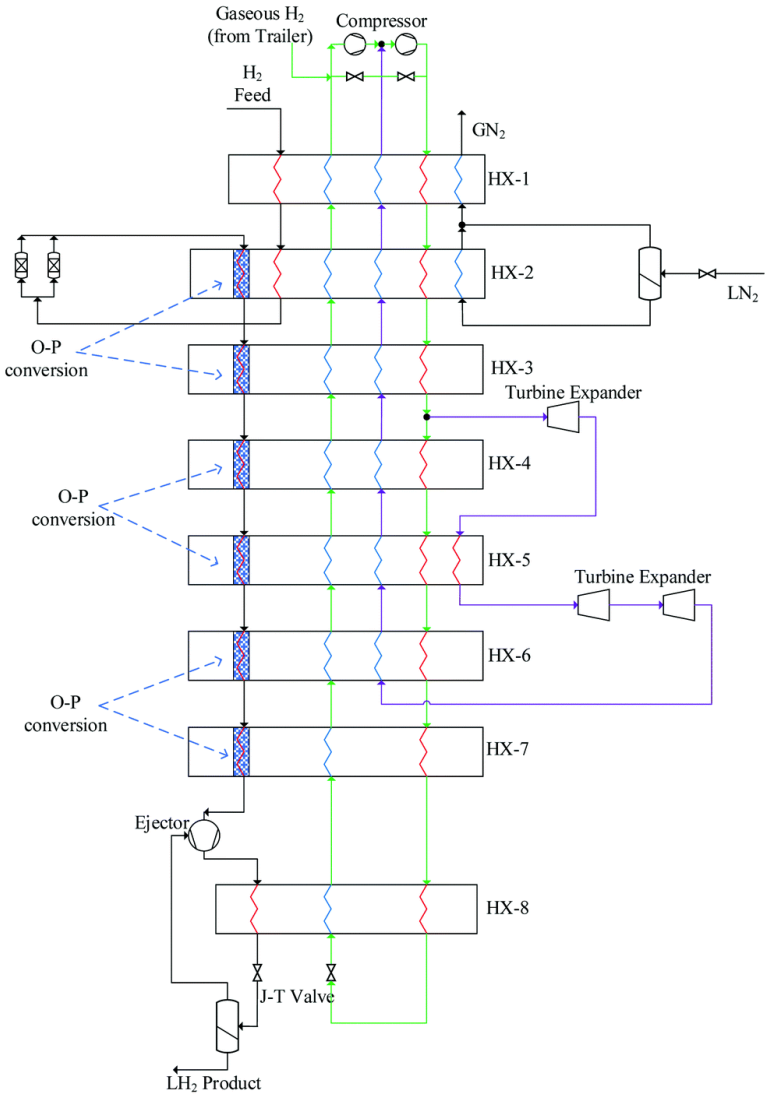

Figure 2.12: Schematic diagram for the Linde-Leuna hydrogen liquefier[f]

software such as Aspen HYSYS, Aspen Plus, UniSim, ChemCAD, et cetera, with limited attention given to overall expenses, operational feasibility, and technological readiness.[2,18,61]

In 2021, researchers collaborated on a thorough literature review on hydrogen liquefaction fundamental physics, engineering practice and prospects.[2] This review offers an extensive overview of feasible concepts for large-scale hydrogen liquefaction, among other aspects. The screening criteria proposed in the review paper[2] for the potentially viable large-scale process are as follows:

- Capacity ≥ 50 TPD,
- SEC values between 4-10 kWh/kg_{LH_2},
- FOM ≥ 0.23,
- Inclusion of novel but attainable technologies

In addition, this review presented a few of the associated cost estimates and projections of the feasible conceptual large-scale methods documented in the original publications. These process economic studies usually provide the plant's specific liquefaction cost (SLC). Specific liquefaction cost is defined as the total cost, which includes CAPEX, OPEX and Operation & Maintenance (OM) annual cost, to produce 1 kg of liquid hydrogen:

$$\mathrm{SLC} = \frac{\mathrm{CAPEX_a} + \mathrm{OPEX_a} + \mathrm{OM_a}}{\dot{m}_{\mathrm{LH_2,a}}}. \tag{2.17}$$

The SLC for current liquefaction processes is in the range 2.5-3.0 US$/kg$_{LH_2}$.[2,22]

The subsequent subsections briefly overview some of the conceptual hydrogen liquefaction processes on a large scale described in recent reviews.[2,34,61] The concepts of large scale hydrogen liquefiers are grouped according to the type of basic cryogenic systems adopted in the designs.

Conceptual Modified-Claude H_2 Liquefier

Kuendig et al.[2,24] developed a conceptual H_2 liquefier with a capacity of 50 TPD using a Claude cycle that incorporates precooling via both LNG and nitrogen gas. LNG was chosen as the working fluid for the liquefaction of hydrogen due to its potential accessibility at the site of liquefaction and its potential for use in generating hydrogen through steam methane reforming. Additionally, the proposed concept utilizes LNG re-gasification at an import terminal as a precooling system, which would help decrease the specific energy consumption (SEC) of the overall process. Similar concepts were also proposed by Faramarzi et al.[62] for larger-scale (369 TPD) applications. Assuming a hydrogen feed pressure of 20 bar, the proposed design's SEC can reach a minimum value of 8.85 kWh/kg$_{LH_2}$ and FOM of 0.47.[62] Based on the economic analysis, the minimum selling price of LH_2 the liquid hydrogen produced from the LH_2-LNG integration plant is 2.07 US$/kg$_{LH_2}$ assuming three years of payback time.

Japan's WE-NET Project, in 1994-2002, reviewed variety of process concept for 300 TPD hydrogen liquefier.[26] The project proposed the hydrogen Claude cycle with a closed loop nitrogen precooling cycle as the favored option. The liquefaction process is complex and necessitates a significant nitrogen liquefaction system to be in place, as it is needed to transform the gaseous nitrogen back into a liquid state following its use in the pre-cooling stage.[2] The calculated SEC and FOM of the WE-NET process concept with 1 bar feed pressure are 8.72 kWh/kg$_{LH_2}$ and 0.46, respectively.

Cardella et al.[22,63–65] designed two 100 TPD H_2 liquefaction concepts through process development and optimization that are highly feasible in the near future. The first process concept is designed with a high-pressure Hydrogen Claude Cycle. The second process concept utilizes two cryogenic refrigeration cycles: Hydrogen-Neon Mixture Brayton Cycle and Hydrogen JT Cycle. The first process suggested by Cardella is deemed more mature from a technical standpoint when compared to the second process. Therefore, this concept has relatively lower technical risks for near-term implementation; thus, this makes it one of the most promising conceptual designs at the time of this writing. After further cost-optimization process and inserting actual unit operations data into the model, the SEC of Cardella's process is around 5.8 kWh/kg$_{LH_2}$ with and 6.5 kWh/kg$_{LH_2}$ without turbine recovery assuming hydrogen pressure feed of 25 bar. Cardella's design also shows that SLC below 1 US$/kg$_{LH_2}$ can be achieved in large-scale hydrogen liquefaction processes. Berstad et al.[21] developed a similar process design for a hydrogen liquefaction plant with a capacity of 125 TPD.

Conceptual Joule-Brayton H_2 Liquefier

The IDEALHY (Integrated Design for Efficient Advanced Liquefaction of Hydrogen) project[59,66] ultimately produced a conceptual design of hydrogen liquefier based on an MR precooled Joule-Brayton refrigeration cycle with 'nelium' (75% helium and 25%) as the primary working fluid. The capacity of the conceptual plant is 50 TPD. The precooling system employs a mixed refrigerant comprising nitrogen, methane, ethane, propane and n-butane to cool the hydrogen stream

[8] Reproduced from Hydrogen Liquefaction: A Review of the Fundamental Physics, Engineering Practice and Future Opportunities[2] with permission from the Royal Society of Chemistry.

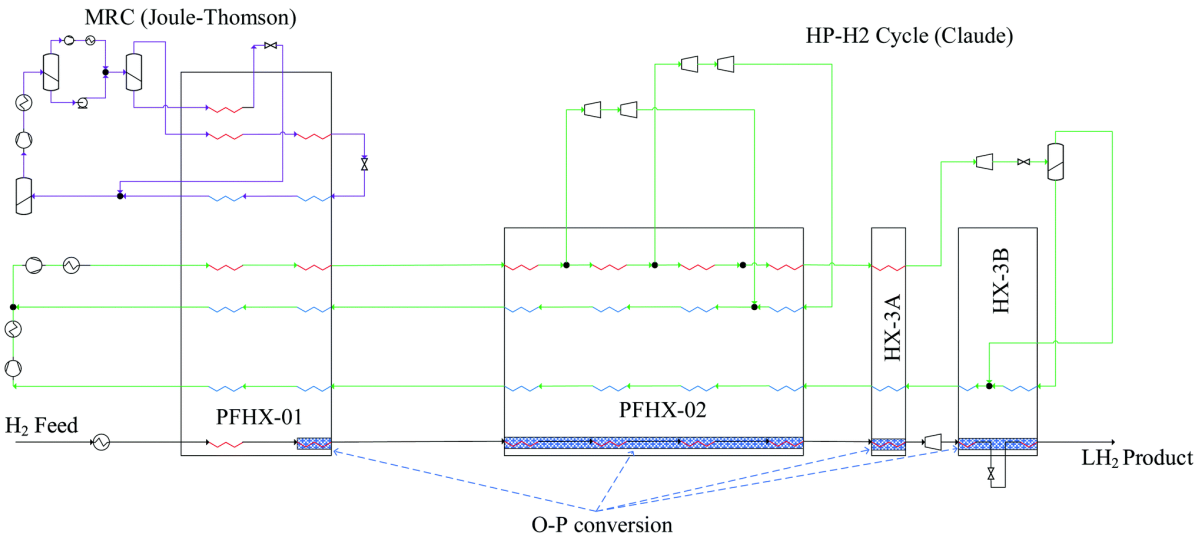

Figure 2.13: Schematic diagram for high pressure H_2 Claude cycle by Cardella et al.[g]

to 130 K. Four adiabatic converters promote ortho to para conversion in the temperature range of 130-85 K and continuously in catalyst-packed heat exchangers at lower temperatures (< 85 K). The reported SEC and FOM values of the system for hydrogen feed pressure of 20 bar are 6.7 kWh/kg_{LH_2} and 0.32, respectively. The IDEALHY Project also claims that heat integration with nearby LNG import and regasification terminals could significantly reduce the SEC to 0.62 kWh/kg_{LH_2}.[66] The SLC of the IDEALHY liquefaction concept is reported to be ≈ 1.93 US$/$kg_{LH_2}$.

Krasae-in[23] proposed a hydrogen liquefier system based on four cascaded hydrogen Joule-Brayton refrigeration cycles with precooling stage using MR of hydrogen, nitrogen, methane, ethane and butane. The conceptual plant capacity is 100 TPD. When the hydrogen pressure supply is 21 bar, the reported SEC and FOM values are 5.91 kWh/kg_{LH_2} and 0.391, respectively. Quack proposes a conceptual design of a 170 TPD hydrogen liquefier.[20] The system is based on propane precooling and helium-neon Joule-Brayton refrigeration cycles. With a hydrogen feed pressure of 1 bar, the reported SEC and FOM of Quack's model are 6.93 kWh/kg_{LH_2} and 0.32, respectively. However, there is a concern raised by NTNU-SINTEF that the high-efficiency value achieved by Quack's model is correct since their internal process simulation indicated that the configuration of the proposed propane refrigeration is impractical for low power consumption.[54] Additionally, the proposed helium-neon mixture has inferior refrigerant heat transfer properties compared to hydrogen, commonly found in today's hydrogen liquefaction plant.[54] Berstad et al.[67] modified the previous model to a more feasible concept by replacing one of the propane precooling stages with a single-stage ethane. The report also shows that a slight improvement in efficiency can be achieved by replacing the propane precooling system with a closed MR cycle with three-stage compression.[67]

Valenti & Macchi[25] developed a 864 TPD hydrogen liquefier process concept involving four cascaded Joule-Brayton refrigeration cycles using helium as the refrigerant. The reported SEC value of this liquefier concept is 5 kWh/kg_{LH_2}, corresponding to an exergy efficiency of approximately 48%. Nevertheless, achieving this idea is quite challenging and may not be feasible in the short term because it demands numerous compressor stages owing to the low molar mass of helium, resulting in increased capital expenses.[2] Additionally, this study assumed a relatively high hydrogen feed pressure of 60 bar, which would significantly enhance the efficiency performance of liquefier systems. It is important to note that performance comparison between hydrogen liquefaction processes should not be taken directly since such direct assessment will only favour models that assume higher H_2 feed pressure. Berstad et al.[68] devised a complete

[h] Reproduced from Hydrogen Liquefaction: A Review of the Fundamental Physics, Engineering Practice and Future Opportunities[2] with permission from the Royal Society of Chemistry.

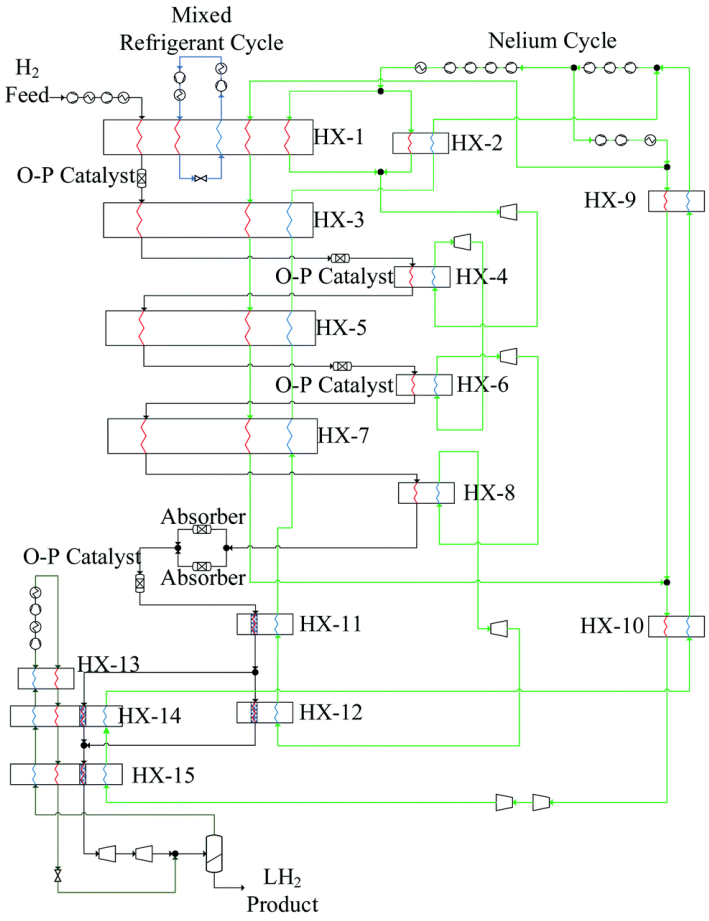

Figure 2.14: Schematic diagram for H_2 liquefier developed in the IDEALHY Project[h]

procedure for comparing multiple hydrogen liquefaction processes while considering variations in feed characteristics, generating a more consistent comparison result. To ensure a more reasonable comparison of all the built and conceptual hydrogen liquefaction processes discussed so far, Berstad et al.[68] recommended adhering to this comparison methodology.

2.3. Equipment for Hydrogen Liquefaction

This section will outline the critical equipment for hydrogen liquefaction and their respective roles in the overall process efficiency. The critical process equipment in industrial hydrogen liquefaction plants are:

- Heat exchangers,
- Compressors, and
- Turbine/turbo expanders

These components will be the main focus of the equipment design part of this thesis. Other essential equipments in hydrogen liquefier are the cryogenic coldbox and JT valve. Other standard equipment commonly found in industrial process plants, such as phase separators, pipes, valves, pumps, coolers, chillers, instrumentation, and measuring devices, are not covered in detail in this thesis.

2.3.1. Heat Exchangers

Heat exchangers are critical in any low-temperature liquefaction and refrigeration system. In industrial hydrogen liquefiers, aluminium plate-fin heat exchangers (PFHX) are widely used due to their versatility in terms of process channels and capacity, as well as providing a large surface area for exchanging heat with minimal internal temperature approaches and pressure drops while requiring comparatively minimal space and low capital expenditure.[18,22,39,69] Aluminium PFHX can be designed to withstand a maximum pressure of approximately 115-130 bar.[2,18,22] Figure 2.15 shows the schematic drawing of a brazed plate-fin heat exchanger. The warm and cold process streams through stacked passages, with up to 200 passages per stack.[18] The main hydrogen passages in the PFHX are often filled with catalyst particulates to promote the continuous and thermodynamically more efficient conversion of ortho- to para-hydrogen within the heat exchangers.[2] Hydrous ferric oxide, $Fe(OH)_3$, is the commonly used catalyst material for this application.[22,47] Figure 2.16 shows an illustration of the catalytic plate-fin heat exchanger.

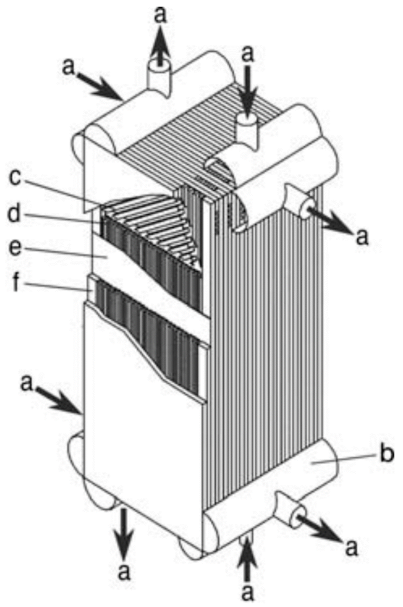

Figure 2.15: Schematic drawing of an brazed plate-fin heat exchanger. Courtesy of Linde AG;[i] a) Process streams; b) Header tank; c) Distribution fins; d) Corrugated heat-transfer fins; e) Partition plate; f) Side bars

According to Cardella,[22] PFHX can be designed to exchange heat between 8 different process streams. Based on the second law of thermodynamics, the temperature differences between streams should be minimized to achieve higher thermal efficiencies. Large and rapid temperature differences should be avoided to keep thermal and mechanical stresses below acceptable limits. Therefore, the temperature differences within the PFHX should be limited to below 30 K. Different types of fins of PFHX are available for heat transfer, which is chosen depending on the application. According to Donaubauer et al.[43], perforated fins are preferred to give an improved catalyst distribution in the reacting hydrogen stream passages. According to Linde AG, the practical fin height is between 4-10 mm while the fin thickness varies between approximately 0.2-0.6 mm.[22]

The irreversibilities associated with the cryogenic heat exchangers are significant to the overall exergy efficiency of the process plant. Ohlig and Decker[5,44] reported that the total exergy losses

[i] Reproduced with permission of John Wiley & Sons - Books, from Cryogenic Technology In: Ullmann's Encyclopedia of Industrial Chemistry,[33] Windmeier, Christoph & Barron, Randall F., Volume 22, 2013; permission conveyed through Copyright Clearance Center, Inc.

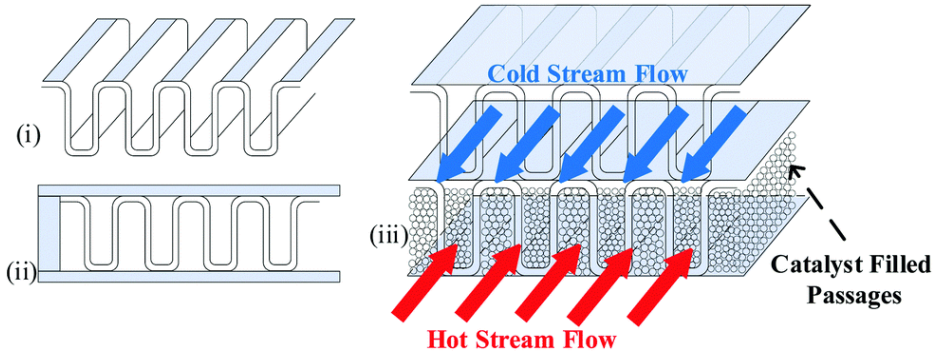

Figure 2.16: Schematic drawing of the (i) fins, (ii) empty channels and (iii) catalyst-filled PFHX[j]

in the heat exchangers could be up to 21.6% of the total exergy input to a typical hydrogen liquefaction process. More recently, Berstad et al.[21] calculated that the cryogenic heat exchangers contributed to approximately 21% of the total irreversibilities in conceptual liquefaction plant with a capacity of 125 TPD. Berstad et al. use the assumption of equilibrium conversion of ortho-para in the heat exchanger; thus, the exergy losses originated only from finite-temperature heat transfer and pressure loss. Skaugen et al.[70] used a more detailed mathematical modelling (non-equilibrium) approach for calculating the exergy losses in these PFHXs, and comparisons show that higher irreversibilities are generated in the heat exchangers.

Generally, increasing the size of the PFHX would provide more heat transfer surface area and volume, which would eventually result in a higher exergy efficiency and increase the capital expenditure of the plant. Although, the size of PFHX is also limited by the manufacturability of the equipment and other practical reasons, such as process design, number of streams, design pressure and available space inside the coldbox.[22] Linde A.G. reported the maximum geometrical dimensions for hydrogen liquefaction application is approximately 8.2 m x 3.4 m x 1.5 m, with a core volume of 15-30 m^3 and a specific surface of 500-2,000 m^2/m^3.[2]

Preliminary Design of Plate Fin Heat Exchangers

The general heat transfer equation between streams across heat exchanger is:[71]

$$\dot{Q} = U \cdot A \cdot \Delta T_{\mathrm{m}}. \tag{2.18}$$

In process simulation, the value of $\dot{Q}$ is determined by applying the first law energy balances, similar to Equation (2.8). On the other hand, the ΔT_{m} is typically evaluated from the composite curves of the cold and warm streams. Finally, the value of $U \cdot A$ is calculated accordingly.

For preliminary sizing of multi-stream aluminium PFHX, the total heat transfer surface area of the PFHX can be from $U \cdot A$ simulation value by assuming the overall heat transfer coefficient value.[22,72,73] The assumed heat transfer coefficients for the PFHX inside the hydrogen liquefier coldbox and the precooling coldbox are 0.1 kW/m^2 and 0.2 kW/m^2, respectively.[22,72] Thus, the total heat transfer surface area can be calculated as follows:

$$A_{\mathrm{hx}} = \frac{(U \cdot A)_{\mathrm{sim}}}{U_{\mathrm{hx}}}. \tag{2.19}$$

Similarly, the PFHX volume requirement can be estimated from the calculated heat transfer surface by assuming the value of the specific surface of the PFHX. According to Cardella,[22]

[j]Reproduced from Hydrogen Liquefaction: A Review of the Fundamental Physics, Engineering Practice and Future Opportunities[2] with permission from the Royal Society of Chemistry.

Häring[72] and ALPEMA[73] the specific surface of indutrial PFHX is approximately 500-700 m^2/m^3; thus:

$$V_{hx} = \frac{A_{hx}}{a_{s,hx}}. \tag{2.20}$$

Cardella[22] suggested that if the required PFHX volume is larger than the maximum feasible volume of PFHX, given in the design constraints, then multiple PFHX cores are assumed to be installed in parallel arrangement inside the coldbox. Due to size limitations of the coldbox, the number of parallel PFHX units should be restricted to a certain extent.[22]

Another option for performing the preliminary design of PFHX is to use commercial heat exchanger design software, such as ASPEN Exchanger Design and Rating (EDR)™ or HTRI Xchanger Suite®. These tools offer advanced thermal process design including sizing, checking/rating, and various rigorous simulations backed by applied research and data collected on industrial heat transfer equipment. In ASPEN EDR™ the *design* programme options for PFHX is capable of giving a quick preliminary design of the geometry and configuration as well as the thermal and hydraulic calculation of the equipment based on process data from the user. The software claims that the default software setups are appropriate for most cases. However, ASPEN EDR™ also stated that the design produced from this feature is a "first-shot" design. A full design can normally only be produced by a manufacturer, who will have proprietary performance data for specific fins, and will undertake full mechanical calculations and layer pattern definition, which are beyond the scope of a "first-shot" design.[k]

For the sizing and preliminary design of the catalyst-filled PFHX with ortho-para H_2 conversion, the kinetic PFHX model by Donaubauer et al.[43] has been used.[22] Donaubauer et al.[43] developed a steady-state one-dimensional pseudo-homogeneous continuum reactor model of the counterflow-cooled catalytic plate-fin heat exchanger, combining kinetics with heat, mass and momentum transfer correlations along with the state-of-the-art EOS. Donaubauer et al.[43] evaluated the first-order and Langmuir-Hinshelwood approach for ortho-para conversion kinetics over the hydrous ferric oxide ($Fe(OH)_3$) catalyst and found the former to be the most accurate kinetic model for this case. Therefore, the first-order kinetics, shown in Equation (2.15), is implemented in the PFHX model. The equation of state for n-H_2, o-H_2 and p-H_2 by Leachman et al.[49] in REFPROP[50] is used.

The sizing of the PFHX model by Donaubauer et al.[43] mainly refers to the geometrical dimensions of the aluminium PFHX by Linder AG, with several additional assumptions. As reported by Donaubauer et al.[43], the PFHX model can be used to calculate the temperature profiles of the hydrogen stream and refrigerant streams as well as the mole fraction of para-hydrogen as a function of the axial length of the PFHX. Cardella[22] utilized the kinetic PFHX model in the process modelling and equipment design of a large-scale hydrogen liquefaction process (100 TPD). The model is used to compute the outlet temperature, outlet pressure and the outlet mole fraction of p-H_2, as well as the necessary geometrical specifications of the PFHX due to the catalytic conversion of ortho- to para-hydrogen in the hydrogen feed stream flowing across the exchanger. Based on these results, the required $Fe(OH)_3$ catalyst volume can be determined.[22]

Recently, O'Neill et al.[45] expanded the kinetic modelling study of PFHX with ortho-para conversion kinetics of Donaubauer et al.[43] but with several distinctions: 1.) More precise analysis of the catalyst fraction; 2.) More comprehensive understanding of the reactor design by examining factors like alternative refrigerants (e.g. Helium/Neon) and reactor length; 3.) The simulation study investigates the impact of various modelling parameters on reactor design to determine the relative influence of conversion kinetics versus heat transfer. O'Neill et al.[45] also adjusted the a and b first-order rate constants in Equation (2.16) (from the original values by Donaubauer et al.[43]) to take into account the space-velocity and catalyst fraction. Based on their simulations, O'neill et al.[45] discovered that the pressure drop of the hydrogen stream across

[k] As mentioned in ASPEN EDR™ V12 software *Help* pages

the catalyst-filled channels is insignificant due to the low velocity and viscosity of the reacting hydrogen. Moreover, the outlet para-hydrogen fraction is greatly more sensitive to changes in kinetic-related parameters than the alterations in the cold-side heat transfer coefficient, indicating that conversion kinetics are the limiting factor of the outlet hydrogen composition.

2.3.2. Compressors

Compressors are crucial for the optimization of scale-up hydrogen liquefaction plants. Feed compression and compression required in the refrigeration cycle account for over 90% of overall power consumption.[2,22,59] Higher feed pressure can reduce the work needed in the liquefaction system; although, the maximum allowable pressure in the heat exchanger often limits them.[2,74] Typically, hydrogen is delivered at a pressure above 15 bar from SMR and electrolysis plants.[2] Additionally, Berstad et al.[21] reported that the compression system, which comprises compressors and intercoolers, contributes to a large portion of the exergy losses in a conceptual hydrogen Claude cycle liquefier. Due to the significant contribution of irreversibilities, the performance of compressors significantly affects the plant's operating expenses.[59] However, higher compression performance also demands higher capital cost. A custom-made compression system can easily account for up to 50% of the total expenses for equipment investment.[59]

The efficiency of the compressor greatly influences the exergy efficiency of the hydrogen liquefaction process. The compressor's isentropic efficiency is determined by its type, capacity, and design. Electric motors are commonly used to drive compressors in hydrogen liquefiers, with mechanical efficiencies up to 0.96. On the other hand, electrical efficiencies up to 0.97 can be achieved when using large motors.[22]

The selection of compressor varieties is limited to the highest attainable capability.[22] Figure 2.17 shows the type and application conditions of compressors that are commonly found in process industry. Generally found in built liquefiers are the reciprocating piston and rotary screw compressors.[22,44] In conceptual hydrogen liquefactions, reciprocating piston and turbo/centrifugal compressors have been widely considered.[2,34] Oil-injected rotary screw compressors require relatively lower CAPEX; however, the efficiencies of these machines are low (η_{is} = 0.65-0.75) have not seen significant improvements over time.[22,44] Hence, to this day, the use of rotary screw compressors are limited to small-scale hydrogen liquefaction plant (< 3 TPD).[5] For this reason, rotary screw compressors will not be considered in developing the large-scale hydrogen liquefaction process in this thesis.

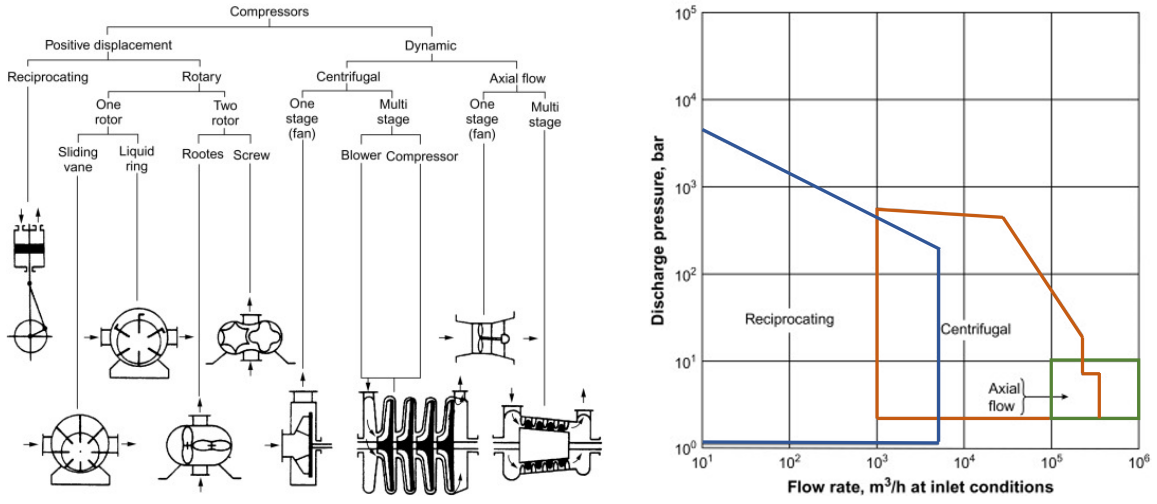

(a) Type of compressors

(b) Compressors operating ranges

Figure 2.17: Type and operating range of compressors commonly found in process industry[l]

Reciprocating piston compressors are state-of-the-art for compressing hydrogen gas streams in industrial hydrogen liquefiers.[22,59] The advantages of reciprocating piston compressors are the relatively high efficiency range (η_{is} = 0.75-0.92) and high compression ratio that is feasible per stage, even for fluids with low molar mass such as hydrogen.[22]. It also offers high design flexibility, as these machines can be designed in many different configurations and orientations.[34,76] However, reciprocating compressors have relatively high maintenance demands and most cannot meet the minimum requirement of continuous, uninterrupted operation for two years. Therefore, if the required flow is sufficient for a centrifugal compressor, or if the necessary head is not so high that it would not require an excessive number of stages, a centrifugal compressor is typically preferred.[77] As discussed in later chapters (3 and 4) of this thesis, the operational parameters of the studied hydrogen liquefaction plant lean towards the conditions suitable for centrifugal compressors. Hence, the selection and preliminary design of compression equipment in this thesis will primarily focus centrifugal compressors.

Turbo compressors are the most efficient compressor type available on the market[59] and generally offer greater throughput than piston compressors; therefore, they are better suited for large-scale applications.[2,22] Turbo compressors can be classified into two main types: centrifugal (also known as radial-flow) and axial-flow turbo compressors. When handling large-volume flow, axial compressors are more efficient than centrifugal compressors, as seen in Figure 2.18; however, the centrifugal compressors are more reliable, less vulnerable to fouling and have wider operating ranges.[77] Additionally, axial-flow types usually require higher CAPEX than centrifugal types, although may be justified based on smaller diametral size and efficiency at a high volumetric rate.[77]

Despite of their advantages, hydrogen's low molar mass makes its compression challenging in a turbo compressor.[78–86] Light gases possess high specific heat values, leading to reduced compression ratios. To attained a higher pressure ratio, the enthalpy difference across the compressor, referred to as "head", needs to be increased; thereby, demanding increased power input. Increasing the head can be achieved through various methods. The first approach involves increasing the impeller tip velocity by operating the compressor at a higher rotational speed or by utilizing a larger impeller diameter. While other common process gases' tip velocities are typically constrained by Mach numbers, the high speed of sound in hydrogen eliminates this constraint.[82] Nonetheless, the limiting factors for hydrogen compression are presently the mechanical strength and stress levels of the impeller, which cap the attainable tip velocity.[80–82] Moreover, the selection of compressor materials with higher strength for hydrogen compression is further restricted by hydrogen embrittlement, a phenomenon wherein ferrous alloy materials lose ductility due to the penetration of H_2.[78,81] State-of-the-art industrial centrifugal compressors can have a maximum impeller wheel tip velocity of about 400-500 m/s.[22]

An alternative method to increase the head involves adding more compressor stages. However, due to rotordynamics reasons, there are finite limits to the shaft length of the centrifugal compressor, which generally restrict the number of stages to around 10-12 per casing.[80–82] Moreover, a substantial increase in the number of turbo compressor stages would result in higher CAPEX.[87] Pressure ratios per compression stage of 1.1 are typical in hydrogen applications.[80,82] Recent research projects[88–92] focusing on advanced high-speed centrifugal compressors using high-strength titanium-based alloys have facilitated for higher wheel tip velocity, up to 701.04 m/s,[88] with a higher compression ratio of up to 1.45 per stage[83,84] However, to the best of the author's knowledge, these advancements in hydrogen radial compressors are primarily within the research realm, with their integration into industry applications yet to be realised.

Other progressions in centrifugal compressors have presented the process industry with multi-shaft integrally-geared centrifugal compressors.[22] Single-shaft multi-stage turbo compressors op-

[l] Reprinted from Chemical Engineering Design (Second Edition), Gavin Towler, Ray Sinnott, Chapter 20 - Transport and Storage of Fluids,[75] 1207-1265, Copyright 2013, with permission from Elsevier

[m] Reprinted from Chemical Engineering Design (Second Edition), Gavin Towler, Ray Sinnott, Chapter 20 - Transport and Storage of Fluids,[75] 1207-1265, Copyright 2013, with permission from Elsevier

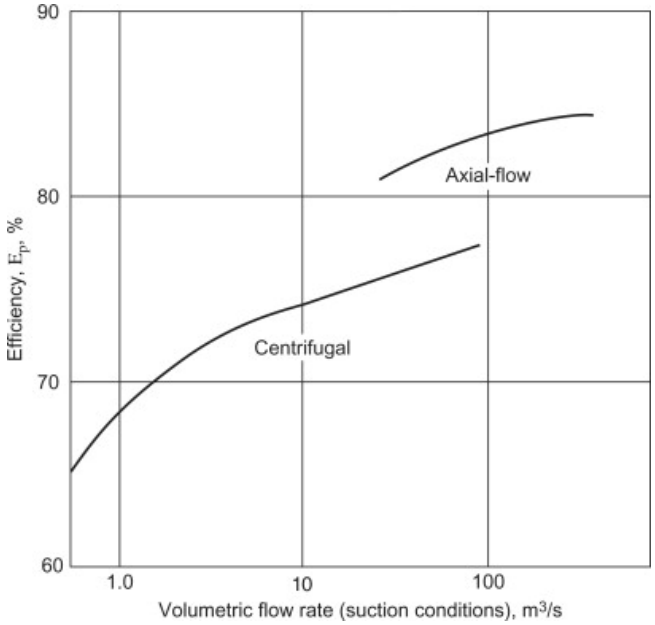

Figure 2.18: Approximate polytropic efficiencies of turbo-compressors[m]

erate at a fixed rotational speed, whereas integrally-geared centrifugal compressors can optimize each impeller wheel (stage) speed, resulting in greater efficiency. Integrally-geared turbo compressors are attractive for industrial cryogenic refrigeration processes because they offer high efficiency and low capital expenses for the necessary compressor capacity.[22] According to MAN ES,[22] these types of compressors are typically limited to a maximum of 8-10 impeller stages. Additionally, the impeller wheel diameter ranges between 0.1-1.5 m, with a maximum rotational speed of 50,000 rpm.

According to Bahadori,[77], multi-stage centrifugal compressors are usually considered for inlet volumes between 850-340,000 m^3/h. Multi-stage compressors need to rely on interstage cooling when the temperature of the gas at the compressor inlet and the desired compression ratio are such that the gas discharge temperature reaches approximately 150°C.[77] According to performance calculations, the head and power of the compressor are directly related to the absolute gas temperature at each impeller.

Ensuring effective sealing (and safety) systems becomes particularly crucial for hydrogen compressors, given hydrogen's low autoignition temperature and wide flammability range. Adequate sealing mechanicsm is also important in any systems in order minimize make-up feed due to continuous leakage loss of the working fluid through the compressor. According to Cardella,[22,65] Carbon ring seals are often used for nitrogen turbo compressors with relatively high loss rates. Dry gas seals can minimize the loss of compressor refrigerant leakage, but require a higher CAPEX. Hermetically-sealed compressors can be used with a much higher initial investment to achieve near-zero losses during operation. Furthermore, hermetically-sealed compressors are currently limited to applications with low maximum feasible capacity and power efficiency.[22,65]

Turbo Compressors Selection Process

The design procedure of turbo compressors has been described extensively in the literature.[76,77,93] A specific book entitled *Turbomachinery: Fundamentals, Selection and Preliminary Design* authored by Gambini and Vellini,[94,95] offers a comprehensive approach to the selection process and preliminary design procedure of turbomachinery. The selection process,[94] as well as the consequent preliminary design of turbo compressor,[95] that are described in this book relies on the simili-

tude theory. Similitude theory enables the knowledge gained from a previously built machine to be applied to a new, similar machine. This theory allows using previous experience in the turbomachinery field to design a new turbomachine with greater efficiency.

The selection procedure follows the fundamental but effective, Baljé's method.[96,97] The method is based on statistical diagrams of turbomachine efficiency as a function of two dimensionless parameters obtained from examining many turbomachines.[94] Baljés expressed the efficiency as a function of specific speed and specific diameter, which are defined as follows:

$$\omega_s = \omega \frac{\dot{V}^{1/2}}{\dot{W}^{3/4}}, \tag{2.21}$$

and

$$D_s = D \frac{\dot{W}^{1/4}}{\dot{V}^{1/2}}. \tag{2.22}$$

For compressor, work W, in the above expressions, is the isentropic enthalpy increase in the stage; the volumetric flow rate V is referred to the stage inlet; the diameter D is the rotor external diameter (outlet diameter for radial impellers); the efficiency is the isentropic efficiency of the stage. Note that the specific speed is indicative of the shape and not of the size of a turbomachine; different-sized turbomachines, having the same specific speed, are in the same shape (for example: axial, radial, mixed flow). On the other hand, the specific diameter takes into account the size of a turbomachine. Baljé diagram for turbocompressors are shown in Figure 2.19a and 2.19b. As illustrated, the Baljé method allows for identifying the type of turbocompressors stages for a specific application.

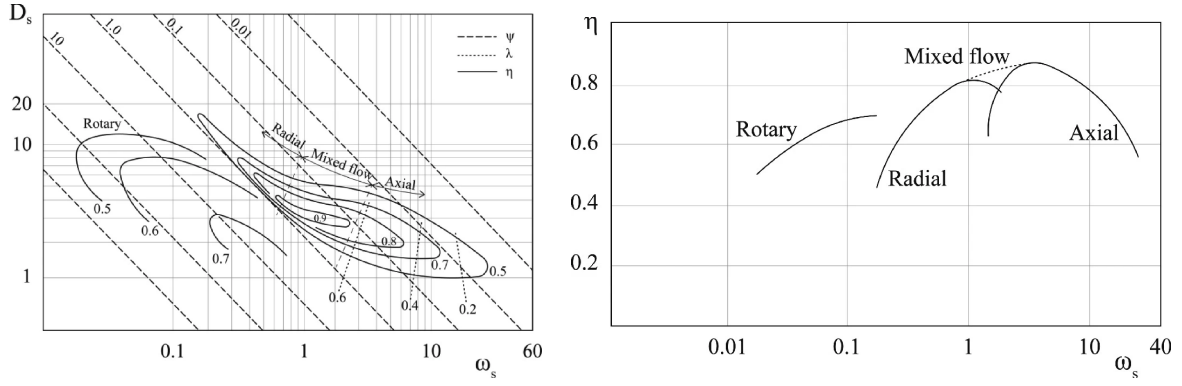

(a) Baljès diagram

(b) Variation of efficiency with specific speed

Figure 2.19: Compressors Baljès diagram[n]

Besides selecting the type of turbo compressors, this selection procedure implies the preliminary evaluation of specific speed and the number of compressor stages required, assuming the specific application provides the following information:

- Type of fluid
- Mass flow rate (kg/s)
- Inlet temperature (°C)
- Inlet pressure (bar)
- Outlet pressure (bar)

With these parameters, determining the isentropic enthalpy change across compressors is straightforward. If the reversible stage work is assumed to be the same at all stages of the compressor, then the specific speed can be expressed as:

[n]Reproduced with permission from Springer Nature, from Turbomachinery Selection In: Turbomachinery Fundamentals, Selection and Preliminary Design,[94] Marco Gambini and Michela Vellini, 2021; permission conveyed through Copyright Clearance Center, Inc.

$$\omega_s = \omega \frac{\dot{V}^{1/2}}{\dot{W}^{3/4}} = \frac{2\pi n}{60} \frac{\dot{V}^{1/2}}{(\Delta h_{is}/z)^{3/4}}. \tag{2.23}$$

Where n is the rotational speed in RPM and z is the total number of stages. It is therefore:

$$\omega_s = f(n, z). \tag{2.24}$$

For compressors, this implies that the stage-specific speed decreases from the first to the last stage since the fluid volumetric flow rate varies between the turbomachinery inlet and outlet. Since pressures and temperatures in the downstream stages of compressors can be calculated using $\Delta h_{is}/z$, the volumetric flow rates at the inlet of each stage can be determined.

Equation (2.23) enables the plotting of the specific speed as a function of z for any rotational speed, providing a straightforward means of analysis. In the book, Gambini & Vellini[94] refer to them as the *basic diagram for $n-z$ selection*. An example of compressor $n-z$ selection diagram is shown in Figure 2.20. These diagrams allow us to choose a range of rotational speed ($n_{min} < n < n_{max}$) and the number of stages ($z_{min} < z < z_{max}$), to ensure a suitable specific speed for attaining maximum efficiency and optimum dimensions of the compressor, with considering possible constraints that were mentioned in the previous section.

Once n, z, and thus ω_s are selected, the optimum value for D_s can be determined using Baljé's or Cordier's[93] other empirical correlation. Finally, the rotor's external diameter can be evaluated as follows:

$$D = D_s \frac{\dot{V}^{1/2}}{(\Delta h_{is,stg})^{1/4}}. \tag{2.25}$$

The impeller tip velocity (also referred to as the blade speed) corresponding to the diameter is thus:

$$u = \frac{\pi n}{60} D. \tag{2.26}$$

The blade speed values, u, play a crucial role in the compressors selection process, as specific limits must be obeyed.

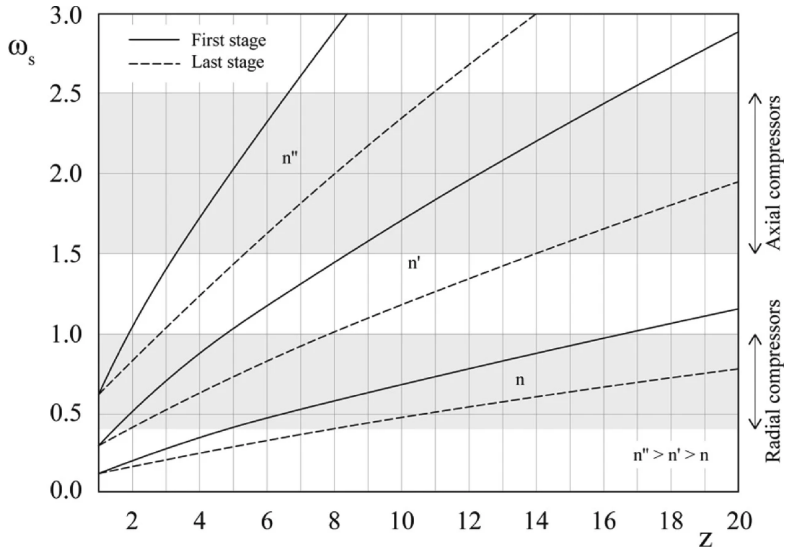

Figure 2.20: Basic diagram for compressor n-z selection[o]

[o]Reproduced with permission from Springer Nature, from Turbomachinery Selection In: Turbomachinery Fundamentals, Selection and Preliminary Design,[94] Marco Gambini and Michela Vellini, 2021; permission conveyed through Copyright Clearance Center, Inc.

Centrifugal Compressor Preliminary Design

As mentioned previously, the operational parameters of the hydrogen liquefaction system studied in this thesis lean towards the conditions suitable for centrifugal compressors. Hence, the preliminary design of the compression equipment that will be discussed in this thesis will be only for centrifugal compressors. Once centrifugal compressors have been selected, along with the selected preliminary rotational speed and number of stages, the kinetic, thermodynamic, and geometric parameters, as well as the stage efficiencies of the compressors, can be evaluated by following the preliminary design procedure described by Gambini & Vellini[95].

The preliminary design procedure proposed by Gambini & Vellini[95] is an iterative calculation. The conceptual framework of this procedure is summarised into two block diagrams for the stage and multistage calculations shown in Figure 2.21a and Figure 2.21b, respectively. The calculations in each step of this procedure are highly detailed and many fall outside the preliminary design scope required for this thesis. Therefore, this thesis introduces a new and simpler approach building upon the calculations provided by Gambini & Vellini[95], though it is less accurate. The details of this approach are outlined in Chapter 4.

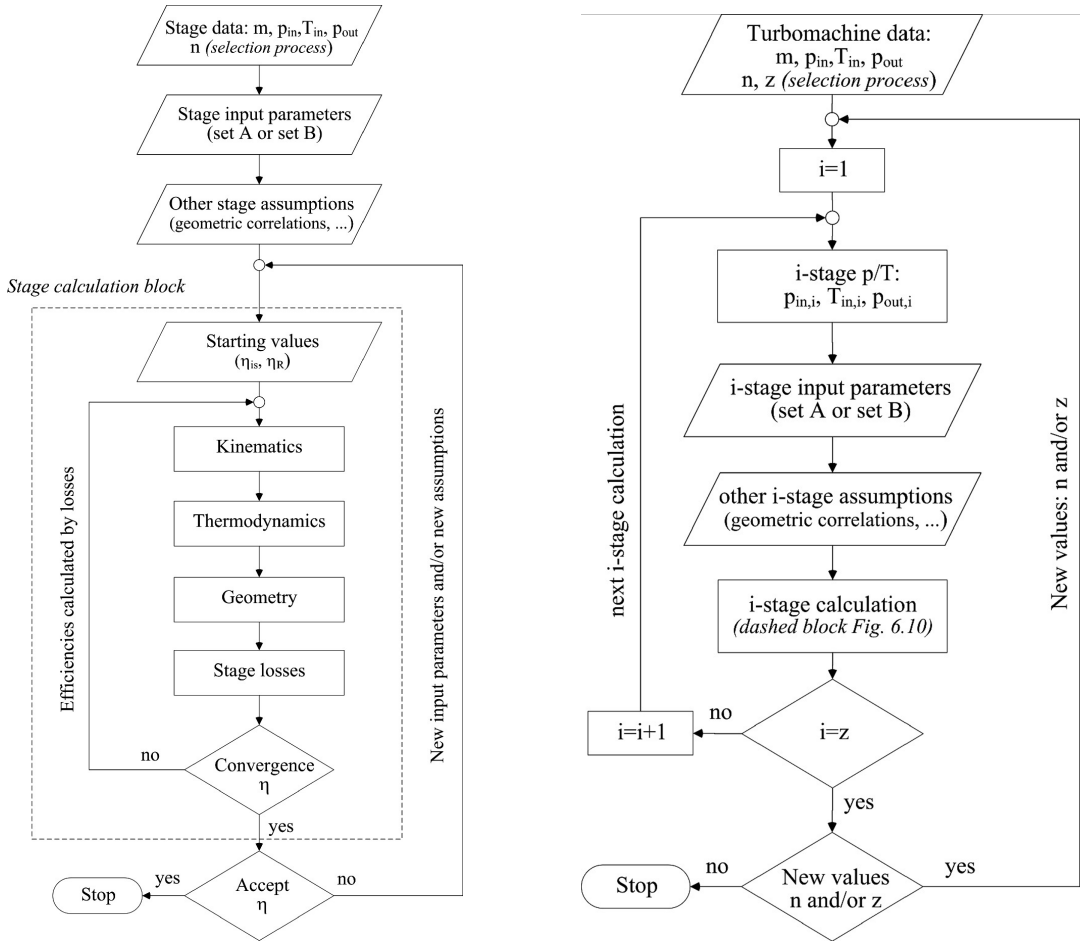

(a) Stage calculation block diagram

(b) Multistage compressor calculation block diagram

Figure 2.21: Framework of the iterative procedure for centrifugal compressor preliminary design[p]

[p] Reproduced with permission from Springer Nature, from Preliminary Design of Centrifugal Compressors In: Turbomachinery Fundamentals, Selection and Preliminary Design,[95] Marco Gambini and Michela Vellini, 2021; permission conveyed through Copyright Clearance Center, Inc.

2.3.3. Turbine/Turbo Expanders

Expansion turbines, or turbo expanders, achieve greater cooling through isentropic expansion compared to the Joule-Thomson valve's throttling effect. However, turbines require a higher initial investment.[2] Consequently, the utilization of turbine expanders increase the FOM of the liquefier significantly when the mechanical energy from the rotation of the turbine is recovered.[2] Berstad et al.[21] reported that for large-scale liquefier plants, recovering 80% of the power from the turbines for compression, could reduce the SEC by up to 7%. Due to the additional CAPEX, energy recovery is only economically attractive for large turbines ($>$ 100 kW) when the electricity cost is high.[22,98] Without turbine power recovery, turbine power dissipation is typically achieved through a braking system, such as air or oil brake.[99] This is the current system employed in existing hydrogen liquefiers.[5,22] Nonetheless, implementing turbine power recovery is feasible within a medium-term timeframe, but several technical challenges must be addressed.[22]

In turbo expander design, the important parameters are the isentropic enthalpy drop across the expander and the volume flow rate at the expander discharge, which determine the rotor speed and wheel flow area, respectively. Within stress and mechanical limits, these two determine the configuration of the hydraulic channel and, thus, the expander efficiency.[98] As reported in the literature, the isentropic efficiency of cryogenic expanders is in the range of 80-90%.[2]

The limitations in state-of-the-art turbo expander capacity posed a significant challenge in the up-scaling of hydrogen liquefaction systems.[22] The capacity requirement of cryogenic turbines governs the suitable bearing systems that can be implemented. Cryogenic turbo expanders employ oil or gas-bearing systems in state-of-the-art industrial hydrogen liquefiers.[22,100] According to Bischoff et al.,[100] oil-bearing technology is a well-established and proven technology in the liquefaction industry. However, this approach has some drawbacks, including losses due to sealing gas taken from the process line, higher investments, and extensive maintenance requirements for the complex oil supply system. Gas-bearing systems are further categorized into static and dynamic types. The main difference is the requirement of an external supply of process gas to the bearing in the former,[22,100] with 2-5% lower efficiency compare to dynamic gas-bearing turbines.[5] Figure 2.22 shows a schematic drawing of the state-of-the-art expansion turbine bearing systems used in industrial helium and hydrogen liquefiers.

Dynamic gas bearing turbine, previously restricted to helium applications, has been effectively adapted to hydrogen application in Linde-Leuna H_2 liquefier.[5,100,101] Some advantages

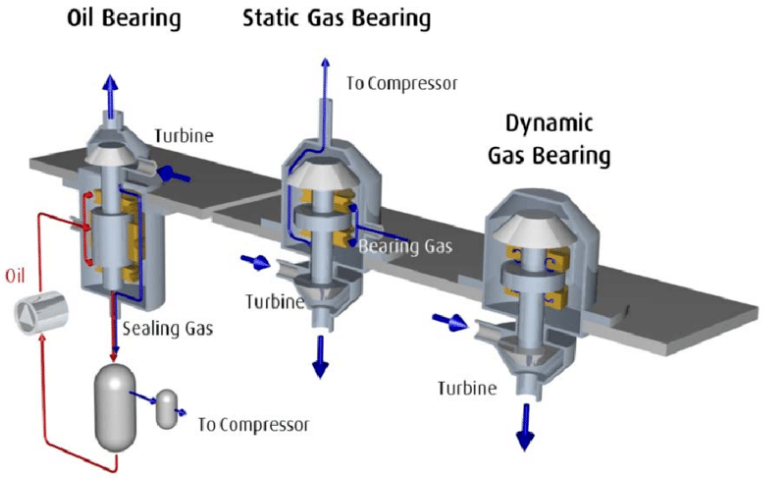

Figure 2.22: Bearing technologies for expansion turbines[q]

[q]Reprinted from The Latest Developments and Outlook for Hydrogen Liquefaction Technology In: AIP Conference Proceedings, K. Ohlig and L. Decker,[5] with the permission of AIP Publishing; permission conveyed through Copyright Clearance Center, Inc.

of dynamic gas-bearing turbines are their high efficiency, elimination of oil systems, and high reliability.[101] In addition to its compact design, the dynamic gas-bearing turbine promises to reduce total expenditures of hydrogen liquefaction systems.[101] However, the maximum installed capacity of dynamic gas bearing turbines is less than 50 kW,[22,100] which is much smaller than the power capacity that would be required for future up-scaling of hydrogen liquefiers.[22]

For large-scale applications, oil and magnetic bearing turbines are often employed in industrial cryogenic processes, with turbine power of up to several megawatts. These turbines can have impeller wheel diameters greater than 1 m.[22,99] However, more extensive versions of these large turbines are not yet proven for extreme cryogenic applications, such as hydrogen liquefaction.[22] Moreover, magnetic bearing turbines require high capital, and adding a permanent magnet is heavy and prone to hydrogen embrittlement that requires careful treatment.[59] For small power turbine, less than 1 kW, cryogenic static gas bearing turbine can be manufactured with impeller wheel diameters less than 0.02 m.[22,100]

Apart from bearing and brake systems, turbo expanders can be further distinguished by the type of fluid phase in the outlet stream of the turbine: single-phase (dry) expanders or two-phase (wet and dense fluid) expanders. According to Bloch & Soares[99], the design of two-phase turbo expanders would need special adjustment to avoid droplets interfering with turbine performance and eroding the blades. There are a significant amount of effective turbo expanders that are currently in operation involving condensing streams in the industry.[99]

In most present air separation and petrochemical process specifications, turbo expanders are generally radial reaction turbine because this geometry is often the most efficient.[99,102] Compared to axial flow expanders, they experience lower stresses at a given tip speed, allowing them to operate at a higher rotational speed, resulting in higher efficiencies.[102] Axial turbines may have higher efficiency at high Reynolds number ($Re > 10^6$), but they require a higher capital cost.[2] Radial in-flow turbines, also termed centrifugal turbines, are highly reliable and require low maintenance.[59] Since centrifugal turbines are proven to be ideal for cryogenic turbo expanders, this thesis exclusively consider centrifugal turbines as the expansion-with-work equipment essential in the hydrogen liquefaction investigated in this thesis.

Turbo Expanders Selection Process

The design procedure of turbo expanders, particularly radial in-flow turbines, has been described in the literature.[93,99,103] Like compressors, Gambini & Vellini[94,104] in their book *Turbomachinery: Fundamentals, Selection and Preliminary Design* present a comprehensive procedure for the selection and preliminary design of axial and radial turbines.

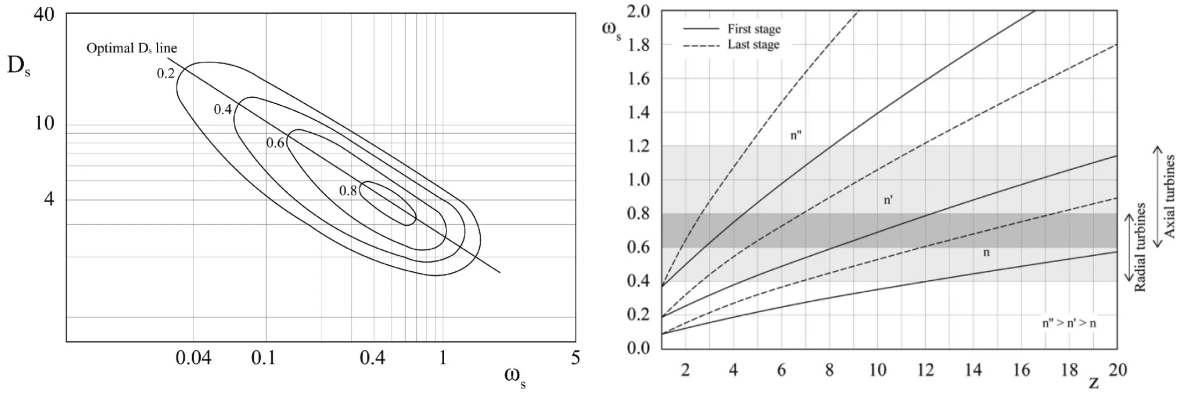

(a) Radial turbines Baljès diagram

(b) n-z selection diagram

Figure 2.23: Turbines Baljès diagram and n-z selection diagram[r]

The selection process for turbines is almost the same as for compressors. However, the work, W, in the expressions of ω_s and D_s (in Equation (2.21) and (2.22), respectively) refers to the reversible work, i.e., the isentropic enthalpy drop in the stage of the turbine; the volumetric flow rate, V, refers to the stage outlet; and the diameter, D, is the external diameter of the rotor (inlet diameter of radial turbines). An example of Baljé diagram for radial turbines is shown in Figure 2.23a. An example of a basic $n-z$ selection diagram of turbines is shown in Figure 2.23b.

Similar to turbo compressors, preliminary information can be gathered about the rotational speed range, the number of stages, the external diameter and the speed of the blade during the selection process. However, it should be noted that these initial findings remain subject to potential readjustment throughout the preliminary design phase. As in turbo compressors, the preliminary design procedure for turbines given by Gambini & Vellini[104] consists of thorough iterative calculations, with a comprehensive framework that follows the same structure shown in Figure 2.21.

Many of these calculations extend beyond the scope of the equipment preliminary design necessary for this thesis. Therefore, a new and simpler procedure is developed based on the calculations provided by Gambini & Vellini,[104] as will be elaborated upon in Chapter 4. While this method might not offer the same level of comprehensiveness as the detailed guidelines provided in the reference literature,[104] it effectively serves its intended purpose within the context of this thesis.

2.3.4. Cryogenic adsorbers

Prior to entering the liquefaction plant, the hydrogen feed coming from either electrolysis or steam reforming plant typically achieves purity of above 99.50-99.99%, with ≤ 10-100 ppm of residual impurities.[21,44] The concentration of these impurities like nitrogen, methane, argon, and carbon monoxide must be reduced to approximately below 1 ppm since these elements will condense and solidify during the liquefaction process, potentially blocking or damaging the machinery.[22,44] Consequently, additional adsorber vessels are usually required and installed in the downstream of the precooling system at (typically at liquid nitrogen temperature, T ≈ 80K).[22,44] Henceforth in this thesis, this asdsorber will be refered as "cryogenic adsorbers".

According to Haüssinger,[105] temperature-swing adsorber (TSA), also termed thermal-swing,[106] is applied as the cryogenic adsober in hydrogen liquefaction. The adsorber vessels are typically filled with charcoal or molecular sieve adsorbent material.[22,105] The regeneration is done with pure hydrogen from the recycle gas at ambient temperature.[105] The adsorption vessels are installed in parallel configuration and usually switched alternately.[22,105] While one adsorber is adsorbing, the other is either being regenerated or kept ready. This switching occurs in a specific order, with the adsorption time intentionally set shorter than the calculated time for impurity breakthrough. The usual cycle durations for these procedures span from a few hours to multiple days.[105] Cardella et al.[65] noted that the total number and size of adsorber vessels that can be installed are restricted by the space within the hydrogen liquefier coldbox.

The design complexity of fixed-bed adsorption systems is significant, and unlike various other processes, it cannot be directly calculated through process simulation. Campbell has provided simple manual calculations applicable for preliminary designs, scoping studies and troubleshooting.[106] As per Campbell's guidelines, the initial steps of adsorption system sizing involve defining the design basis (including factors such as feed gas flow rate, composition, and product gas water content) and specifying parameters like the number of towers, type and size of adsorbents, flow direction, and cycle times for each tower. These two steps are usually performed by the end-user of the adsorbers system.[106] Next, the diameters of the adsorber vessels need to

[r] Reproduced with permission from Springer Nature, from Preliminary Design of Centrifugal Compressors In: Turbomachinery Fundamentals, Selection and Preliminary Design,[95] Marco Gambini and Michela Vellini, 2021; permission conveyed through Copyright Clearance Center, Inc.

be estimated, which is set by the superficial gas velocity and allowable pressure drop. The last sizing step is to estimate the height of the bed and the adsorber vessel, along with the expected initial gas pressure drop through the bed. The complete procedure and equations for these steps are described in the literature.[106]

Following the preliminary sizing steps, Campbell also provided a guided procedure to determine the regeneration process, which is the a function of step times, the source of regeneration gas and type of adsorbent used, based on insulation type, gas composition, heating and cooling temperatures, pressures as well as flow directions.[106] This step determines the required heating and cooling of the vessels during the regeneration process. Due to the limited scope of this thesis, this part of the adsorber design will not be covered in this study.

2.3.5. Coldbox

Equipment operating at cryogenic conditions must be placed inside one or multiple cryogenic coldbox vessels to minimize heat leaking into the cryogenic equipment.[2] Coldboxes for hydrogen liquefaction can be cylindrical or rectangular vessels erected in a horizontal or vertical configuration, although the latter is more often applied.[22] The precooling system of hydrogen liquefiers is usually stored in a precooling coldbox which is typically insulated with perlite material as in an air separation unit (ASU).[22,98]

Cryogenic coldbox, on the other hand, is typically a vacuum-insulated coldbox vessel with multilayer superinsulation (MLI).[22,29] Vacum-insulated coldboxes are usually pre-fabricated offsite and transported to the construction site;[98] thus, the feasible transportation weight and size limits of coldboxes should be considered as a constraint for conceptual designs of large-scale liquefiers.[22] According to IDEALHY report, the typical restrictions for coldbox within Europe are approximately 4.2 m for road transport and 5.5 m for waterway transport.[59] According to Cardella, the maximum length of pre-fabricated cryogenic coldbox are between 20-40 m.[22]

Air liquide reported their HYLIAL hydrogen liquefiers of 600, 800 and 1,500 L/h liquefaction capacities to have dimensions of (8.1×4.8×5.5), (8.1×4.8×5.5) and (9×4.5×5.5) metres, respectively (with gangway included in the first two liquefiers dimensions).[107] KHI has showcased their 5 TPD demonstration plant, featuring a coldbox measuring four metres in diameter and standing at a height of 12 metres.[56] To enhance insulation efficiency and minimise the amount of radiant heat that could affect heat exchangers and piping systems, KHI cover all components inside their coldbox with a type of metallic, super-insulation sheets similar to those used for satellites and spacesuits.[56] Chart industries offers standardised hydrogen liquefaction plant design with liquefaction capacities of 5, 9, 12, 15 and 30 TPD.[55] Notably, their 10 TPD liquefier has dimensions of 3.048 metres in diameter and 12.192 metres in height. Coldbox size information for other hydrogen liquefiers has not yet been found in the literature.

2.4. Process Economics

One of the main objectives of process economics evaluation is to calculate and evaluate the specific liquefaction cost (SLC) during the development of the large-scale hydrogen liquefaction concept. The SLC represent the total costs of ownership of the hydrogen liquefaction plant and can be easily used to perform cost-benefit analyses and further hydrogen supply chain assessment.[22] The SLC of existing hydrogen liquefaction plants is between 2.5 and 3.0 US\$/kg_{LH_2}.[2,22] Recent studies have shown that large-scale hydrogen liquefiers should be able to attain an SLC of less than 1 US\$/kg_{LH_2} without requiring novel technologies.[2]

As shown in Equation (2.17), to determine the cost of liquefaction for the facility, it is necessary to take into account both the capital expenditure (CAPEX) and operating expenditure

(OPEX). The following sections will briefly explain both terms and associated cost estimation models found in the literature.

2.4.1. Capital Expenditure

Capital expenditure (CAPEX), also referred to as capital expenses or fixed capital investment, is the complete expense incurred in designing, constructing and installing a plant and the necessary modifications to prepare the plant site. Numerous scientific literature[108–112] offer methodologies, correlations, and models to facilitate the estimation of "Class 4" capital costs. "Class 4" cost estimates, according to the Association for the Advancement of Cost Estimating International (AACE International), are the preliminary estimates ("approximate","study","feasibility"), with an accuracy of ± 30% which are typically used to make comparisons between design alternatives.[108] These estimates rely on limited cost information and preliminary design results, details which are in line with the scope of this thesis.

According to Towler & Sinnot,[108] CAPEX consists of the following costs:

- The inside battery limits (ISBL) investment – The cost of the plant comprises the direct and indirect field costs. The **direct field costs** include: 1.) Costs of major process equipment, such as reactors, heat exchangers, compressors, et cetera; 2.) Bulk items, such as piping, catalysts, instruments, et cetera; 3.) Civil works; and 4.) Installation labor and supervision. The **indirect field costs** include: 1.) Construction costs such as construction equipment, temporary construction, water, power, et cetera; 2.) Field expenses and services; 3.) Insurance; 4.) Labour benefits and burdens; and 5.) Miscellaneous overhead items, including agent's fees, legal costs, import duties, et cetera.
- Offsite costs or outside battery limits (OSBL) investment – The cost of additions or modifications that must be made to the site infrastructure to accommodate adding a new plant. This may include power generation plants, cooling towers, workshop and maintenance facilities, air separation plants to provide site nitrogen (inert gas), et cetera.
- Engineering costs – Sometimes referred to as the home office costs or contractor charges, it is the expenses associated with detailed design and other engineering services necessary for project execution. This comprises of 1.) Detailed engineering of process equipment, piping system, et cetera; 2.) Procurement of main plant items and bulks; 3.) Construction supervision and services; 4.) Administrative charges such as project management, inspection, et cetera; 5.) Bonding; and 6.) Contractor's profit
- Contingency charges – Additional expenses incorporated into the project budget to accommodate any discrepancies or deviations from the estimated cost.

In accordance with Towler & Sinnot,[108] offsite costs are typically estimated as a percentage of ISBL costs during the early design phase, usually ranging from 10% to 100% depending on the project scope and its impact on-site infrastructure. For petrochemical projects, offsite costs typically fall between 20% and 50% of ISBL cost, with an initial estimate of 40% if site details are unknown. Established sites, like in "brownfield" projects with well-developed infrastructure, generally have lower offsite costs. Alternatively, completely new areas, such as in "greenfield" projects, will likely experience higher offsite costs.

A rule of thumb for estimating engineering costs is 30% of ISBL plus OSBL costs for relatively smaller projects and 10% of ISBL plus OSBL costs for larger projects.[108] On the other hand, the contingency charge should be at least 10% of ISBL plus OSBL costs for any projects. If the plant's technological readiness is low, higher contingency charges should be used. In this case, contingency costs can be as high as 50% of ISBL plus OSBL costs.[108]

In addition to the fixed capital investments, the working capital expenditure must also be considered. Working capital is the additional money needed to start the plant up and run it until it starts earning income,[108] or simply the cost for the commissioning and start-up of the plant.[22] This can be as low as 5% of the total fixed capital for simple processes and as high as

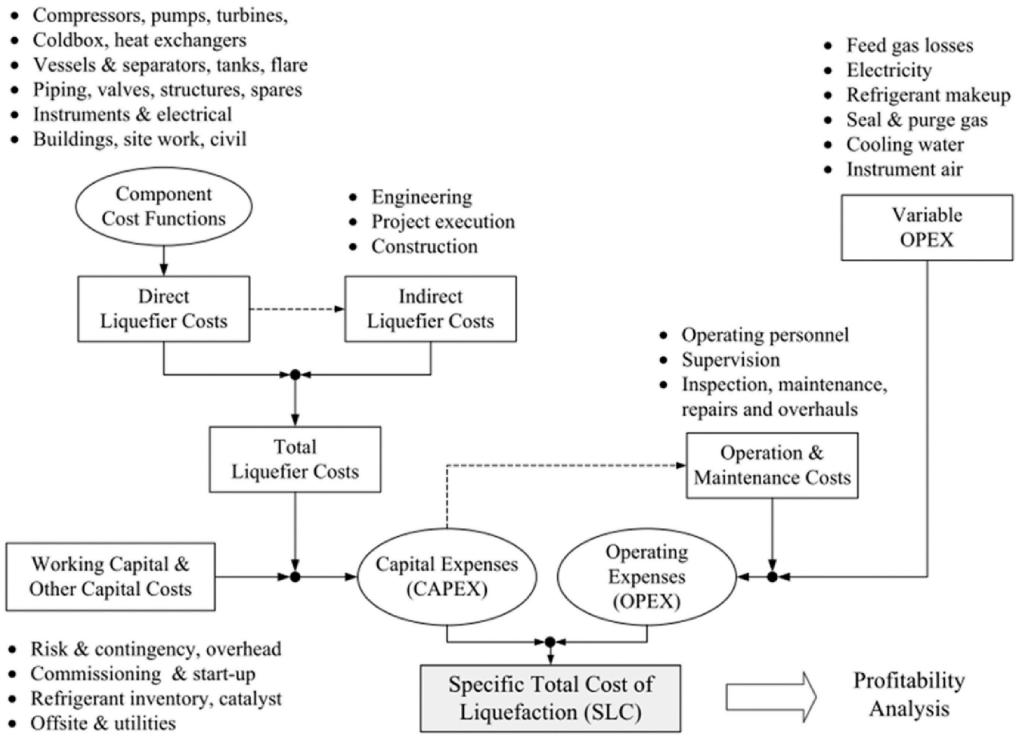

Figure 2.24: Schematic procedure for the liquefier SLC estimation proposed by Cardella et al.[s]

30% complex, multiple products process plant.[108] In the petrochemical industry, a typical figure for working capital is approximately 15% of the fixed capital.[108]

Syed et al.[113] and Cardella et al.[22,63] conducted capital cost estimations specific for hydrogen liquefaction systems. Both employ a cost estimation model based on process equipment cost functions and adapted factors from literature to estimate ISBL investment. However, Cardella et al. have developed and fitted most of their cost correlations specifically for hydrogen liquefier equipment and validated the model with cost data from industrial manufacturers. The resulting correlations from the fittings remain unpublished. Figure 2.24 shows the schematic procedure for the process economics of hydrogen liquefaction plants proposed by Cardella et al.[63]

It is challenging for engineers and researchers outside the Engineering, Procurement and Construction (EPC) sector to gather current cost information from many actual process plant projects and maintain precise and up-to-date cost-estimation models.[108] Even large operating companies acknowledge the difficulty of creating accurate cost projections, which typically hires a few cost engineering specialists who gather data and collaborate closely with the EPC companies.[108]

One of the alternatives for non-EPC related design engineers and academia is to utilise equipment cost data and costs correlations found in the open literature.[108] As mentioned previously, there is an abundance of equipment cost data and correlations published in the literature. However, much of it is of poor quality due to the continuous significant development in the relative contributions of each cost element since the cost models were published.[108] The more prevailing approach for estimating cost in chemical plant projectrs involves the utilization of commercial cost estimating software. There is a wide selection of cost estimating programs, such as Cleopatra Enterprise (Cost Engineering Consultancy), CostLink/CM (Building Sytems Design, Inc.), Cost Track (OnTrack Engineering Ltd.), Aspen Capital Cost Estimator (Aspen Technology Inc.), PRISM Project Estimator (ARES Corp.), Success Estimator (U.S. Cost), Visual Estimatior

[s]Reprinted from International Journal of Hydrogen Energy, 42/17, U. Cardella,L. Decker,J. Sundberg,H. Klein, Process optimization for large-scale hydrogen liquefaction,[63] 12339-12354, Copyright 2017, with permission from Elsevier

(CPR International Inc.), WinEst (Win Estimator), and etc.[108] Aspen Technologys Aspen Process Economic Analyzer (APEA) is one of the most simple-to-use cost estimating software, which performs estimation based on Aspen ICARUS Technology robust algorithm. APEA is included in the standard Aspen Plus/Hysys package, with the ability to linked to process simulator programs from AspenTech, Chemstations, Hyprotech, SimSci[t] and is available in most universities as well as most chemical companies.[114]

The foundation of Aspen ICARUS Technology relies on mathematical modeling technology that has undergone development, enhancement, and application by a team of cost engineers based on data collected from EPC companies and equipment manufacturers ever since ICARUS Corporation was founded in 1969.[115] Costs can be estimated for a whole plant or for one piece of equipment at a time.[115] Costs are based on the materials and labor required (following the practice used for detailed estimates) rather than installation factors.[114] When used properly, APEA can provide reasonably good and defensible estimates without requiring a lot of initial design data.[114] Details on the evaluation of capital costs by APEA have been described in the literature.[114–117]

Cost Escalation

Any approach to cost estimation relies on past data to predict future expenses. However, material prices and labor costs are susceptible to inflation. Consequently, a means must be employed to rejuvenate outdated cost data for estimating during the design phase and to project the plant's forthcoming construction expenses. Typically, historical cost data is refreshed using publicly available cost indices.[108] The following equation provides a means to adjust equipment and process plant construction costs from one period to another using cost indices:[108]

$$\text{Cost in year A} = \text{Cost in year B} \times \frac{\text{Cost index in year A}}{\text{Cost index in year B}}. \tag{2.27}$$

To obtain the best estimate, it is advisable to deconstruct every task into its elements, employing distinct measures for both labor and materials.[108] However, utilising the various composite indices published by trade journals is often more convenient. Chemical Engineering Plant Cost Index (CEPCI or CE index), published monthly in the journal *Chemical Engineering*, is probably the most widely used cost index in United States process plant industry.[118] CEPCI consists of a composite index assembled from a set of four sub-indexes: Equipment; Construction Labor; Buildings; and Engineering & Supervision. Other journals such as the *Oil and Gas Journal*, *Engineering News Record*, and *Process Engineering* also maintain and publish monthly cost indices.[108]

2.4.2. Operating Expenditure

The operating expenditure (OPEX), also termed as the cash cost of production (CCOP),[118] is the expense of operating the process plant to manufacture a product, which can include up to the packaging, shipping, selling and distribution as well as the general overhead expenses.[109] In general, OPEX can be classified into variable and fixed costs of production.[118]

Variable production costs are production expenses that vary with a plant's output or rate of operation.[118] Based on Towler & Sinnot,[118], these include:

- Raw materials that are being used or converted within the process plant
- Utilities – such as fuels, steam, cooling water, electricity et cetera.
- Consumables – such as solvents, acids, inert materials, catalyst et cetera that require regular or frequent replacement.

[t] As mentioned in APEA™ V12 software *Help* pages

- Effluent disposals – such as running costs for treating emissions or waste products from the plant.
- Packaging and shipping – drums, tankers, freight charges, et cetera.

In chemical plants, costs of raw materials are usually the major component of the overall operating costs, which are typically around 80-90% of the OPEX.[118] Utility costs are generally about 5-10% of the OPEX.[118] The number of raw materials and utilities required to make the desired product at the plant's design capacity can be estimated from the process model's mass and energy balances.[109,118] Consumables typically cost less than 3% of the OPEX.[118] Methods for estimating variable costs of production are described in the literature.[109,113,118]

In the context of hydrogen liquefaction processes, particularly when assessing liquefaction costs, the expense associated with the raw materials (in this instance, hydrogen gas) is generally not factored in, except when accounting for losses. This is because the liquefaction process is not designed to enhance the intrinsic value of hydrogen; rather, its purpose lies in enabling the storage or transportation of hydrogen across extended time frames and distances. Consequently, when considering a hydrogen liquefier, the predominant factor contributing to total operating costs pertains to utilities, mainly electricity. Additionally, as noted in literature,[2] these utility costs play a substantial role in shaping the overall expense of hydrogen liquefaction.[u] Cardella et al.[22,63] listed the costs of electricity, hydrogen feed gas losses, liquid nitrogen, refrigerant make-up, cooling water make-up, and seal and purge gas as the variable operating expenses of large-scale hydrogen liquefier. The specific costs of each variable cost element within cost estimation models are usually based on informed assumptions and vary significantly across different literature sources.[2]

In contrast, fixed production costs are expenses independent of the level of plant operation or production output.[118] Even if the plant reduces production, these costs remain the same and do not decrease. Based on Towler & Sinnot,[118] fixed production costs consist of:

- Operating labor – Depends on number of shift positions and salaries of each operator. Operator salaries vary by region and experience level.
- Supervision – usually taken as 25% of operating labor
- Direct salary overhead – usually 40% to 60% of operating labor plus supervision.
- Maintenance – usually estimated as 3-5% of ISBL investments, depending on the expected reliability of the plant.
- Property taxes and insurance – typically 1-2% of ISBL fixed capital.
- Rent of land and buildings – typically 1-2% of ISBL plus OSBL cost.
- General plant overhead – charges to cover corporate overhead functions such as human resources, research and development (R&D), information technology, finance, et cetera.
- Allocated environmental charges to cover superfund payments – typically 1-2% of ISBL plus OSBL cost.
- Running license fees and royalty payments.
- Capital charges – these include interest payments due on any debt or loans used to finance the project, but do not include expected returns on invested equity capital.
- Sales and marketing costs – Near zero for commodities, but can be as high as millions of US dollars annually for branded items (food, drug, cosmetics et cetera).

These costs should always be addressed, even at early design stages, as they can contribute highly to the overall process economics. Methods for estimating fixed operating costs that were not previously mentioned above are given in the literature.[109,118] Some of the above costs may also be considered semi-variable costs of production. Semi-variable expenses have both fixed and variable components with respect to production.[109] They tend to decrease with increasing

[u] During the time of this study, the annual energy inflation in the EU have reached record level following the undergoing conflict in the area. The annual energy inflation rate exceeded 40% in June 2022,[119] with the maximum wholesale day-ahead electricity price reach 823.29€/MWh and then prices began falling gradually. On 31 July 2023, the price of electricity in the EU is between 32.56-125.82€/MWh. Electricity prices based on `https://ember-climate.org/data/data-tools/europe-power-prices/`, accessed on 7 August 2023.

production but do not completely vanish at zero production. Maintenance, supervision, labor costs, and, in some cases, utilities may fall into this category.[109]

Towler & Sinnot[118] provide a systematic procedure to calculate and summarize production costs and revenues associated with a process plant project. This help to simplify the process of evaluating the economic aspects of the project and comprehending how the various elements contribute to the total production cost. Another tool that can be utilized for performing production cost calculation is the previously mentioned Aspen Process Economic Analyzer (APEA), which has built-in feature for investment analysis. APEA computes the complete operating expenses by factoring in both variable and fixed production costs, based on user-provided values at each components (or the default settings if chosen by the user).[115–117] Additionally, APEA lets the user to perform profitability analysis and project cash flow based on investment parameters and product pricing. Details on the evaluation of operating costs by APEA have been described in the literature.[115–117]

2.4.3. Economy of Scale

As mentioned in the Introduction, one of the objectives of this thesis is to be able to predict a learning curve for the hydrogen liquefaction plant based on the cost study of this thesis. To understand the concept of the learning curve, it is essential to also comprehend the notion of economy of scale. The economies of scale are cost advantages that companies obtain due to their scale of operation.[108] This economic principle traces its origins back to Adam Smith and the notion of achieving enhanced production returns through the utilization of division of labor.[120] In the context of the process plant industry, this principle is evident, as larger plants tend to exhibit lower construction costs per unit of product manufactured.[108]

The economies of scale of chemical plants can be exhibited by the cost curve method, which is one of the fastest ways for design engineers to make an order-of-magnitude (Class 5)[v]estimate of plant capital cost. The cost curve method relates the capital cost of a plant to its' capacity using the following equation:[108]

$$C_2 = C_1 \left(\frac{S_2}{S_1} \right)^n . \tag{2.28}$$

Another form of this equation that is also commonly used in the industry is as follows:[108]

$$C_2 = \frac{C_1}{S_1^n} \times S_2^n = a S_2^n . \tag{2.29}$$

From Equation (2.29), the capital cost per unit of production of product is calculated as follows:[108]

$$\frac{C_2}{S_2} = a S_2^{n-1} . \tag{2.30}$$

In the context of hydrogen liquefaction, these correlations have been used in multiple studies to estimate the capital investment for the liquefaction facility. For example, in 1998, Amos[121] deduced the base cost/size and constant n values of Equation (2.29) based on published cost data in studying the cost of hydrogen storage and transport. In the IDEALHY project, Equation (2.29) has been used to estimate the capital cost of a 40 TPD liquefier from the initial quoted investment cost for a 50 TPD liquefier. In this study, constant n was assumed as 2/3, while constant a was determined to be 7.37 million€ from the investment for 50 tpd and zero investment for a 0 tpd plant. Several researchers, have also used the same 2/3 value for n to extrapolate capital costs;[13,27,28] however, used in the correlation in the form of Equation (2.28).[27,28]

[v]Order of magnitude estimates (ballpark estimate, guess estimate, Class 5 estimate), accuracy typically ±30% to 50%, usually based on the costs of similar processes and requiring essentially no design information. They find application in initial feasibility assessments and for preliminary screening objectives.[118]

In 2008, Nexant, Inc. along with other companies, team up to carried out US DOE hydrogen delivery infrastructure project and reported their cost projection curve for hydrogen liquefier capital investment based on quotes from major gas processing companies.[122] However, the vendor quotes are preliminary, with significant uncertainty, and are limited to relatively small scale plants (less than 50 TPD). The model that was developed and evaluated in this project is the Hydrogen Delivery Scenario Analysis Model (HDSAM).[123,124] Since its initial public release in 2006, HDSAM has annually updated its data on delivery pathways, component technologies, and costs relevant to government agencies and industry stakeholders. The latest HDSAM version[124] (V4.0) estimates hydrogen liquefier installed costs with a form of Equation (2.29), with constant a and n of 5.6 million US$ and 0.8, respectively.

It can be seen in literature and many journals that the value for exponent n, for almost any kind of chemical plants, in above equations is less than 1.0.[108] Therefore, the value for $n-1$ is always less than zero, thus, as S_2 increases the cost per unit of production, C_2/S_2, decreases. A lower capital cost per product unit allows the owner of larger plants to use more competitive pricing while still recovering their capital investment.[108] This encourages chemical companies to build larger plants.

The negative correlation between specific costs and production volume was first noticed and documented for aeroplane production by T.P. Wright as far back as the 1930s.[125,126] He observed that as more aeroplanes were built over time, there was a consistent reduction in the amount of labor hours and materials needed for each aircraft. This phenomenon is now known as a "*learning curve*".[126] Since then, this idea has been used mainly to analyse the overall costs of a product, encompassing the combined impact of learning, economies of scale, and potentially other variables.[126,127] Today, this concept is also frequently extended to whole industries, rather than just individual firms. The broader understanding of the concept of learning curves formulates what is now known as the "*experience curve*".[126,127w]

An experience curve typically describes the relationship between a technology's specific costs (expressed in real terms) as the dependent variable and the technology's experience (or cummulative capacity) as the independent variable.[126,127] The logarithmic linear function is probably the most common model used for representing such learning phenomena due to its simplicity and generally high goodness-of-fit to observed data. The log-linear equation for experience curve is as follows:[127]

$$c = c_0 \left(\frac{q}{q_0} \right)^{-b} = a \cdot q^{-b}. \tag{2.31}$$

Notice that the equation has the striking similarity with the previous capital cost projections. The central parameter within the experience curve model is the exponent that establishes the incline of a power function, known as the learning coefficient (b).[127] The learning coefficient is used to calculate the progress ratio (PR) and learning rate (LR) of the technology, also called the learning ratio, by means of the following equations:

$$\mathrm{PR} = 2^{-b}, \tag{2.32}$$

and

$$\mathrm{LR} = (1 - \mathrm{PR}). \tag{2.33}$$

The learning rate is the rate at which a technology's costs are found to decrease for each doubling of experience.[126] The progress ratio informs about the relative technology costs remaining after a doubling of experience.[126]

An important implication of the experience curve is that increasing the accumulated experience in the early stages of a technology is a dominant strategy to maximise the profitability of

[w] However, as noted in literature,[126] many still use the term learning curve as a synonym for experience curve

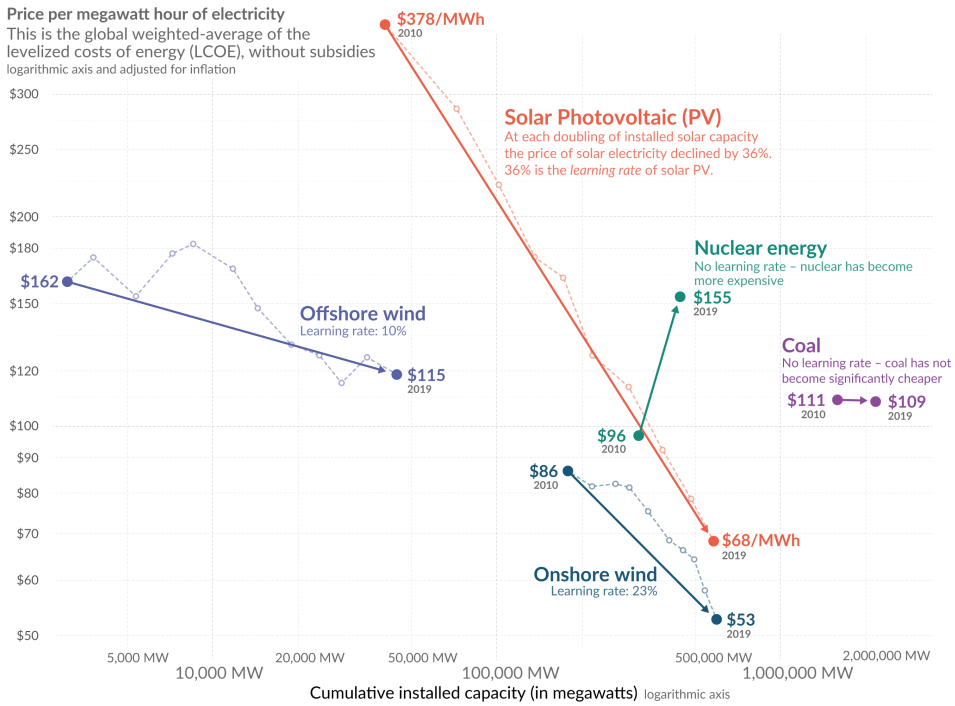

Figure 2.25: Learning curves of several electricity generation technologies[x]

firms and the societal benefits of technology-related public policy.[126,128] This concept has been an important tool for modelling technical change, informing policy decisions and anticipating future costs related to energy technology in the last two decades.[126] Figure 2.25 depicts the experience curves of several electricity generation technologies using global cumulative installed capacity as the definition of technological experience i.e. the independent variable, reported by Ritchie et al.[129] based on data from various works. Based on assumptions about future deployment levels, this relationship can be used to anticipate future changes in the cost of electricity generation, e.g. by assuming that the learning rates observed in the past will remain stable in the future.[126]

[x] Reproduced from *Why did renewables become so cheap so fast?*,[129] Energy, Published in Our World in Data by Hannah Ritchie and Max Roser, 2021; available online at ourworldindata.org/cheap-renewables-growth

3

Process Modelling

3.1. Reference Process

Various large-scale hydrogen liquefaction concepts and cycle configurations have been reviewed by Aasadnia & Mehrpooya.[34] These concepts have theoretically demonstrated how energy consumption in hydrogen liquefaction can be minimised. However, a prevailing concern arises from the fact that many of these modern investigations focus on "pure" process simulation and often overlook the viability of integral hardware components, such as compressors, turbines, heat exchangers, pumps, and columns.[18] Many efficient but very intricate liquefaction systems, which may not be technically or economically attainable, have been developed. As noted by Berstad et al.[21], the development of new processes should not merely be a "race to the bottom" in power requirements. Instead, the focus should be directed towards identifying rational and economically viable pathways for improving efficiency.

Based on the literature review, it can be infer that most large-scale H_2 liquefaction concepts are developed by adopting either one of these basic systems:

- Precooled Claude cycle
- Joule-Brayton cycle
- Integration with LNG Production

As the main focus of this thesis is not the integration of LH_2 and LNG production, the options naturally narrows down to the Precooled Claude and Joule-Brayton hydrogen liquefaction systems.

Furthermore, Al Ghafri et al.[2] provide a synopsis and lists of viable large-scale liquefaction concepts that were selected based on the criteria outlined in Section 2.2.2. By using this approach, numerous conceptual processes were eliminated and only the following processes remain:

- **Quack (2002)**; 170 TPD, MR He-Ne JB cycle[20]
- **WE-NET (2004)**; 300 TPD, LN_2 precooled H_2 Claude cycle[26]
- **Berstad et al. (2010)**; 86 TPD, MR He-Ne JB cycle[67]
- **IDEALHY (2013)**; 50 TPD, MR precooled He-Ne JB cycle[19,59,66]
- **Krasae-in (2014)**; 100 TPD, MR precooled H_2 JB cycle[23]
- **Cardella et al. (2017)**; 100 TPD, MR precooled H_2 Claude cycle[22,63]
- **Berstad et al. (2021)**; 125 TPD, MR precooled H_2 Claude cycle[21,70]

These concepts were the primary candidates for the investigation of the large-scale hydrogen liquefaction processes in terms of both technical viability and economic feasibility within the scope

of this thesis. According to Al Ghafri et al.[2], the high pressure hydrogen Claude cycle concept using a mixed-refrigerant Joule-Thomson precooling cycle proposed by Cardella et al.[22,63] and Berstad et al.[21] is regarded as one of the most promising conceptual designs for near-future implementation.

Based on the process optimisation performed by Cardella et al,[22,63] the SEC of the plant can be reduced to about 6 kWh/kg while reducing the SLC by nearly 67%, compared to small-scale 5 TPD plants, to below 1€/kg. Furthermore, the use of the MR pre-cooling system eliminates the need for the LN_2 pre-cooling system, which requires a considerable portion of the total H_2 liquefaction energy.[2,130] Another challenge with the use of nitrogen is the large temperature difference between the cooling and heating curves of nitrogen and hydrogen, which limits heat recovery[2] and increases irreversibilities.[21,23] Mixed refrigerants (MR) are advantageous because its mixture compositions can be readily modified to adjust the evaporation curve so that it aligns with the cooling of hydrogen gas. This minimisation of temperature discrepancies in the heat transfer enhances the overall thermodynamic efficiency.[2,21,23,63]

Based on these factors, the high-pressure hydrogen-Claude cycle with MR precooling concept is selected to be the base process for the case study in this thesis. The process model is predominantly constructed in reference to the conceptual plant of 125 TPD proposed by Berstad et al.[21], which presents the complete stream data for this particular process.

3.1.1. Process Description

Figure 3.1 illustrates the process flow diagram of the hydrogen liquefaction process under consideration. Gaseous hydrogen is fed to the process plant at a rate of 125 TPD at 20 bar and 298.15 K (*GH_2*). The hydrogen is first cooled by the MR precooling system as it enters heat exchanger **HX-1**. The process flow diagram for the MR precooling cycle is shown in Figure 3.2. The cycle utilises a five-component refrigerant mixture to cool the hydrogen feed to 114 K. Details of the mixed refrigerant composition follow the composition used by Skaugen et al.,[70] given in Table 3.1. The main specification of the gas hydrogen feed, liquid hydrogen product and ambience conditions are given in Table 3.2.

Mixed-refrigerant compression in the precooling module is provided by two compressors equipped with aftercoolers. The aftercoolers cools incoming streams to 298.15 K by means of cooling water that is assumed to be readily available within the plant. The first compressor, **MRC-1**, takes the refrigerant (*MR1*) to a pressure of around 12 bar and after the first aftercooler stage, the refrigerant partially condenses (*MR2*). The multiphase stream is then separated in a vapor-liquid separator, **V-200**. The liquid condensate from the separator is collected and pressurised to 35 bar using a pump (*MR3*), while the vapor flow is compressed by the second compressor, **MRC-2**, to the same pressure. The vapor refrigerant re-condenses partially after the second aftercooler (*MR4*) and then mixes with the pressurised liquid from the pump before entering **HX-1** (*MR5*). In **HX-1**, the multiphase pressurised refrigerant and the hydrogen feed, are cooled to a temperature of 114 K (*M01* & *MR6*). The exiting refrigerant is expanded via Joule-Thomson valve to a pressure of 3.6 bar, which accordingly decreases its temperature to

Table 3.1: Mixed refrigerant composition[70]

Component	Mole fraction
Nitrogen	0.101
Methane	0.324
Ethane	0.274
Propane	0.031
n-Butane	0.270

Table 3.2: Main H_2 Liquefaction Process Specifications

Gas hydrogen feed	Values	Unit
Pressure	20	bar
Temperature	298.15	K
Mole fraction of p-H_2	0.25	
Liquid hydrogen product	Values	Unit
Mass flow (plant capacity)	125	TPD
Pressure	1.500	bar
Temperature	≤21.67	K
Mole fraction of p-H_2	≥0.98	
Ambient conditions	Values	Unit
Pressure	1.013	bar
Temperature	298.15	K
Cooling water temperature	293.15	K

about 111.3 K (*MR7*). The cold and low pressure refrigerant is routed back to the **HX-1** cold side to absorb the heat from the two hot streams of pressurised refrigerant and hydrogen feed. This configuration of **HX-1** gives a tight thermal match between the streams and thus an exergy efficient heat transfer.[21]

As mentioned in the literature review, the typical hydrogen feed in a liquefaction plant has impurities of 10-100 ppm. The concentration of these impurities needs to be reduced to below 1 ppm, since they could condense and freeze during cryogenic cooling, potentially degrading the ortho-para catalysts inside the heat exchanger. Therefore, cryogenic adsorber beds, **TS-ADS**, are added after **HX-1** to basically purify the main hydrogen stream. The pure hydrogen (*M02*) feed now enters the main cryogenic cooling system, where it is cooled from a temperature of 114 to 30 K (*M02-M06*) through a series of catalytic heat exchangers (**HX-3**-**HX-6**). These heat exchangers are filled with ortho-para catalyst on the main hydrogen feed side, which for now is assumed to be sufficiently long to allow the hydrogen spin isomers to convert to the equilibrium state. The cooling capacity required to cool the incoming H_2-feed and dissipate the extra heat from exothermic ortho-para conversion in these heat exchangers is provided by the cold hydrogen gas produced within the high pressure Claude refrigeration cycle. After cooling the hydrogen gas feed to 30 K, it is expanded from 20 bar to 1.85 bar through a Joule-Thomson valve which cools down and liquefy the hydrogen. The temperature of the LH_2 at this point is about 22.49 K (*M07*).

The hydrogen Claude refrigeration cycle, high-pressure hydrogen stream (*C01*) is pre-cooled within heat exchangers **HX-2** and **HX-3** to a temperature of 112 K (*C02-C03*). Beyond this point along the high-pressure line (*C03-C05*), auxiliary streams are extracted from the primary high-pressure conduit. These streams (*C16*, *C19*, *C22*) are expanded to an intermediate pressure level (*C17*, *C20*, *C23*) through cryogenic hydrogen turbines, to promote temperature reductions. Subsequently, they are introduced into an intermediate pressure gas return line (*C18*, *C21*, *C24*, *C25*, *C26*), which plays a central role in providing cooling for **HX-2** to **HX-6**. The remaining fraction of high-pressure hydrogen, which exits **HX-6** at about 33.2 K (*C06*), is expanded in a series of dense-phase turbo-expander and throttling valve to a pressure of 1.25 bar (C07-C08), resulting in a partially condensed hydrogen flow. The resulting two-phase is sent to a vapor-liquid separator column, **V-100**, where the liquid hydrogen, at a temperature of 21.1 K (*RX1*), is then sent to the last catalytic heat exchanger, **HX-7**. This ensures further cooling and ortho-para conversion of the LH_2 product. The LH_2 product stream (*M08*) exits **HX-7** at a temperature of around 21.6 K is further expanded to 1.5 bar for storage and transport (LH_2). In this study, the liquid hydrogen storage and the related boil-off management system are considered to be outside the battery limit of the hydrogen liquefaction plant; thus, they will not be modelled or further evaluated in the technical and economic analysis.

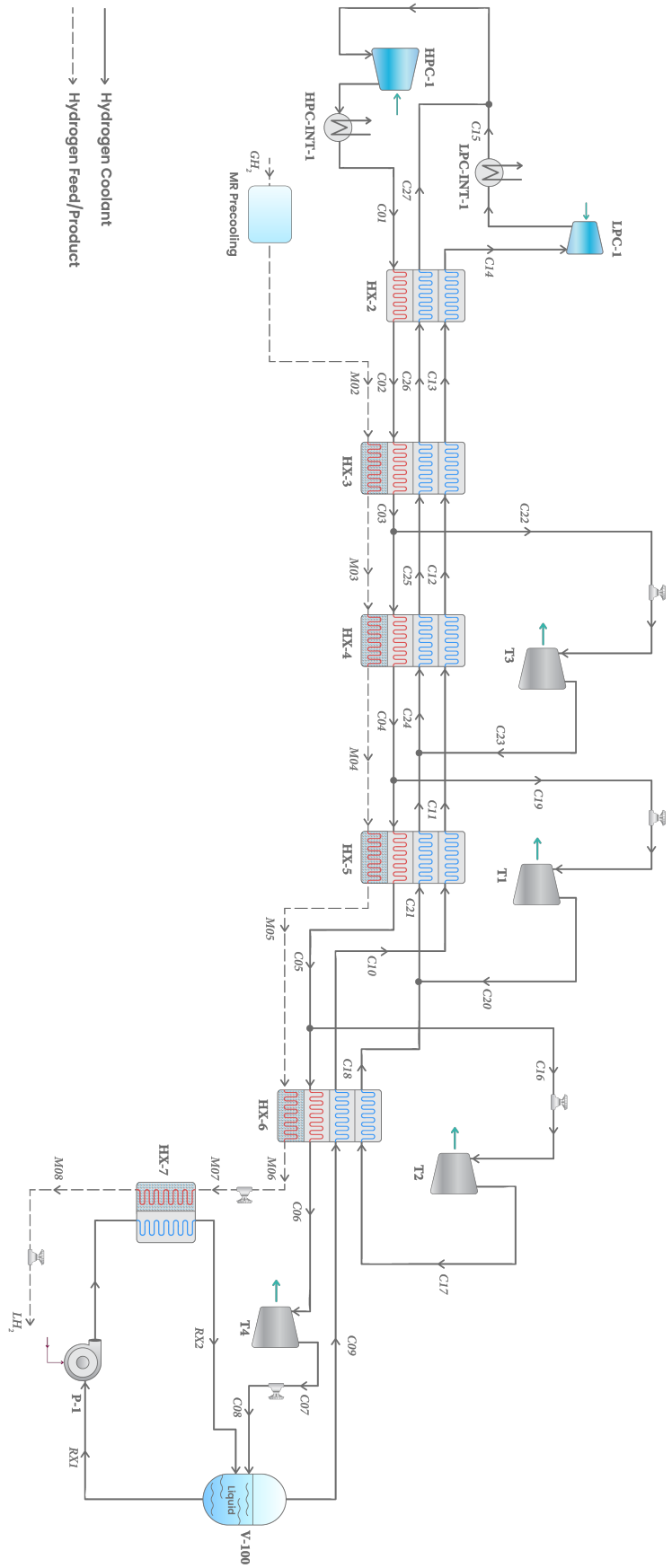

Figure 3.1: High-Pressure Hydrogen Claude Cycle Hydrogen Liquefier Process Flow Diagram

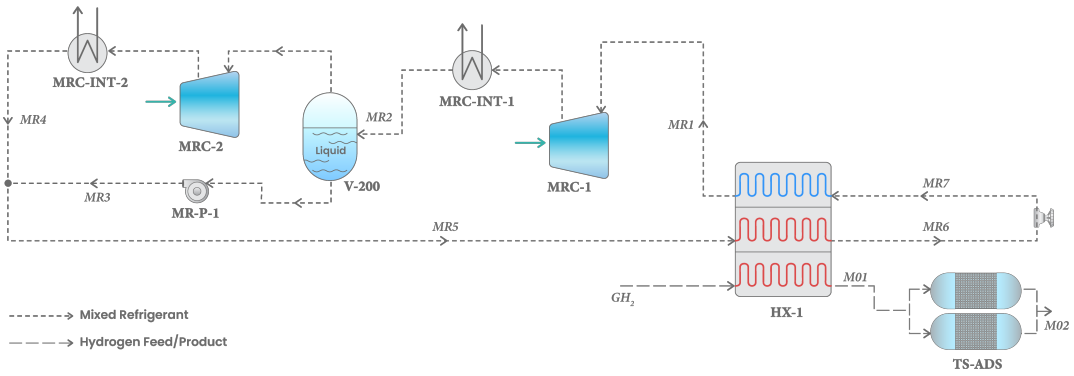

Figure 3.2: Mixed Refrigerant Precooling System Process Flow Diagram

The hydrogen vapours from the cold side of **HX-7** and the expander-valve expansion (*RX2* & *C08*) are collected in the vapour-liquid separator and drawn into the low-pressure compressor (**LPC**). This flow (*C09-C14*) then passes through all the heat exchangers in the main Claude cycle (from **HX-6** to **HX-2**) before it is compressed by the **LPC** to a pressure of 7.395 bar (*C15*). Subsequently, the compressed hydrogen is combined with the returning intermediate-pressure stream (*C27*) and subjected to further compression, raising it to a higher pressure of 30 bar (*C01*) using the high-pressure compressor (**HPC**). As with precooling compressors, both the **LPC** and **HPC** systems are configured with an aftercooler to reduce the gas temperature exiting the compressors to 298.15 K through the utilization of cooling water.

3.1.2. Process Simulation

As mentioned in Section 2.2.2, recent conceptual studies have been carried out using commercial process simulation tools. Commercial process simulation programs can thoroughly evaluate plant steady-state operations and some are capable of estimating the plant's total cost under different scenarios. According to Al Ghafri et al.[2], the choice of simulation platform, in general, is less important than the accuracy of the models used to represent the properties of the hydrogen and refrigerant fluids, and the design constraint imposed on the critical items of process equipment such as heat exchangers, turbines and compressors. In this thesis, process modelling and simulation will be performed in the steady-state process simulator Aspen HYSYS V12.

In the process simulation, the built-in unit operation models from Aspen HYSYS are used to calculate the process operation of components such as the heat exchangers, commpressors, expanders, etc. For the calculation of the multi-stream counter-current PFHX in the hydrogen liquefaction process simulation model, the built-in "LNG exchanger" model in Aspen HYSYS is used. In order to consider economically and technically viable industrial equipment designs, parameter constraints are imposed in the preliminary design of the equipment, which will be described in greater detail in Chapter 4. Additionally, in the initial phase of modelling the liquefaction process within the process simulation, the efficiencies of the pressure-altering equipment are taken as assumptions. In this context, the isentropic efficiencies of all compressors within the precooling and cryogenic cycles are assumed to be 85%. Cryogenic turbo-expanders are also assumed to possess isentropic efficiencies of 85%. For condensate pumps, an assumed isentropic efficiency of 75% is used. These efficiency values will be subject to refinement based on preliminary design outcomes and will be reincorporated into the simulation. Similarly, pressure drops associated with adsorbers and heat exchangers, including aftercoolers, which are initially assumed to be negligible, are adjusted and reintroduced into the simulation after the preliminary equipment designs were established.

The hydrogen liquefaction simulation model is divided into one primary flow sheet and two subflowsheets. The primary flow sheet, referred to as the main *cryogenic liquefier system*, encompasses the primary Claude refrigeration cycle, excluding the compressors, along with the final hydrogen liquefaction process. The first subflowsheet is the *compression system*, which features the Claude-cycle HPC and LPC units, including their respective aftercoolers. The other subflowsheet is for the *MR precooling system*, which consists of all the equipment shown in Figure 3.2.

The process simulation model employs different fluid property packages with equation of state (EOS) according to the respective fluids. This is elaborated further in the following segment:

Estimation of Fluid Properties

As Aspen HYSYS is capable of calling REFPROP databank of NIST,[50] the thermodynamic property estimation for normal-, ortho- and para-hydrogen can be calculated using the state-of-the-art EOS of Leachman et al.[49] The hydrogen feed stream that is cooled in the heat exchangers with continuous catalytic ortho- to para-hydrogen conversion can be simulated by assuming equilibrium-hydrogen. For this purpose, the pseudo-equilibrium-hydrogen heat-capacity model developed by Valenti et al.[51] shall be utilized. Although the model has faced some criticism in recent literature,[53] it has been demonstrated to be a helpful idea for accurately modelling heat exchanger unit operations in hydrogen liquefaction simulations.[21,22] The kinetic aspects of the conversion will be considered in the heat exchanger sizing and preliminary design phase.

In this work, the pseudo-e-H_2 model is utilised to calculate the properties of the main GH_2 feed from the exits of the adsorbtion systems to the final LH_2 product. The pseudo-e-H_2 model by Valenti et al.[51] is implemented by modifying the REFPROP[50] fluid file (.FLD file) of the parahydrogen and subsequently calling the REFPROP's parahydrogen model from Aspen HYSYS. On the other hand, the properties of the H_2 refrigerant in Claude refrigeration system are simulated by calling the normal-H_2 model using EOS by Leachman et al.[49] from REFPROP. The properties of the mixed-refrigerant fluid in the precooling cycle are calculated using the Peng-Robinson cubic EOS available in Aspen HYSYS.

The author recognises that employing the pseudo-e-H_2 model directly for the H_2 feed stream at the entrance of the Claude refrigeration cycle overlooks the additional heat originating from the conversion of ortho- to para-hydrogen resulting from the temperature drop of hydrogen from 298.15 K to 114 K. However, it has been calculated that the influence of this exothermic reaction on the plant's energy consumption estimation remains modest. The calculated heat release from this reaction is approximately 82.81 kJ / kg. Integrating this additional heat into the energy equilibrium of **HX-3** within the simulation leads to a mere 0.04 kWh/kgLH_2 increase in the overall SEC of the plant. The ensuing impact on the plant's SLC as a result of this slight rise in the SEC is also considered negligible in the context of the plant's economic evaluation. Specifically, the increase amounts to less than 0.001/kgLH_2 at low electricity prices (0.02/kWh) and 0.016/kg_{LH_2} at very high electricity prices (0.40/kWh).

To thoroughly incorporate this reaction into the simulation, a more sophisticated fluid model of the hydrogen ortho-para mixture is necessary. Alternatively, another approach involves the introduction of an adiabatic ortho-para reactor downstream of the cryogenic adsorbers to equilibrate the hydrogen's ortho-para composition, as observed in prior literature[21,22,63]. However, due to the absence of adequate design tools for such reactors during this study, this solution was unfeasible for the technical and economic analysis undertaken in this thesis. Moreover, considering that adiabatic ortho-para reactors are not a fundamental component for this large-scale hydrogen liquefaction concept, developing a new reactor design procedure is deemed unnecessary within the scope of this thesis.

Calculation of Specific Energy Consumption

The specific energy consumption (SEC) for the large-scale hydrogen liquefaction process is calculated within process simulation model using the built-in spreadsheet feature within Aspen HYSYS. The calculation follows Equation (2.3). In this study, two distinct SEC values are under assessment: SEC with electric power recovery (SEC_{recov}) and SEC without electric power recovery (SEC_{base}) from turbines. This comparison aims to quantify the economic advantages of incorporating turbine power recovery systems (turbo-generators) into the larger liquefaction system.

For SEC_{base}, the net total power requirement is the sum of electrical power needed to drive the compressors and pumps within the liquefaction plant. On the other hand, for SEC_{recov}, the net power requirement is the difference between the total electric power consumption and the electric power that would be generated by installing turbo-generators in the plant. In this work, only turbo-expanders generating mechanical power exceeding 100 kW are considered suitable for coupling with generators. The conversion efficiency of mechanical energy from turbines to electrical energy is assumed to be 80%.

For analysis purposes, the main reference process in this study, the high-pressure hydrogen Claude-cycle conceptual liquefier of 125 TPD capacity proposed by Berstad et al.[21], was reported to have an SEC value of 7.09 kWh/kg_{LH_2}. This value can be potentially reduced about 7%, to about 6.57 kWh/kg_{LH_2} by recovering mechanical power from turbines through electric generators. The minimum specific work requirement to transform the 20-bar hydrogen feed to liquid hydrogen at 1.50 bar and 0.2 K subcooled state is estimated by Berstad et al.[21] to be equal to 2.67 kWh/kg. Therefore, the FOM, or exergy efficiency, of this process is equal to 37.66%. This value increases to 40.64% when the addition of a turbine power recovery system is considered.

4

Equipment Preliminary Design

Numerous conceptual approaches to large-scale hydrogen liquefaction have been developed over the years. However, only a limited number of these concepts have undergone thorough evaluations of their technical and economic viability. This thesis aims to address this gap by introducing a comprehensive framework for assessing the technical and economic aspects of conceptual large-scale hydrogen liquefaction systems. This chapter describes the methodology employed in this study for preliminary sizing, design calculations, and estimation procedures. Most of these design procedures have been operationalised through algorithmic calculations within a self-developed Python programme. The programme's source code is accessible in the GitHub repository: `https://github.com/pbtamarona/h2liquefaction`.

As mentioned in Section 2.3, the preliminary equipment designs presented in this thesis mainly focus on plate-fin heat exchangers, compressors, and turbines. Additionally, a brief discussion on the preliminary sizings of cryogenic adsorbers and coldboxes are presented. The sizing of the remaining equipment is estimated using the APEA mapping and sizing functionality, which will be briefly explained in Chapter 5. The chapter also outlines the design constraints for each type of equipment which are based on current technological limitations.

The core objective of the equipment design phase encompasses two key aspects: first, it aims to evaluate the technical feasibility of the base process introduced in Chapter 3; second, it lays the foundation for a reliable estimate of the costs associated with the plant, as elaborated in Chapter 5. The degree of detail of the preliminary sizing and designs, as elucidated in this chapter, is determined by the specific design constraints and cost estimation models chosen for the analysis.

A comprehensive account of the results stemming from preliminary sizing and design across all case study scenarios is provided in GitHub repository: `https://github.com/pbtamarona/h2liquefaction/tree/main/thesisResults`.

4.1. Plate-Fin Heat Exchanger

Preliminary sizing and design of the non-catalytic PFHXs, *HX-1* and *HX-2*, is performed in Aspen EDR *design mode*. The input for the design is imported directly from the Aspen HYSYS simulation file of the Claude-liquefier described in Section 3.1.1-3.1.2. The design constraints assumed for the preliminary design of noncatalytic PFHX are summarised in Table 4.1.

Table 4.1: Design limitations of plate-fin heat exchangers

Parameter	Values	Unit
Max. Length	8.2	m
Max. Width	1.5	m
Max. Height	3.0	m
Volume	15-30	m^3
Specific surface	500-1,800	m^2/m^3
Max. Temperature Difference	25.0	K
Min. Temperature Difference	1.0	K

If the heat transfer requirement cannot be fulfilled in a single PFHX while meeting the design constraints provided in Table 4.1, additional PFHX(s) shall be added in parallel configuration to the process. In practise, the number of PFHX cores that can be added is limited by the maximum feasible dimension of the precooling and liquefier coldbox. Therefore, the results of the preliminary design of PFHX have a significant influence on the technical feasibility of the coldboxes, which will be discussed further in Section 4.5.

The *design mode* in Aspen EDR performs various calculations of geometric (mechanical), thermal, and hydraulic parameters. Furthermore, Aspen EDR provides the estimated stream properties and wall temperature at every calculation node. These values are used to check whether the minimum and maximum temperature differences have met the PFHX design constraints. Additionally, the Aspen EDR also estimated the pressure drops of each stream, which can be used to refine the pressure values in the Aspen HYSYS simulation. Figure 4.1 shows some snippets of the result windows obtained from Aspen EDR PFHX *design mode*.

For noncatalytic PFHXs, the main outcomes of the preliminary designs within this study are all the calculation results from Aspen EDR *design mode*, that fulfil the criteria described in Table 4.1. The full results of the preliminary designs of noncatalytic PFHXs for all simulation scenarios are given in the GitHub repository: `https://github.com/pbtamarona/h2liquefaction/tree/main/thesisResults`.

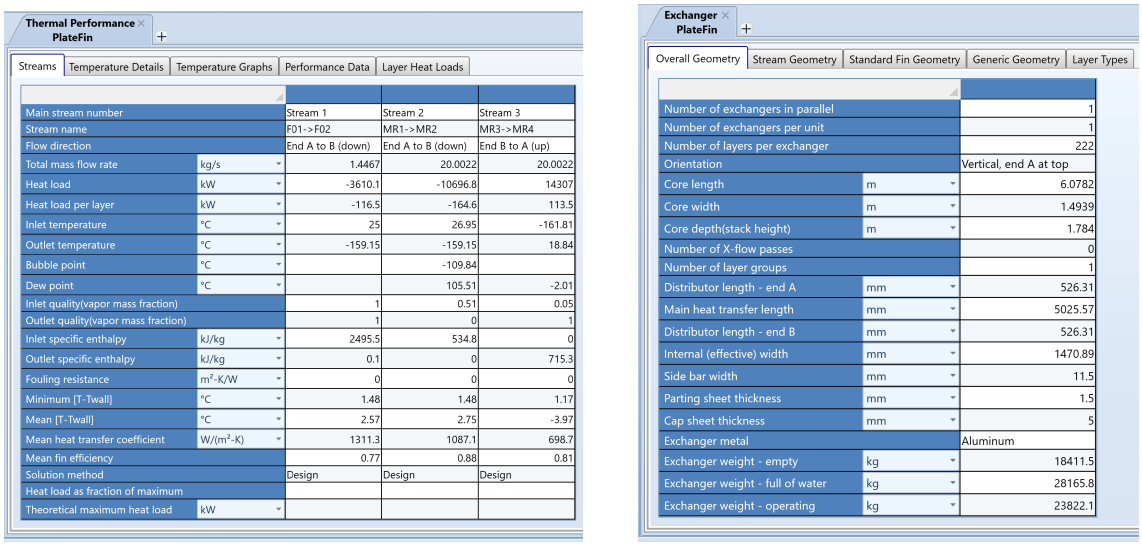

(a) Plate-fin thermal performance Summary

(b) Plate-fin overall geometry Summary

Figure 4.1: Exemplary of Aspen EDR plate-fin heat exchanger *design mode* results

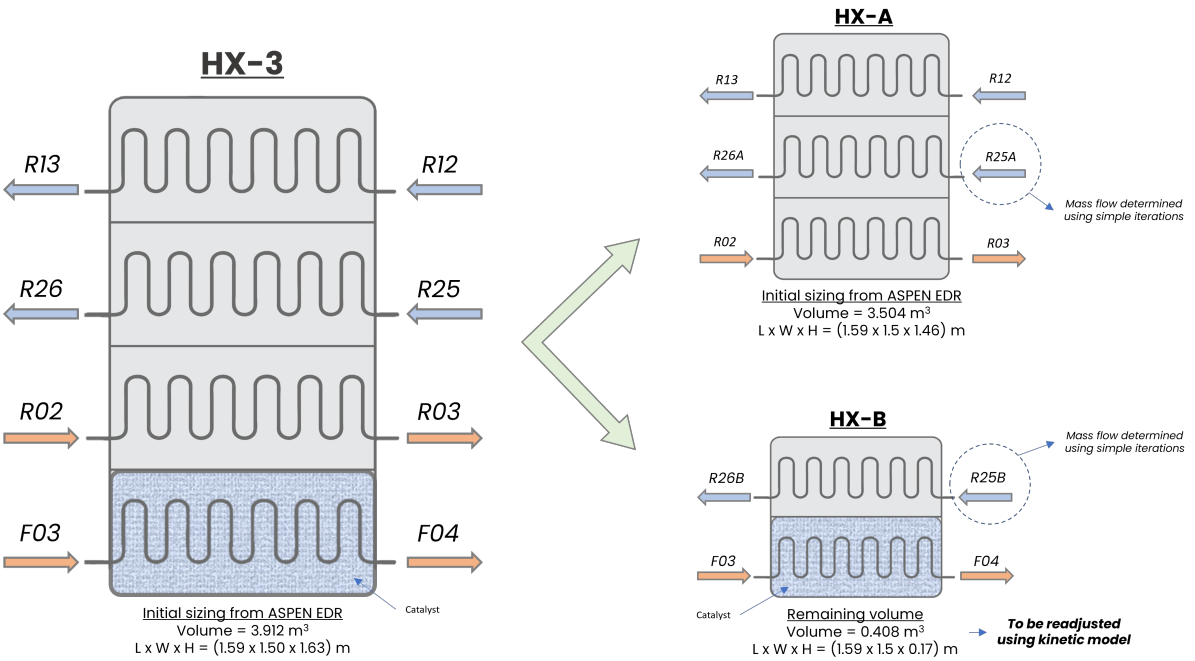

Figure 4.2: Schematic for dividing the sizing process of HX-3 into two sizing procedure of noncatalytic and catalytic PFHXs

4.1.1. Catalyst-Filled Plate-Fin Heat Exchanger

For PFHX with ortho- to para-hydrogen conversion, **HX-3**-**HX-6**, the above sizing procedure is not sufficient, since conversion kinetics is the limiting factor of the design. The steady-state one-dimensional pseudo-homogeneous continuum reactor model of the counterflow-cooled catalyst-filled PFHX model recently developed by O'Neil et al.[45] has been publicly shared on GitHub and thus is used to approximate the geometric specifications for the catalytic PFHX as well as the required catalyst volume.

The PFHX model developed by O'Neil et al.[45] is developed to simulate the dynamic processes of hydrogen spin-isomer conversion, heat transfer, and pressure loss that occur in a two-stream plate-fin heat exchanger filled with ortho-para catalyst in the hot-stream channel. However, the catalytic heat exchangers assumed in the liquefaction process simulation are multi-stream catalytic heat exchanger models, with both hot and cold streams having two streams each. Therefore, in this thesis, the preliminary design of the multistream catalytic PFHX is separated into two sizing processes: 1.) The noncatalytic HX sizing; 2.) The catalytic HX sizing. Figure 4.2 shows a schematic for the process of dividing the four-stream PFHX of **HX-3**, into one three-stream noncatalytic PFHX (with one cold stream and two hot streams) and two-stream counterflow catalyst filled PFHX.

Using the catalytic plate-fin heat exchanger of **HX-3**, from the base simulation described in Chapter 3, as an example (as shown in Figure 4.2), the full step-by-step procedure for this approach is as follows:

1. First, the initial size of the **HX-3** is determined using Aspen EDR *design mode*. Here, the process data is directly imported from the Aspen HYSYS simulation; thus, the main-H_2 streams, *F03-F04*, are evaluated using the pseudo-e-H_2 model of Valenti et al.[51]
2. Subsequently, the four streams of **HX-3** are segregated into two virtual heat exchangers: **HX-A** and **HX-B** (illustrated in Figure 4.2). As depicted in the schematic, **HX-A** incorporates three streams, while **HX-B** handles two streams. The configuration is established by splitting

the incoming cold stream with the larger mass flow, *R25* in this case, into two virtual streams, namely *R25A* and *R25B*, entering **HX-A** and **HX-B** respectively.

3. The mass flows of *R25A* and *R25B* are established iteratively using the heat-exchanger energy balance equation (Equation (2.8)).
4. Once flow rates are determined, **HX-A** is sized using Aspen EDR *design mode* with predefined length and width based on the dimensions obtained for **HX-3** from Step 1. Consequently, the height of **HX-A** consistently remains smaller than that of **HX-3**.
5. The initial length and width of **HX-B** follows those for **HX-3** and **HX-A**, while the height is set to be equal to the difference between the height of **HX-3** and **HX-A**.
6. With these specifications, **HX-B** is subjected to simulation using O'Neil et al.'s catalytic PFHX kinetic model[45]. From the resulting plots of this simulation, the temperature profile of the streams and the final para-H_2 composition of the main-H_2 stream can be evaluated. The simulation results of **HX-B** using the initial dimensions are shown in Figure 4.3a.
7. As described by O'Neil et al.[45], the geometry of catalytic heat exchangers is primarily governed by conversion kinetics. Thus, the initial sizing of the catalytic PFHX is likely to be insufficient for the conversion process to reach equilibrium, as observed in the initial simulation of **HX-3**. In such cases, the initial dimensions of **HX-3** need to be readjusted, followed by a re-assessment of **HX-B** with its size recalculated using the same procedure (from Step 5 onward).
8. Adjustment of **HX-3's** dimensions and reevaluation of **HX-B's** simulation results are repeated until the desired temperature profile and para-H_2 compositions are attained in **HX-B**.

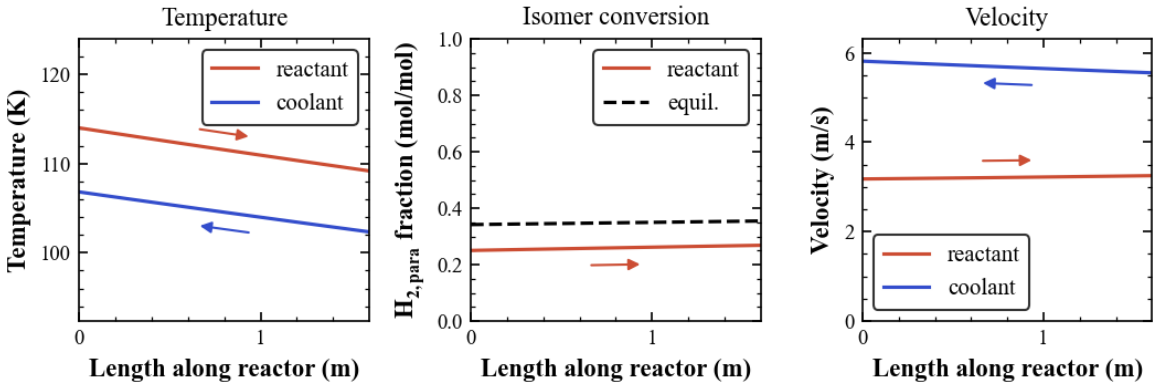

(a) Simulation results using initial **HX-B** dimensions, (1.59×1.5×0.17) m

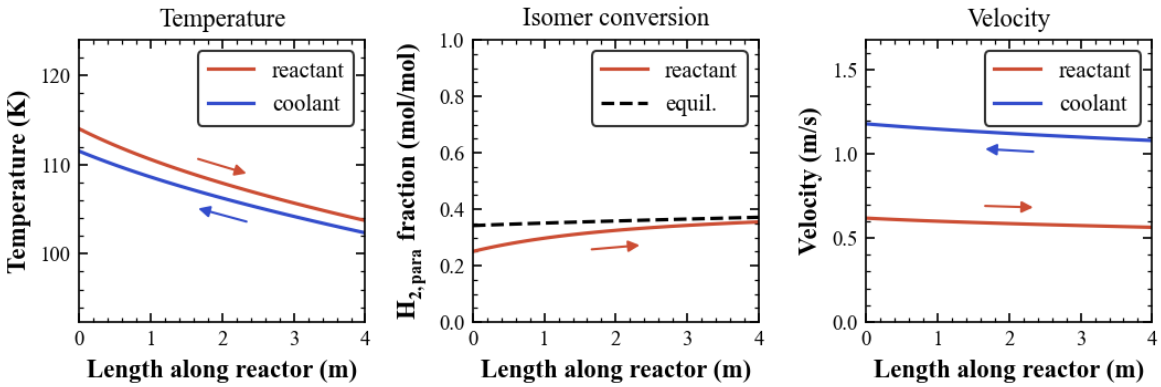

(b) Simulation results using final **HX-B** dimensions, (4.00×1.50×1.54) m

Figure 4.3: Stream profiles along the length of the **HX-B** obtained from the 1-D PFHX with ortho- to para-H_2 conversion kinetic model of O'Neil et al.[45]

9. For the preliminary design of **HX-3**, its' initial dimensions of (1.59×1.50×1.63) m are readjusted to (4.00×1.50×3.00) m in order for the para-H_2 composition to reach the equilibrium composition at the exit of **HX-B**. The results obtained from the simulation using the final **HX-B** dimensions, (4.00×1.50×1.54) m, are shown in Figure 4.3b.
10. In this study, the final size of the PFHX is established through an iterative process of trial and error. No formal optimization procedure is employed within this framework.

In addition to evaluating the stream temperature profile and conversion of hydrogen spin-isomers, the PFHX kinetic model is also capable of calculating the pressure drop for both the main hydrogen and the coolant streams in the PFHX. The calculated pressure drop values from the kinetic model are used to adjust the pressure values of the main hydrogen stream in the hydrogen liquefier simulation model. On the contrary, the pressure values of the hydrogen cooling streams are approximated with the pressure drops resulting from the initial sizing of the catalytic PFHX in Aspen EDR.

The step-by-step sizing procedure described above applied for the preliminary sizing of **HX-3** to **HX-6**. The preliminary design of heat exchanger **HX-7**, however, does not involve the utilisation of the simulation tool developed by O'Neil et al.[45]. This is because the influence of ortho-para conversion on the sizing of **HX-7** considered negligible. Given that the conversion of hydrogen spin isomers associated with the temperature drop in **HX-7** is estimated to be very small, less than 1% of its overall composition, the heat released as a result of this conversion is expected to be inconsequential. Therefore, the preliminary sizing and design of **HX-7** is solely conducted in Aspen EDR *design mode*, similar to the noncatalytic PFHXs of **HX-1** and **HX-2**.

During the preliminary sizing of **HX-3** to **HX-6** in this study, it is observed that most of the temperature values of the hydrogen coolant at the exit of the PFHX, calculated by the kinetic model, do not match the expected values from the calculation of the energy balance using the pseudo-equilibrium model by Valenti et al.[51] There is a possibility that the quantification of the exothermic energy resulting from the conversion of ortho- to para-H_2 has been approached differently by O'Neil et al.[45] and Valenti et al.[51] This matter necessitates further investigation, which is currently deferred for future works.

Due to the complexity of the process and equipment, unlike the non-catalytic PFHXs, the main focus of the preliminary designs for catalytic PFHXs in this study is only on determining the required dimensions of the PFHX cores. The procedure developed in this thesis ensures that the PFHX designs are sufficiently large to facilitate the necessary heat transfer process and enable the equilibrium conversion of hydrogen spin-isomers, while adhering to the dimensional constraints outlined in Table 4.1. These geometric parameters are considered to be sufficient for making sound cost estimations which are further described in the next chapter. The full results of the preliminary designs of catalytic plate-fin heat exchangers for all simulation scenarios are given in the GitHub repository: `https://github.com/pbtamarona/h2liquefaction/tree/main/thesisResults`..

4.2. Compressors

From the base process simulation in Aspen HYSYS, the inlet volumetric flow rates of the compressors **MRC-1**, **MRC-2**, **LPC** and **HPC** are calculated to be in the range of 4,000-85,000 m3/h with a maximum discharge pressure of 30 bar. As shown in Figure 2.17b, centrifugal compressors are the most suitable type of compressors for these operating conditions. Therefore, only the design of radial-flow turbo compressors is considered in this study. In this study, it is assumed that each radial-flow turbo-compressor design is equipped with an aftercooler that cools the compressor outlet gas to 298.15 K by means of cooling water.

As of this writing, radial-turbo compressors have not been implemented in the hydrogen

liquefaction industry. Some of the main challenges of implementing turbo-compressors for hydrogen application have been addressed in the literature review. To ensure that the outcomes of the centrifugal compressor preliminary designs of this thesis are technically feasible for the realisation of large-scale hydrogen liquefiers, this study strictly follows compressor design constraints that have been derived in accordance with the current technological limitations of turbo-compressors. The design limitations assumed for the preliminary design of centrifugal compressors are summarised in Table 4.2.

Table 4.2: Design limitations of centrifugal compressors

Parameter	Values	Unit
Max. Number of Stages per Compressor	8	stages
Min. Volumetric Inlet Flowrates	1,000	m^3/h
Max. Volumetric Inlet Flowrates	300,000	m^3/h
Max. Compressor Power	37,000	kW
Max. Impeller Tip Velocity	500	m/s

4.2.1. Selection of Number of Stages and Rotational Speed

As described in the literature review, Section 2.3.2, the initial selection for the number of stages and the rotational speed of turbo-compressors can be performed using the *n*-*z* selection diagram. To illustrate the selection process, the process data of the high-pressure compressor (**HPC**) from the base simulation are taken as an example. Table 4.3 below shows the initial design specification of HPC:

Table 4.3: High-Pressure Compressor System Initial Specification

Parameter	Values	Unit
Fluid	Hydrogen	
$\Delta h_{\text{is, comp}}$	2,093.06	kJ/kg
Isentropic power	29,948.72	kW
Mass Flowrate	14.31	kg/s
Inlet Condition		
Pressure	7.40	bar
Temperature	293.76	K
Enthalpy	3,871.75	kJ/kg
Entropy	44.96	kJ/kg·K
Isentropic Outlet Condition		
Pressure	29.8	bar
Temperature	437.62	K
Enthalpy	5,964.81	kJ/kg
Entropy	44.96	kJ/kg·K

The first step in the selection process is to determine the minimum number of stages of **HPC** to achieve the required pressure ratio. The pressure ratio of **HPC** is about 4.03. The minimum number of stages that can be selected for HPC is restricted by the compressor's impeller tip velocity. The impeller or blade tip velocity in the base scenario is limited to 500 m/s. Later in this thesis, the impact of using higher tip velocity will be evaluated.

The minimum number of compressor stages required can be determined from the maximum impeller tip velocity by following this approach:

1. Using the following equation below, the maximum isentropic enthalpy change, $\Delta h_{\text{is, stg}_{\text{max}}}$,

across one compressor stage can be determined:

$$\Delta h_{\text{is, stg}_{\text{max}}} = \psi_{\text{is}} \cdot u_{2,\text{max}}^2. \tag{4.1}$$

Here, the input value for the isentropic work coefficient, ψ_{is}, is assumed to be 0.45, as the polytropic efficiency of the centrifugal compressor is in its optimal range at $0.4 < \psi_{\text{is}} < 0.5$.[95]

2. Once the maximum isentropic enthalpy change per stage, $\Delta h_{\text{is, stg}_{\text{max}}}$, has been determined, one can estimate the minimum number of stages required by dividing the isentropic enthalpy difference, $\Delta h_{\text{is, comp}}$, required in the compression process by $\Delta h_{\text{is, stg}_{\text{max}}}$:

$$z_{\text{min}} = \text{Round}\left(\frac{\Delta h_{\text{is, comp}}}{\Delta h_{\text{is, stg}_{\text{max}}}}\right). \tag{4.2}$$

Note that in Equation (4.2), the minimum value is rounded to the nearest integer since the stipulation of $\psi_{\text{is}} = 0.45$ is not a strict requirement. Additionally, the actual impeller tip speed velocity of each compressor stage will be reevaluated throughout the preliminary design process, based on the rotational speed and number of stages of the compressor selected in each iteration. Nonetheless, through this method, it can be determined that for a maximum impeller tip velocity of 500 m/s, $\Delta h_{\text{is, stg}_{\text{max}}}$ is approximately 112 kJ/kg. This would correspond to a minimum number of compression stages of 19 for the **HPC** system. However, as stated in Table 4.2, the number of stages per compressor is limited to 8. Therefore, it is evident that the required HPC pressure ratio cannot be attained in a single high-pressure compressor.

In this study, the **HPC** system is designed as a series of three high-pressure compressors, namely **HPC-1**, **HPC-2** and **HPC-3**, with each compressor equipped with an aftercooler, as depicted in Figure 4.4. The pressure ratio in each compressor is approximately 1.59, which is determined using the following equation:

$$PR_{\text{comp}} = \left(\frac{P_{\text{dis,HPC}}}{P_{\text{suc,HPC}}}\right)^{1/z_{\text{comp}}}. \tag{4.3}$$

With this configuration, the minimum number of stages required for **HPC-1** and **HPC-2** is calculated to be equal to 5 stages, while **HPC-3** requires a minimum number of stages of 6.

Once the minimum number of stages is determined, the n-z selection diagram for each compressor can be plotted. To make the diagram useful, the number of stages that are included on the x-axis of the diagram will be in the range of $z_{\text{min}} < z < z_{\text{min}} + 2$, as compressors with $z > z_{\text{min}} + 2$ are considered undesirable, since this would significantly increase the CAPEX of the compressor. Furthermore, only curves for rotational speed, in the range of $z_{\text{min}} < z < z_{\text{min}} + 2$, which would correspond to a specific speed between $0.4 \geq \omega_s \geq 1$ (range of ω_s for the optimal efficiency of the centrifugal compressor), are plotted in the diagram. The specific speed, ω_s,

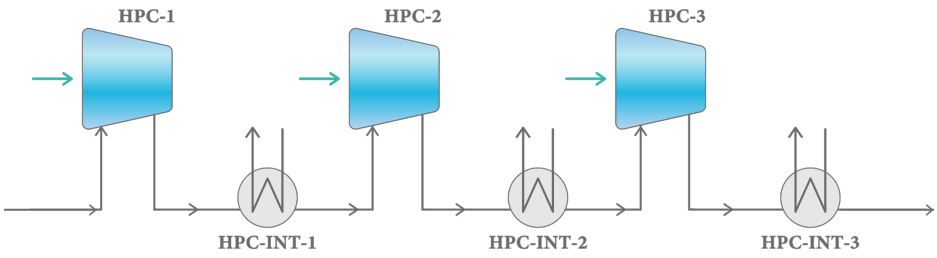

Figure 4.4: HPC system designed as three high-pressure compressors (with aftercoolers) in series

is calculated using Equation (2.21), with the inlet volumetric of the last compression stage approximated from isentropic calculations. Figure 4.5a and 4.5b show the n-z selection diagram for **HPC-1** and **HPC-2**, respectively. The source code of the programme to generate compressor n-z selection diagram based on the simulation process data, developed in this thesis, is accessible through the GitHub repository: `https://github.com/pbtamarona/h2liquefaction/tree/main/equipmentDesign`.

The n-z selection diagram evidently serves as a valuable tool for compressor designers, offering a spectrum of rotational speed and stage number options for compressor design. However, to make a feasible choice for compressor speed and stages, it is essential to calculate and validate various kinematic, thermodynamic and geometric stage parameters of the compressor. This includes the estimation of the isentropic efficiency of each compression stage. The following subsection delves into the calculation guidelines and design constraints for the preliminary kinematics, thermodynamics, and geometry of the centrifugal compressors used in this thesis.

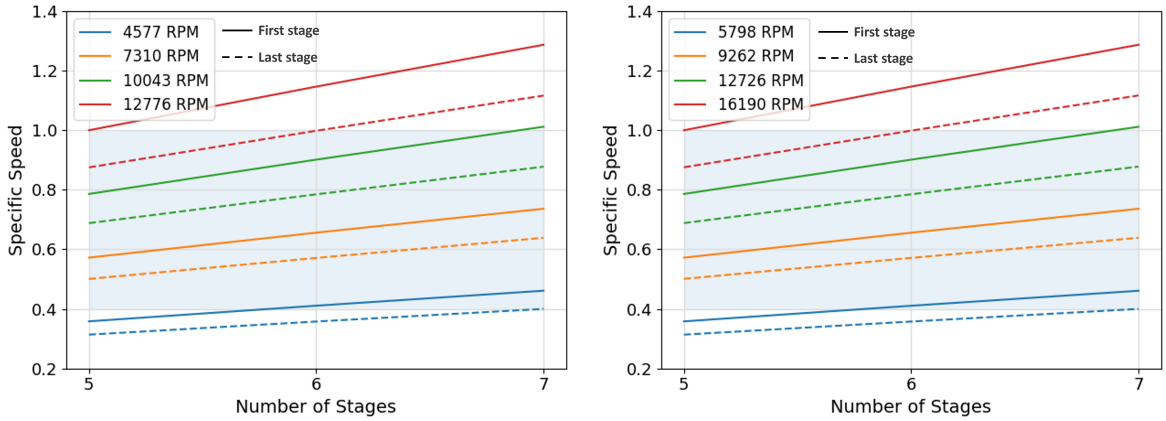

(a) HPC-1 **(b)** HPC-2

Figure 4.5: *n-z selection diagrams* for the high pressure compressors

4.2.2. Calculation of Kinematic, Thermodynamic and Geometry Parameters

The calculation procedure developed in this thesis is a simplification of the calculation procedure provided by Gambini & Vellini.[95] The block diagram of the centrifugal compressor stage calculation procedure is shown in Figure 4.6. The main difference between this procedure and the original stage calculation by Gambini & Vellini[95], shown in Figure 2.21a, is the stage losses calculation process in the original procedure which is used as the final calculation to verify the initial assumption of compressor efficiency. However, the stage losses calculation is an exhaustive process that requires a full evaluation of all kinematic, thermodynamic, and geometric parameters of the centrifugal compressor.

As shown in Figure 4.6, in this thesis, compressor stage losses will not be evaluated and compressor efficiency will be estimated based on correlations of polytropic efficiency as a function of the specific speed of the compressor stage. However, the results of kinematic, thermodynamic, and geometry calculations are compared with the constraints of the radial stage design parameters proposed by Gambini & Vellini.[95], in an iterative process. The preliminary design of centrifugal compressors is considered acceptable once the selection of the input parameters satisfies the design constraints during all stage calculation. The parameters constraints assumed for the preliminary design of multistage centrifugal compressors are summarised in Table 4.4. Considering that these constraints are not stringent for compressor design; instead, they represent recommended values intended to optimise efficiency, a 10% tolerance is granted for certain parameters when specified values are difficult to meet.

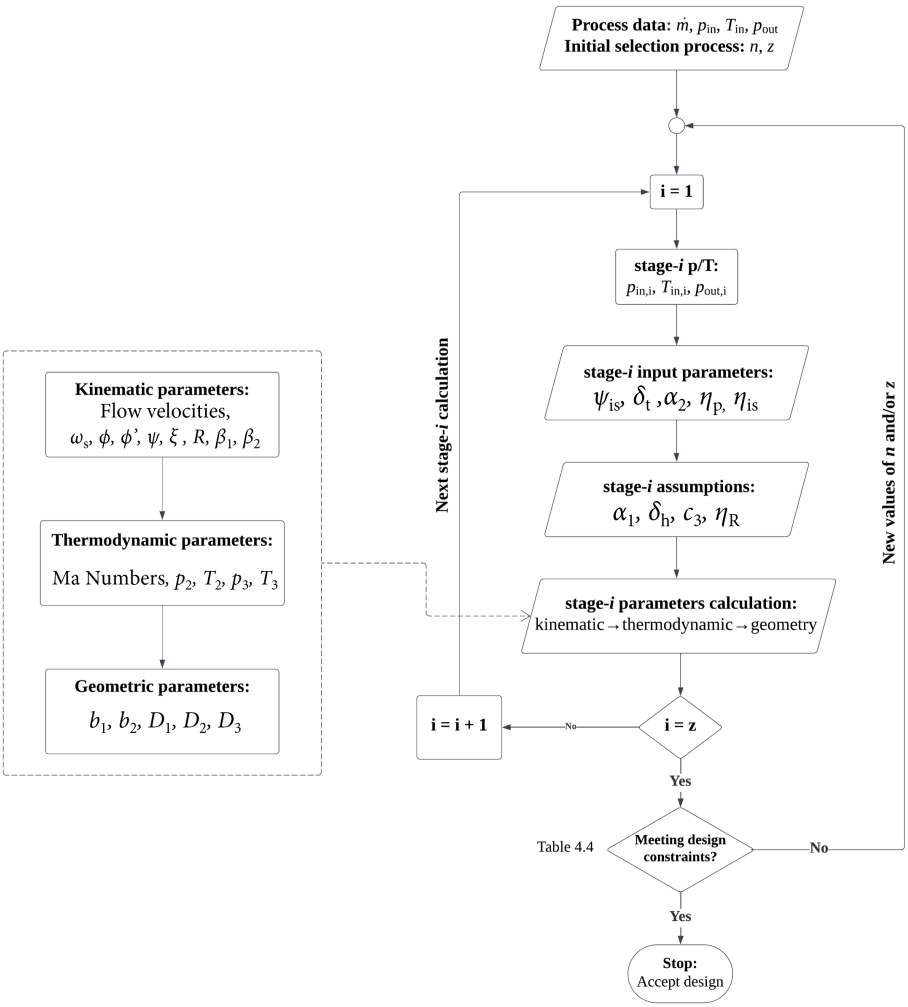

Figure 4.6: Multistage centrifugal compressor calculation block diagram

The main set of input parameters, in this *guided procedure*, can be expressed as functions of specific speed. Therefore, the related correlations suggested by various authors can be applied to choose the values for the input parameters. These correlations are as follows:

- Isentropic work coefficient, ψ_{is}, as proposed by Casey et al.[131]:

$$\psi_{is} = \psi_{medium} \cdot (1 - A) + \psi_{high} \cdot A + \psi_{medium} - \psi_{low} \cdot B, \tag{4.4}$$

where

$$\psi_{low} = 0.45, \qquad \psi_{medium} = 0.55, \qquad \psi_{high} = 0.02,$$

$$A = \frac{1}{1 + e^{-t_1}},$$

and

$$B = e^{-t_2},$$

where

$$t_1 = K_1 \cdot (K_2 + \log_{10} \omega_s), \qquad K_1 = 4, \qquad K_2 = -0.3,$$

and

$$t_2 = K_3 \cdot (K_4 + \log_{10} \omega_s), \qquad K_3 = 5, \qquad K_4 = 1.0.$$

Table 4.4: Parameter contraints of centrifugal compressors

Parameter	Range	Remarks
Specific speed, ω_s	0.4-1.0	
Flow coefficient, φ	0.2-0.3	
Work coefficient, ψ	0.5-0.6	
Degree of Reaction, R	0.6-0.7	10% tolerance
Rotor tip diameter ratio, δ_t	0.5-0.75	
δ_t/δ_h	0.2-0.7	
Rotor outlet absolute flow angle, a_2	60°-70°	10% tolerance
Rotor outlet relative flow angle, β_2	0°-60°	10% tolerance
Impeller tip speed velocity, u_2	< 500 m/s	
Mach Number, Ma	< 0.9	

- Rotor tip diameter ratio, δ_t, as proposed by Hazby et al.[132]:

$$\delta_t = 0.5 + 1.5\frac{\omega_s^2 \psi_{is}^3/2}{\pi}. \tag{4.5}$$

- Rotor outlet absolute flow angle, a_2, as proposed by Aungier et al.[133]:

$$a_2 = 72° - 0.5 \cdot \log\left(\frac{\omega_s^2 \cdot \psi^{3/2}}{\pi}\right) - 585 \cdot \left(\frac{\omega_s^2 \cdot \psi^{3/2}}{\pi}\right)^2. \tag{4.6}$$

- Stage polytopic efficiency, η_p, as proposed by Bommes et al.[131,134]:

$$\log_{10}(\eta_p) = -0.097358 - 0.0800538 \cdot \log_{10}\left(\frac{\omega_s}{2.9809}\right) + 0.151771 \cdot \left[\log_{10}\left(\frac{\omega_s}{2.9809}\right)\right]^2 + 0.340467 \cdot \left[\log_{10}\left(\frac{\omega_s}{2.9809}\right)\right]^3. \tag{4.7}$$

The stage's isentropic efficiency can be calculated from the polytopic efficiency using a simple iteration procedure based on the known fluid states, properties, and the definition of the two efficiencies.[a]

This thesis also used some stage parameters assumptions those are generally taken in radial compressor designs, such as:

- Inlet absolute flow angle, $a_1 = 0$, unless the relative Mach number need to be reduced.[95]
- Rotor hub diameter ratio, $\delta_h = 0.35$, as proposed by Hazby et al.
- Absolute velocity at the stator outlet, $c_3 = c_1$, which is a general initial assumption.[95]
- Rotor isentropic efficiency, $\eta_R = \eta_{is}$, which is a general starting assumption prior to stage loss calculation.[95]

Using the aforementioned set of input parameters and the above assumptions, the following parameters can be calculated immediately:

- Impeller tip velocity (blade speed at the rotor outlet), u_2:

$$u_2 = \sqrt{\frac{\Delta h_{is}}{\psi_{is}}}. \tag{4.8}$$

[a]This iterative process, along with the complete centrifugal compressor preliminary design algorithm developed in this thesis, is implemented in a Python programme, which can be accessed through the GitHub repository, at the following URL: `https://github.com/pbtamarona/h2liquefaction/tree/main/equipmentDesign`

- Work coefficient, ψ:

$$\psi = \frac{\psi_{\text{is}}}{\eta_{\text{is}}}. \tag{4.9}$$

- Rotor outlet diameter, D_2:

$$D_2 = \frac{60 \cdot u_2}{\pi \cdot n}. \tag{4.10}$$

- Blade height at rotor inlet, b_1:

$$b_1 = \frac{D_2}{2} \cdot (\delta_{\text{t}} + \delta_{\text{h}}). \tag{4.11}$$

- Rotor inlet meridional velocity, $c_{1\text{m}}$:

$$c_{1\text{m}} = \frac{2 \cdot \dot{V}_1}{\pi \cdot D_2 \cdot (\delta_{\text{t}} + \delta_{\text{h}}) \cdot b_1}. \tag{4.12}$$

- Flow coefficient, φ:

$$\varphi = \frac{c_{1\text{m}}}{u_2}. \tag{4.13}$$

- Rotor meridional velocity ratio. ξ:

$$\xi = \frac{1}{\varphi \cdot \tan a_2} \cdot (\psi + \varphi \cdot \delta_{\text{t}} \cdot \tan a_1). \tag{4.14}$$

- Degree of reaction, R:

$$R = 1 - \frac{\psi}{2} + \frac{\varphi^2}{2 \cdot \psi} \cdot \left[(1 - \xi^2) + \tan^2 a_1 \cdot (1 - \delta_{\text{t}}^2)\right] - \varphi \cdot \delta_{\text{t}} \cdot \tan a_1. \tag{4.15}$$

- Flow angles, β_1 & β_2:

$$\tan \beta_1 = \frac{\delta_{\text{t}}}{\varphi} - \tan a_1, \tag{4.16}$$

and

$$\tan \beta_2 = \frac{1}{\varphi \cdot \xi} \cdot (1 - \psi) - \frac{\delta_{\text{t}}}{\xi} \cdot \tan a_1. \tag{4.17}$$

Once the previously mentioned parameters are established, it becomes possible to compute the complete set of kinematic, thermodynamic, and geometric parameters (or even the stage losses). Velocity triangles of the flow at the inlet and outlet of each compression stage of the centrifugal compressors can also be constructed based on these results. The velocity triangles can be used for further analysis and development of the compressor design. The inlet and outlet velocity triangles for **T-3** are shown in Figure 4.7a and 4.7b, respectively.

The outstanding variables not yet outlined in this document, including the complete set of absolute, relative, and blade velocities at both the inlet and outlet points, as well as the Mach number assessment, along with a subset of geometric properties, are accessible within the source code of the compressor design software developed for this thesis. Given that stage losses are not assessed in this process, only a small subset of geometric parameters associated with design limitations and other kinematic/thermodynamic assessments are derived during this initial design phase.

In summary, the main results of the preliminary designs of the centrifugal compressors within this study are the number of compressor modules that are needed in the process to

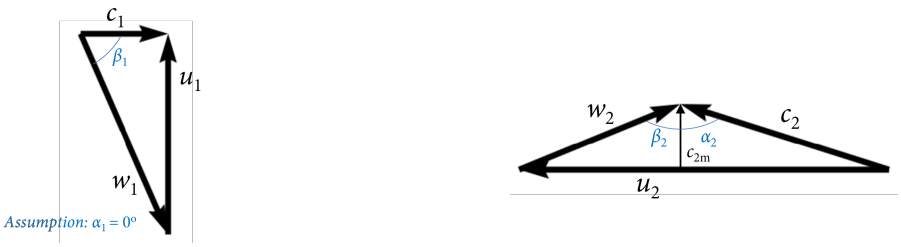

(a) Stage inlet

(b) Stage outlet

Figure 4.7: Velocity triangles in the first stage of centrifugal compressor **HPC-1**

achieve the required flow compression, along with the number of stages and rotational speed of each compressor. The required number of stages and speed of the compressors are selected initially with the *n-z* selection diagram and verified using the kinematics, thermodynamics, and geometry calculations. The efficiencies of the compressor stages are estimated by using the correlation of polytropic efficiency as a function of the specific speed (Equation (4.7)). The full results of the preliminary designs of the centrifugal compressors in all simulation scenarios are given in the GitHub repository: `https://github.com/pbtamarona/h2liquefaction/tree/main/thesisResults`.

4.3. Turbo-expanders

As explained in the literature review, only radial in-flow turbines, also called centrifugal turbines, are considered for the design of turbo-expanders required in the hydrogen liquefaction process described in this thesis. The initial selection process for the number of stages and rotational speed is nearly identical to the compressor selection process. The main difference, as described in the literature review, is on the definition of the reversible work, volumetric flow-rates and rotor's diameter in the expressions of the specific speed, ω_s and specific diameter, D_s. Similar to compressors, the preliminary design of turbo-expanders is in accordance with the design limitations assumed in this thesis. These limitations are outlined in Table 4.5.

Table 4.5: Design limitations of radial-inflow turbines

Parameter	Values	Unit
Max. Number of Stages per Turbine	1	stage
Min. Volumetric Inlet Flowrates	8.5	m^3/h
Max. Volumetric Inlet Flowrates	339,800	m^3/h
Max. Rotational Speed	100,000	rpm
Max. Turbine Power	1,500	kW
Max. Impeller Tip Velocity	500	m/s

4.3.1. Selection of Number of Stages and Rotational Speed

For the initial selection of number of stages and rotational speed, *n-z selection diagrams* can be created for the turbines. This can be done using a procedure similar to that used for compressors. However, the main difference between the two procedures lies in the calculations for determining the maximum isentropic enthalpy change across a single radial expansion stage. To illustrate the selection process, the process data of **T-3** obtained from the simulation detailed in Chapter 3 is employed as an example. The initial design specifications of **T-3** are provided in Table 4.6 below.

Table 4.6: Turbo-Expander **T3** Initial Specification

Parameter	Values	Unit
Fluid	Hydrogen	
$\Delta h_{is,comp}$	483.48	kJ/kg
Isentropic power	2,282.9	kW
Mass Flowrate	4.72	kg/s
Inlet Condition		
Pressure	29.48	bar
Temperature	111.99	K
Enthalpy	1,410.73	kJ/kg
Entropy	26.3	kJ/kg·K
Isentropic Outlet Condition		
Pressure	7.70	bar
Temperature	67.11	K
Enthalpy	927.25	kJ/kg
Entropy	26.30	kJ/kg·K

The pressure ratio of **T-3** is 3.83. In this thesis, as is the case for compressors, the minimum number of stages that can be selected for the turbines is limited by the turbine's impeller tip velocity. However, as stated in Table 4.5, the design constraints in this thesis dictate that a single turbo-expander may only consist of one expansion stage; thus, any expansion stage requirement that is higher than one will have to be designed with multiple turbo-expanders in series. The following procedure is used to determine the minimum number of expansion stages required based on the maximum impeller tip velocity:

1. Using the following equation, the maximum isentropic enthalpy change, $\Delta h_{\text{is, stg}_{\text{max}}}$, across one turbo-expander stage can be determined:

$$\Delta h_{\text{is, stg}_{\text{max}}} = \frac{(u_{1,\text{max}}/\nu_s)^2}{2}. \tag{4.18}$$

   Here, the input value for the isentropic velocity ratio, ν_s, is assumed to be 0.7, as the *total-to-static* efficiency of the centrifugal turbine is at maximum values in $0.68 < \nu_s < 0.71$.[95]
2. Once the maximum isentropic enthalpy change per stage, $\Delta h_{\text{is, stg}_{\text{max}}}$, has been determined, one can estimate the minimum number of stages required by dividing the isentropic enthalpy difference, $\Delta h_{\text{is, turb}}$, required in the expansion process by $\Delta h_{\text{is, stg}_{\text{max}}}$:

$$z_{\text{min}} = \text{Round}\left(\frac{\Delta h_{\text{is, turb}}}{\Delta h_{\text{is, stg}_{\text{max}}}}\right). \tag{4.19}$$

In Equation (4.19), the minimum value is rounded to the nearest integer since $\nu_s = 0.7$ is only a starting value for the number of stage selection. These turbine stage parameters will be re-evaluated throughout the preliminary design based on the selected rotational speed and number of stages of the turbine in each iteration. With a maximum impeller tip velocity of 500 m/s, the maximum isentropic enthalpy change per stage , $\Delta h_{\text{is, stg}_{\text{max}}}$, is approximately 255.1 kJ/kg. This would signify a need for a minimum of 2 expansion stages for **T-3**. Due to the constraint of one stage per turbine component, the design of the turbine expansion system for **T-3** is expanded to incorporate two turbo-expanders in series—namely, **T-3** and **T-4**—both operating at the same pressure ratio of 1.79. The original turbine denoted as **T-4** in the base simulation, depicted in Figure 3.1, will now be designated as **T-5**.

While **T-3** and **T-4** are distinct turbo-expanders housed in separate casings and arranged in series, this thesis assumes that they operate on the same rotating shaft. This configuration

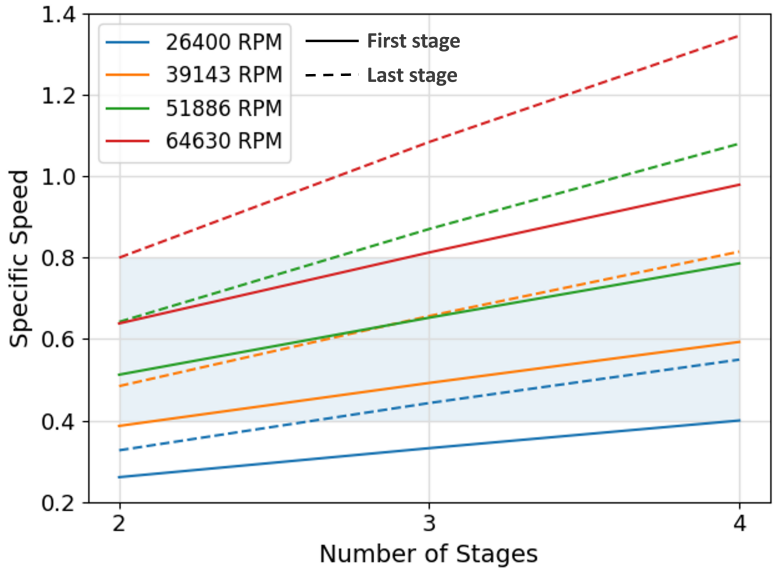

Figure 4.8: n-z selection diagram for the turbo-expander **T-3** and **T-4**

aims to maximise power recovery while minimising the space requirements and overall costs of generators. To determine the appropriate rotational speed, the n-z selection diagram can be created for the combined setup of **T-3** and **T-4** (equivalent to a two-stage turbo-expander system), following a procedure similar to that used for compressors. In this diagram, the rotational speed curves are plotted within the specific speed range known for optimal efficiency in radial inflow turbines, which lies between $0.4 \geq \omega_s \geq 0.8$.[104] Figure 4.8 illustrates the n-z selection diagram for **T-3** and **T-4**.

Following the turbine's n-z selection diagram, the subsequent task involves opting for the most suitable n-z configuration by assessing various parameters of the turbines, encompassing its' kinematics, thermodynamics, and geometry, including the isentropic efficiency of the expansion process. The fundamental framework of this approach bears similarities to the preliminary design process used for centrifugal compressors. Nevertheless, there exist disparities in the specific parameters and equations utilized. The full guideline and design constraints assumed for preliminary design of turbo-expanders is elaborated upon in the subsequent subsection.

4.3.2. Calculation of Kinematic, Thermodynamic and Geometric Parameters

The procedural framework developed in this thesis for radial inflow turbines closely resembles that devised for centrifugal compressors. Both methods simplify the calculation process originally proposed by Gambini & Vellini[95,104], by omitting the stage loss calculation step. However, the set of input and output parameters in the turbine preliminary designs varies from that of compressors. Figure 4.9 illustrates the procedure developed for evaluating turbo-expander parameters, as well as the inputs, assumptions and the resulting kinematic, thermodynamic, and geometric parameters within the process. The parameter constraints adopted for this preliminary design are summarised in Table 4.7. Given that these constraints are not strict, rather these are suggested values aimed for maximising performance, a 10% tolerance is given on some parameters when meeting the specified values becomes difficult.

In this *guided procedure*, the set of input parameters can be selected by using specific speed correlations from the literature. The correlations employed in this thesis are as follows:

- Isentropic velocity ratio, ν_s, as proposed by Aungier et al.[135]:

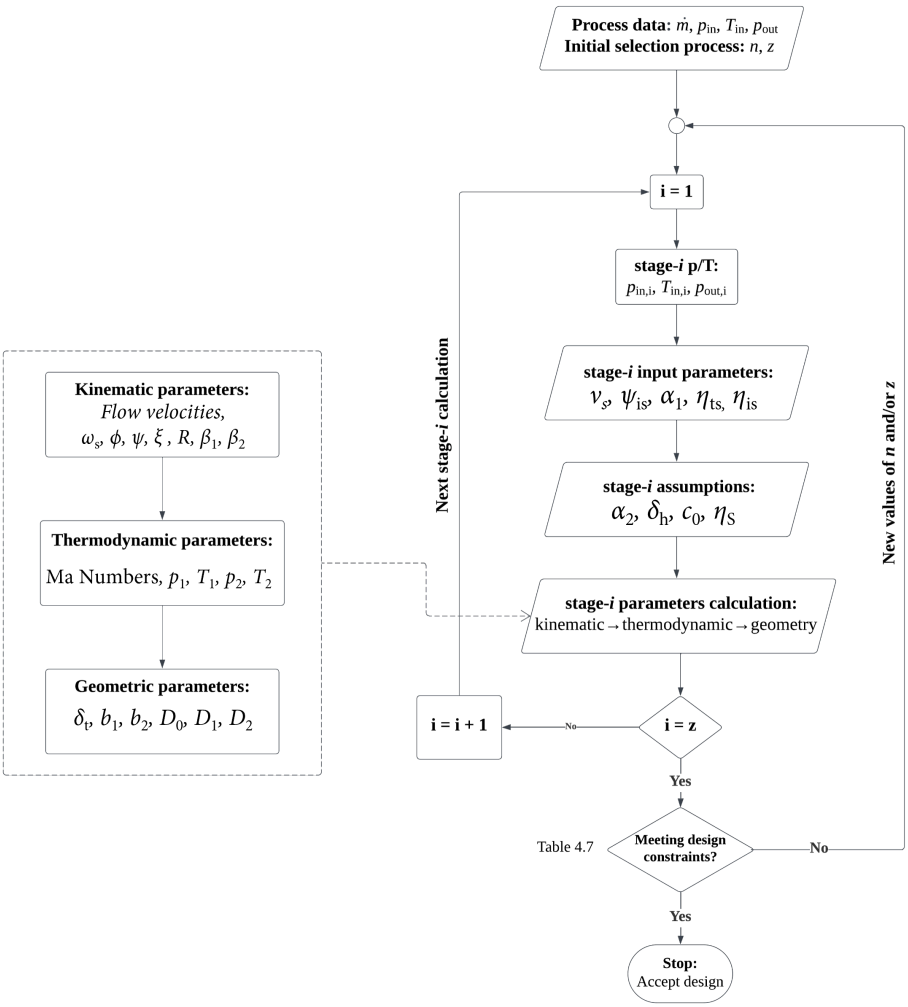

Figure 4.9: Radial in-flow turbine calculation block diagram

$$\nu_s = 0.737 \cdot \omega_s^{0.2}. \tag{4.20}$$

- Isentropic work coefficient, ψ_{is}:

$$\psi_{is} = \frac{1}{2 \cdot \nu_s^2}. \tag{4.21}$$

- Rotor inlet absolute flow angle, a_1, as proposed by Aungier et al.[135]:

$$a_1 = 79.2^\circ - 14.2 \cdot \omega_S^2 \tag{4.22}$$

- Stage *total-to-static* efficiency, η_{ts}, as proposed by Aungier et al.[135]:

$$\eta_{ts} = 0.87 - 1.07 \cdot (\omega_s - 0.55)^2 - 0.5 \cdot (\omega_s - 0.55)^3. \tag{4.23}$$

The stage's isentropic efficiency can be calculated from the *total-to-static* efficiency using a simple iteration procedure based on the known fluid state properties, velocities, and the definition of the two efficiencies.[b]

[b]This iterative process, along with the complete radial in-flow turbine preliminary design algorithm developed in this thesis, is implemented in a Python programme, which can be accessed through the GitHub repository, at the following URL: `https://github.com/pbtamarona/h2liquefaction/tree/main/equipmentDesign`

Table 4.7: Parameter contraints of radial in-flow turbines

Parameter	Range	Remarks
Specific speed, ω_s	0.4-0.8	
Flow coefficient, φ	0.2-0.3	10% tolerance
Work coefficient, ψ	0.8-1.0	10% tolerance
Degree of Reaction, R	0.45-0.65	
Rotor meridional velocity ratio, ξ	0.65-1.0	
Rotor tip diameter ratio, δ_t	<0.7	
δ_t/δ_h	> 0.4	
Rotor inlet absolute flow angle, a_1	66°-78°	10% tolerance
Rotor inlet relative flow angle, β_1	22°-40°	10% tolerance
Impeller tip speed velocity, u_2	< 500 m/s	
Mach Number, Ma	< 0.9	

This thesis also used some stage parameters assumptions those are generally taken in radial in-flow turbine designs, such as:

- Exit absolute flow angle, $a_2 = 0$, in order to minimize the kinetic energy at the rotor outlet.[104]
- Rotor hub diameter ratio, $\delta_h = 0.185$, as proposed by Aungier et al.
- Absolute velocity at the stator inlet, $c_0 = c_2$, which is a general initial assumption.[104]
- Stator isentropic efficiency, $\eta_S = \eta_{is}$, which is a general starting assumption prior to stage loss calculation.[104]

Using the aforementioned set of input parameters and the above assumptions, the following parameters can be calculated immediately:

- Impeller tip velocity (blade speed at the rotor inlet), u_2:

$$u_1 = \sqrt{\frac{\Delta h_{is}}{\psi_{is}}}. \tag{4.24}$$

- Work coefficient, ψ:

$$\psi = \psi_{is} \cdot \eta_{is}. \tag{4.25}$$

- Rotor outlet diameter, D_2:

$$D_1 = \frac{60 \cdot u_1}{\pi \cdot n}. \tag{4.26}$$

- Rotor inlet meridional velocity, c_{1m}:

$$c_{1m} = u_1 \cdot \frac{\psi}{\tan a_1}. \tag{4.27}$$

- Blade height at rotor inlet, b_1:

$$b_1 = \frac{\dot{V}_1}{\pi \cdot D_1 \cdot c_{1m}}. \tag{4.28}$$

- Rotor meridional velocity ratio, ξ, as proposed by Aungier et al.[135]:

$$\xi = \frac{c_{1m}}{c_{2m}} = \left[1 + 20 \cdot \left(\frac{b_1}{D_1}\right)^2\right]^{-1}. \tag{4.29}$$

- Flow coefficient, φ:

$$\varphi = \frac{c_{1m}}{\xi \cdot u_1}. \tag{4.30}$$

- Rotor tip diameter ratio, δ_t:

$$\delta_t = \sqrt{\delta_h^2 + \frac{4 \cdot \dot{V}_2}{\pi \cdot \varphi \cdot u_1 \cdot D_1^2}}. \tag{4.31}$$

- Degree of reaction, R:

$$R = 1 - \frac{\psi}{2} + \frac{\varphi^2}{2 \cdot \psi} \cdot \left[(1 - \xi^2) + \tan^2 a_2 \cdot (1 - \delta_t^2)\right] + \varphi \cdot \delta_t \cdot \tan a_2. \tag{4.32}$$

- Flow angles, β_1 & β_2:

$$\tan \beta_1 = \frac{1}{\varphi \cdot \xi} \cdot (\psi - 1) - \frac{\delta_t}{\xi} \cdot \tan a_2, \tag{4.33}$$

and

$$\tan \beta_2 = \frac{\delta_t}{\varphi} + \tan a_2. \tag{4.34}$$

After establishing the aforementioned parameters, it becomes feasible to compute the comprehensive set of kinematic, thermodynamic, and geometric parameters, or even include stage losses if required. Velocity triangles of the flow at the inlet and outlet of the radial turbine stage can also be constructed based on these results. The velocity triangles can be used for further analysis and development of the turbine design. The inlet and outlet velocity triangles for **T-3** are shown in Figure 4.10a and 4.10b, respectively.

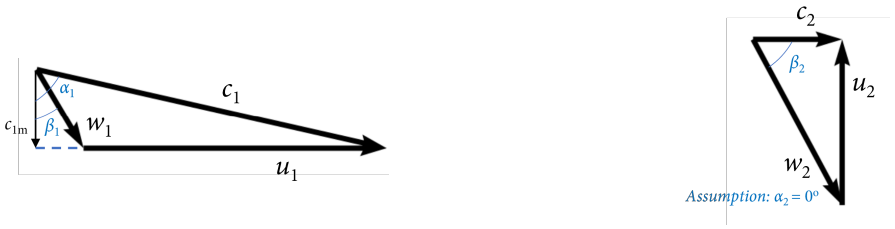

(a) Stage inlet

(b) Stage outlet

Figure 4.10: Velocity triangles in the radial stage of turbine **T-3**

The variables that have not been previously outlined in this document, encompassing absolute, relative, and blade velocities at inlet and outlet points, as well as Mach number analysis and a subset of geometric properties, are available within the source code of the turbine design software developed for this thesis. As the assessment of stage losses is not encompassed in this process, only a limited subset of geometric parameters tied to design constraints and other kinematic/thermodynamic evaluations are derived in the initial design phase.

In summary, the key outcomes of the preliminary radial in-flow turbine designs in this study encompass the determination of the necessary number of turbine modules (which corresponds to the number of the expansion stage due to design constraints) within the process to achieve the required expansion. This is then followed by the determining the acceptable rotational speed for the turbo-expander system. The initial selection of the required operating speed and number of turbines is accomplished using the n-z selection diagram, and their validity is confirmed through iterative kinematic, thermodynamic, and geometric calculations. The efficiency of the expansion stages is approximated using the correlation between *total-to-static* efficiency and specific speed (as shown in Equation (4.7)). A comprehensive presentation of the results of the preliminary radial-inflow turbine designs across all simulation scenarios is provided in GitHub repository: `https://github.com/pbtamarona/h2liquefaction/tree/main/thesisResults`.

4.4. Cryogenic Adsorbers

In this study, temperature-swing adsorbers are selected as the cryogenic adsorption system in the hydrogen liquefaction process. The preliminary design of the TSA system in this study focusses on estimating the required size and number of adsorber columns. These parameters are considered important information necessary for the sizing of the precooling coldbox as well as for making a sound estimation of the plant costs related to the adsorption system.

The size of adsorber column is characterised by the diameter and height of the column. This thesis utilises a python source code for the sizing of the hydrogen adsorption system developed by Kandasamy[136] to determine the size and number of TSA columns required for the hydrogen liquefaction plant under evaluation. The adsorber sizing algorithm developed by Kandasamy[136] is based on the design calculation procedure described by Campbell.[106]

This thesis assumes two adsorption vessels in parallel configuration and is alternately switched every 12 hours, with an operating lifetime of 5 years. The hydrogen feed is assumed to contain water impurities with 100 ppm concentration, since sizing evaluation using high water impurities would give the largest column requirement compared to evaluating with other impurities. The adsorber columns are assumed to be filled with molecular sieve 4A, which according to Campbell[106] is capable of adsorbing molecules with an effective diameter less than 4 angstrom, such as water, nitrogen, methane, etc. Besides calculating the required column diameter and height, the calculation tools provided by Kandasamy[136] also estimate the pressure drop experience by the hydrogen feed as it flows through the adsorption column.

The regeneration process of the adsorbers would most likely to utilise some part of the warm hydrogen streams from the Claude cycle as the high-temperature source, however, the full evaluation of this process will not be covered in this study. The full results of the preliminary designs of the temperature-swing adsorption systems for all simulation scenarios are given in GitHub repository: `https://github.com/pbtamarona/h2liquefaction/tree/main/thesisResults`.

4.5. Coldbox

The preliminary design of coldbox in this study focus on estimating the required coldbox volumes for both the precooling and liquefier system. The precooling coldbox would need to be sufficiently large to encapsulate the components of the precooling system that are fully or partly operating in cryogenic conditions. These consists of **HX-1** and **TS-ADS** columns. Similarly, the cryogenic liquefier coldbox must be suitably sized to contain the Claude liquefier's components that are fully or partly operating in cryogenic conditions. These include the PFHXs (**HX-2** to **HX-7**), turbo-expanders (turbo-generators in power-recovery scenarios), vapor-liquid separator, and cryogenic pump.

In addition to the main equipment, there are also piping and auxiliary process items that are essential to the operation of the liquefier, such as valves, control and measurement devices, etc. To estimate the volume of these elements, the PFHXs and the separator column are given a clearance of 1.3 from their core volumes. For single and multiple turbo-expanders, in both parallel or series configurations, the volume estimations consider the additional space needed for their connections and instrumentation. The estimated footprints of the turbo-expander systems are approximated based on information extracted from turbine brochures from various manufacturers. These estimations are shown in Table 4.8.

The necessary coldbox volume is estimated to be the total volumes of the internal components, including their clearances, accommodated within the vessel. An additional clearance of 10% is further added to the sum of the component volumes to take into account the coldbox's wall thickness and insulation material. In this study, both the precooling and liquefier coldboxes, are

Table 4.8: Estimation of turbo-expanders volume

Expander Systems	Est. Length	Est. Width	Est. Height	Unit
Small turbine (< 300 kW)	158.75	182.9	152.4	cm
1 Turbine	158.75	365.8	304.8	cm
1 Turbine + Generator	317.5	365.8	304.8	cm
2 Turbine	317.5	365.8	304.8	cm
2 Turbine + Generator	476.25	365.8	304.8	cm
3 Turbine	476.25	365.8	304.8	cm
3 Turbine + Generator	635	365.8	304.8	cm
4 Turbine	635	365.8	304.8	cm
4 Turbine + Generator	793.75	365.8	304.8	cm
5 Turbine	793.75	365.8	304.8	cm
5 Turbine + Generator	952.5	365.8	304.8	cm
6 Turbine	952.5	365.8	304.8	cm
6 Turbine + Generator	1,111.25	365.8	304.8	cm

assumed to have a capsule-like structure (spherocylinder), a three-dimensional shape consisting of a cylinder with hemispherical ends. The main geometrical parameters of the vessel are the radius and the height of the cylinder. Once the required volume of the vessel is determined, its optimised radius and height values are determined using Microsoft Excel's GRG Nonlinear Solver. The values of the radius and height of the liquefier coldbox are limited to 5.5 m and 40 m, respectively. These constraints are based on the current logistical limitation of vacuum-insulated coldbox (see Section 2.3.5).

5

Techno-economic Analysis

Techno-economic analysis (TEA) is a method for evaluating the economic performance of a technology. In this thesis, TEA is performed to assess the overall value of a large-scale hydrogen Claude liquefier, enabling analysts to objectively weigh the benefits of liquid H_2 against the cost of liquefaction. The main objective of the TEA in this thesis is to compute the SLC of a large-scale hydrogen liquefaction plant based on the Claude-cycle concept described in Chapter 3. Subsequently, in the following chapter, a range of cost sensitivity analyses will be conducted to investigate how specific parameters impact the cost efficiency of the facility.

Within this TEA, the CAPEX and OPEX of the large-scale high-pressure hydrogen Claude cycle concept are estimated. These expenditures are derived with the help of the Aspen Process Economic Analyzer (APEA) software. APEA is chosen due to its capability to project equipment expenses based on fairly current cost data gathered from actual EPC projects and equipment manufacturers. Besides estimating equipment purchase costs, APEA also assesses total installed costs, encompassing both direct and indirect field costs. A noteworthy advantage of opting for APEA, in contrast to other methodologies, lies in its integration with Aspen HYSYS simulation software, which is employed for the process modelling conducted in this thesis. Estimation of main process equipment is based on their design parameters established from the equipment preliminary design and sizing, as detailed in Chapter 4. Alongside capital costs, APEA also facilitates the calculation of the plant's operating costs, encompassing both variable and fixed operating expenditures.

The subsequent sections discuss about the workflow devised for conducting TEA on hydrogen liquefiers within this thesis. followed by the description of the general specification, equipment input parameters, and process assumptions that serve as the basis for the techno-economic analysis of hydrogen liquefiers performed in this thesis.

5.1. APEA Workflow and Project Basis

The Aspen Process Economic Analyzer is designed to automate the preparation of comprehensive designs, cost estimates, investment analyses, and timelines from minimal project scope definitions. This can include inputs from process simulation outcomes or lists of sized equipment. The recommended project workflow for APEA is depicted in Figure 5.1a. During the project workflow, user is allowed to go back to previous steps to refine the project cost evaluation.

Within the context of this thesis, some adjustments have been made to the APEA workflow.

These modifications permit the calculation of the SLC for the hydrogen liquefaction process under evaluation. The TEA workflow tailored for the cost analysis in this study is illustrated in Figure 5.1.

5.1.1. Project Basis

The project basis defines specifications that pertain to the overall project scenario. These specifications wield an influence over the design and cost estimation process by establishing system defaults and environmental variables. Within APEA, these specifications encompass various components, including **Project Properties**, **General Project Data**, **Basis for Capital Costs**, **Investment Analysis**, **Process Designs**, and **Streams**.

Project Properties and **General Project Data** provide the means for users to specify the project's description and owner. Additionally, users can specify the base unit of measure, the base country, and the base currency for the evaluation of project costs. The setting of the country base has implications on several system default values, including the base cost index, wage rates for crafts, as well as costs associated with engineering, construction office functions, and project management. For the purposes of this thesis, European Union (EU) and Euro (EUR) are selected

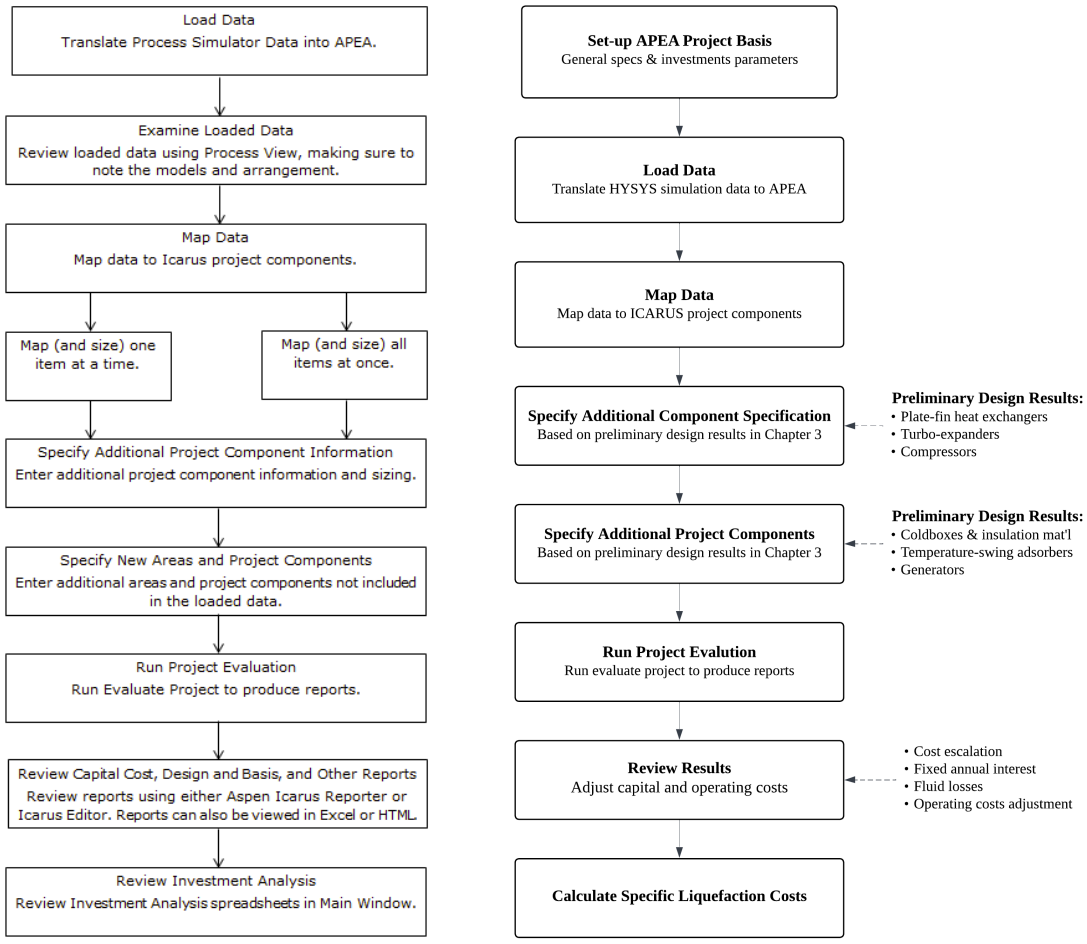

(a) General projeect workflow recommended by APEA[a] **(b)** TEA Workflow developed in this thesis

Figure 5.1: Techno-economic analysis workflow using APEA

[a]Obtained from Aspen Process Economic Analyzer™ V12 software *Help* pages

as the project country and currency base, respectively.

The **Process Design** specifications are used in APEA projects that contain a simulator input. These specs facilitate APEA to map the simulator equipment models into ICARUS project components. In this study, the Aspen HYSYS process simulation file developed in Chapter 3 and refined by the preliminary design results in Chapter 4 is loaded into APEA **Process Design**. All process unit operations from the simulation, including pumps, vapour-liquid separators, etc., are mapped onto APEA (ICARUS) project components and further detailed with additional specifications derived from the preliminary design results (see workflow in Figure 5.1).

In **Process Design** specifications, utilities used for process heating and cooling are outlined within the *Utility Specification*. This includes the specification and unit costs of the cooling water streams intended for aftercoolers in the process model. For both the process simulation and the TEA model, the cooling water for aftercoolers is assumed to operate at a pressure of 3.45 bar, with inlet and outlet temperatures of 20°C and 35°C, respectively. The unit cost of cooling water is set at 2.12×10^{-4} €/MJ.

The **Streams** specifications in APEA serve the purpose of generating, modifying, or removing streams within a project. However, in this particular study, no alterations or additions to the streams originating from the process simulation are necessary.

Basis for Capital Costs

The **Basis for Capital Costs** specifications, consists of *General Specs*, *Construction Workforce*, *Currency* and *Input/Output Units of Measure Customization*. The *General Specs*, specifically, exert a significant influence over both the total capital expenditure and operating costs of the project.

In *General Specs*, there are Process Description, Process Complexity, and Project Type parameters, which combine to generate the contigency percentage (of the total project cost). These independent parameters result in a non-linear combination that produces the final value of the contingency percentage. In addition to adjusting the contigency percentage, Process Description also governs the design allowances for all equipment whose material cost is system generated. Project Type, on the other hand, shapes the configuration of the project's electrical power distribution and process control systems.

The *General Specs* also includes Project Location, wields an impact the cost estimation of domestic freight, ocean freight, and taxes/duty (expressed as a percentage of material costs), as well as the equipment rotating spares (as a percentage of the purchase cost of all rotating equipment). Additionally, within the *General Specs* section, there's a field to input the Estimated Starting Date of Basic Engineering. This date marks the commencement of the project schedule, which involves estimating timelines and durations for design engineering, procurement, material and equipment delivery, site development, and construction. This date also plays a role in determining capital cost escalation or de-escalation from APEA's cost/pricing basis.

For this thesis, APEA Version 12 was used, which estimates equipment costs based on a pricing update from the 1st Quarter of 2019. In this particular study, capital cost escalation is manually calculated using Equation (2.27), based on the 2019 and 2022 CEPCI Index. As a result, the Estimated Starting Date of Basic Engineering is set to 1 April 2019.

Furthermore, *General Specs* entail additional inputs such as Process Control, Soil Conditions Around Site, Equipment Specification, and others. These parameters collectively define the additional general equipment and plant design conditions applied throughout the cost estimation of the entire project. Further details can be found in the APEA *Help* pages. Figure 5.2 shows the input values of APEA *General Specs* for the Base Scenario in this thesis.

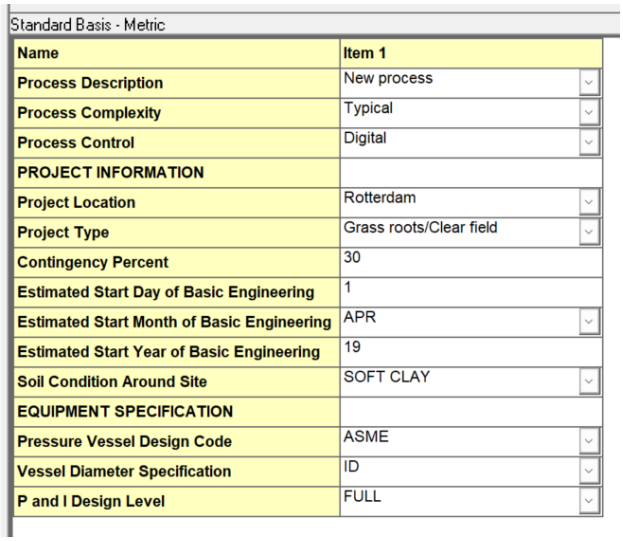

Standard Basis - Metric

Name	Item 1
Process Description	New process
Process Complexity	Typical
Process Control	Digital
PROJECT INFORMATION	
Project Location	Rotterdam
Project Type	Grass roots/Clear field
Contingency Percent	30
Estimated Start Day of Basic Engineering	1
Estimated Start Month of Basic Engineering	APR
Estimated Start Year of Basic Engineering	19
Soil Condition Around Site	SOFT CLAY
EQUIPMENT SPECIFICATION	
Pressure Vessel Design Code	ASME
Vessel Diameter Specification	ID
P and I Design Level	FULL

Figure 5.2: **General Specs** inputs for the techno-economic analysis of the base scenario

Investment Analysis

In addition with *General Specs*, APEA also provides the user the ability to define the project *Construction Workforces*. Construction workforce specifications are divided into General Rates and Craft Rates. Upon selecting a country base location, the user obtains a base set of crafts, wage rates, crew mixes, production rates, and other related parameters for field manpower consistent with the selected country base. Given that this study does not include an analysis on the the latest average wage and productivity rates for common construction workers in Europe, the **Construction Workforces** values are determined using the default settings supplied by APEA for projects centered in Europe.

The **Investment Analysis** specifications, consists of *Investment Parameters*, *Operating Unit Costs*, *Raw Material Specifications* and *Product Specifications*.Given that the primary objective of TEA in this thesis is to compute the SLC of a hydrogen liquefaction plant, detailed specifications for *Raw Materials and Product Specifications* are unnecessary (as these pertain more to the assessment of plant profitability and ROI). Due to the same reason, several parameters within *Investment Parameters* need not be specified for this study, except for the Operating Cost Parameters and the Facility Operation Parameters, which contribute to the calculation of total operating cost per period (the period in this study is set to one year—52 weeks).

The Operating Cost Parameters consist of Operating Charges, Plant Overhead, and G&A Expenses. Operating Charges include operating supplies and laboratory charges, expressed as a percentage of the operating labor costs. Plant Overhead encompasses charges during production for services, facilities, payroll overhead, and similar factors, expressed as a percentage of operating labor and maintenance costs. represent general and administrative costs incurred during production, such as administrative salaries/expenses, R&D expenses, and product distribution and sales costs. This value is specified as a percentage of the subtotal of operating costs.

The Facility Operation Parameters consist of Facility Type, Operating Mode, Length of Start-up Period, Operating Hours per Period, and Process Fluids. Facility Type defines the type of facility, influencing the number of operators per shift and maintenance costs for facility equipment. Operating Mode impacts the same parameters. The Length of Start-up Period doesn't directly affect operating cost calculations, but contributes to APEA project scheduling and cash-flow analysis, which are irrelevant to the calculation of SLC in this study. The Operating Hours per Period influence the total cost calculation for operating labor. Process Fluids indicate the types of fluids involved in the process, influencing both operating and maintenance costs. Figure

Investment Analysis Parameters

Name	Units	Item 1
Period Description		Year
Number of Weeks per Period	Weeks/period	52
Number of Periods for Analysis		20
Tax Rate	Percent/period	40
Interest Rate/Desired Rate of Return	Percent/period	20
Economic Life of Project	Period	10
Salvage Value (Percent of Initial Capital Cost)	Percent	20
Depreciation Method		Straight Line
ESCALATION PARAMETERS		
Project Capital Escalation	Percent/period	5
Products Escalation	Percent/period	5
Raw Material Escalation	Percent/period	3.5
Operating and Maintenance Labor Escalation	Percent/period	3
Utilities Escalation	Percent/period	5
PROJECT CAPITAL PARAMETERS		
Working Capital Percentage	Percent/period	5
OPERATING COSTS PARAMETERS		
Operating Supplies	Cost/period	25
Laboratory Charges	Cost/period	25
Operating Charges	Percent/period	25
Plant Overhead	Percent/period	50
G and A Expenses	Percent/period	8
FACILITY OPERATION PARAMETERS		
Facility Type		Chemical Processing Facility
Operating Mode		Continuous Processing - 24 Hou
Length of Start-up Period	Weeks	20
Operating Hours per Period	Hours/period	8,328
Process Fluids		Liquids and Gases

Figure 5.3: *Investment Parameters* inputs for the techno-economic analysis of the base scenario

5.3 shows the input values of APEA *Investment Parameters* for the Base Scenario in this thesis.

The *Operating Unit Costs* form specifies Labor Unit Costs and non-heat transfer Utility Unit Costs. Labor Unit Costs are given for Operators and Supervisors. The total cost of operating labor is computed through the following steps: 1.) Determining the total number of operators and supervisors necessary to run the facility for a certain number of hours; 2.) Adjusting that number for the number of hours the facility operates per period; 3.) Multiplying that number by the respective Labor Unit Costs and adding them together.

Operator labor includes all labor works that are associated with operating the facility, while supervision includes all the labor involved with overseeing the personnel that operate the facility. In this thesis, the values for the Operator and Supervisor Labor Unit Costs followed the default values given by APEA, which are 20 and 35 €/personnel·H.

The non-heat transfer Utility Unit Costs consist of Electricity, Potable Water, Fuel and Instrument Air costs. However, for this study, only the electricity cost holds relevance, as the other utilities aren't defined in the process plant model. In the base scenario, the electricity cost is set at 0.1 €/kWh. Nevertheless, a sensitivity analysis regarding electricity costs is executed within the TEA model, with outcomes discussed in the next chapter.

5.2. Equipment Mapping and Specifications

5.2.1. Compressors

The process simulation's compression unit operations are mapped to components within the ICARUS project. As the compressors in this analysis are of the centrifugal type, the models of

compression systems from HYSYS process simulations are mapped to the ICARUS' Gas Centrifugal Compressor - Horizontal (GC CENTRIF) model.

After each compressor is mapped to the APEA system, the minimum input parameters for estimating their capital costs are the actual gas flow rate at the inlet, and the design gauge pressure inlet and outlet. These elements, along with others, are filled automatically upon equipment mapping from HYSYS units. Although, two particular parameters remain unspecified, which are the number of impellers (or stages) and the rotational speed of the compressor. These values can be defined based on the preliminary design of the compressor conducted in this research. An exemplary representation of the APEA centrifugal compressor project specification interface is depicted in Figure 5.4. For compression system that required multiple compressors to be installed in parallel configuration, due to the centrifugal compressor design limitations, the total direct costs of the system can be estimated at once by specifying the number of parallel compressors in the "number of identical items" column within the specification form.

As explained previously, each compressor design is equipped with an aftercooler to bring the gas outlet temperature back to 25°C. In this study, the compressors' aftercoolers are mapped to ICARUS's TEMA Shell and Tube Heat Exchanger - Fixed tube, float. head, u-tube exchanger

HPC-1_@Compression System - Centrifugal compressor - horizontal

Name	Units	Item 1
Item Reference Number		1
Remarks 1		Equipment mapped from 'HPC-1_@Compression System'.
Remarks 2		
Item description		HPC-1_@Compression System
User tag number		HPC-1_@Compression System
Drawing reference number		
Structure tag		
Component WBS		
Quoted cost per item	EUR	
Currency unit for matl cost		
Source of quote		
Number of identical items		1
Installation option		
Code of account		
Icarus/User COA option		
Casing material		CS
Actual gas flow rate Inlet	M3/H	93,227.285046
Design gauge pressure Inlet	KPAG	638.15108
Design temperature Inlet	DEG C	20.613286
Design gauge pressure Outlet	KPAG	1,075.43599
Design temperature Outlet	DEG C	71.020792
Number of impellers		6
Compressor speed	RPM	8,000
Driver power	KW	10,404.739116
Molecular weight		2.01588
Specific heat ratio		1.406127
Compressibility factor Inlet		1.004399
Compressibility factor Outlet		1.006309
Intercooler required		NO
Intercooler type		WATER
Aftercooler required		NO
Aftercooler type		WATER
Inter/Aftercooler excess area	PERCENT	0
Maximum interstage temperature	DEG C	175
Intercooler outlet temperature	DEG C	30
Interstage pressure drop	KPAG	35
Driver type		MOTOR
Turbine gauge pressure	KPAG	2,050
Gear reducer type		
Lube oil system		YES
Allow resizing		

Figure 5.4: Centrifugal compressor HPC-1 component specification form in APEA

(HE TEMA EXCH) model. Since compressor aftercoolers were not included in the equipment preliminary design in this thesis, the default sizing and design results from APEA mapping are used as the basis of the aftercoolers capital estimate.

Once a process component is mapped and specified within APEA, users can run the item evaluation and generate a capital costing report to evaluate the direct capital costs estimation of the component.

5.2.2. Turbo-expanders (and Turbo-generators)

The simulation models of expansion turbines from Aspen HYSYS simulations are mapped to ICARUS project's Turbine Turbo-expander (TUR TURBOEXP) component model. Similar to compressors mapping, certain initial specifications of the turbine are automatically populated within the turbo-expander specification based on the process data imported from Aspen HYSYS. These specifications include the turbine's actual gas flow rate at the inlet and the design gauge pressure at the inlet and outlet of the turbine, which are the mandatory input parameters required for APEA to compute turbine capital costs.

Within the specification form, the refinement of turbine capital cost evaluation is possible by inputting the inlet design temperature parameter based on the turbine's process specifications. An exemplary representation of the APEA turbo-expander project specification interface is shown in Figure 5.4. For expansion system that required multiple turbo-expanders to be installed in parallel configuration, due to the turbo-expander design limitations, the total direct costs of the system can be estimated at once by specifying the number of the parallel components in the specification form.

T1 - Turboexpander

Name	Units	Item 1
Item Reference Number		30
Remarks 1		Equipment mapped from 'T1'.
Remarks 2		
Item description		T1
User tag number		T1
Drawing reference number		
Structure tag		
Component WBS		
Quoted cost per item	EUR	
Currency unit for matl cost		
Source of quote		
Number of identical items		1
Installation option		
Code of account		
Icarus/User COA option		
Actual gas flow rate Inlet	M3/H	1,690.767603
Design gauge pressure Inlet	KPAG	2,836.67108
Design temperature Inlet	DEG C	-199.2
Design gauge pressure Outlet	KPAG	678.17108
Power output	KW	1,127.271766
Molecular weight		2.01588
Specific heat ratio		1.493449
Compressibility factor Inlet		0.953206
Isentropic efficiency	PERCENT	89.69
Number of spare cartridges		0
Allow resizing		

Figure 5.5: Turbo-expander **T-1** component specification form in APEA

As explained in Section 3.1.2, two distinct SEC values of the hydrogen liquefier will be evaluated in this study, i.e. the SEC with electric power recovery (SEC_{recov}) and SEC without

electric power recovery (SEC_{base}) from turbines. For SEC_{recov} calculation, the additional capital and operating costs due to generators are necessary to be taken into account. Since the electric generators models are not included in the loaded process simulation file, the generators need to be added manually in APEA. The power generators are added by adding ICARUS project component Electrical generator - Steam or gas turbine drive (EG TURBO GEN) in the APEA project for each turbo-generators system. In the specification form, the driver type is specified to "NONE" in order to estimate solely the generator component costs (without including again the costs of the turbine system).

For a series of turboexpanders that operate on the same rotating shaft (such as T-3 and T-4, illustrated in Section 4.3), only one generator component is assumed to be added to this system, converting the accumulation of mechanical power from both turbines into electric power with the efficiency of 80%.

5.2.3. Plate-fin Heat Exchangers

The LNG multi-flow heat exchanger model from Aspen HYSYS simulations are mapped to ICARUS project's Heat Exchanger - Multi-stream, plate fin heat exchanger (HE PLATE FIN) component model. In APEA, the minimum input information so that the software can give an estimate for the direct cost of the plate fin heat exchangers are the dimensions of the PFHX core. These values are not automatically filled when the equipment are mapped in APEA. Therefore, the resulting dimensions from the preliminary equipment study must be entered.

HX-2 - Multi-stream, plate fin heat exchanger

Name	Units	Item 1
Item Reference Number		57
Remarks 1		Equipment mapped from 'HX-2'.
Remarks 2		
Item description		HX-2
User tag number		HX-2
Drawing reference number		
Structure tag		
Component WBS		
Quoted cost per item	EUR	
Currency unit for matl cost		
Source of quote		
Number of identical items		2
Installation option		
Code of account		
Icarus/User COA option		
Material		*A3003*
Core length	M	4.3976
Core width	M	1.5
Core height	M	2.8789
Number of streams		3
Parting sheet thickness	MM	1.5
Cap sheet thickness	MM	5
End bar width	MM	11.5
Side bar width	MM	11.5
Core weight	KG	17,910.7
Pipe material		AL
Layer data		
Stream data		
Allow resizing		

(a) HX-2

HX-3 - Multi-stream, plate fin heat exchanger

Name	Units	Item 1
Item Reference Number		56
Remarks 1		Equipment mapped from 'HX-3'.
Remarks 2		
Item description		HX-3
User tag number		HX-3
Drawing reference number		
Structure tag		
Component WBS		
Quoted cost per item	EUR	
Currency unit for matl cost		
Source of quote		
Number of identical items		1
Installation option		
Code of account		
Icarus/User COA option		
Material		*A3003*
Core length	M	4
Core width	M	1.5
Core height	M	3
Number of streams		4
Parting sheet thickness	MM	1.5
Cap sheet thickness	MM	6.35
End bar width	MM	38
Side bar width	MM	38
Core weight	KG	
Pipe material		AL
Layer data		
Stream data		
Allow resizing		

(b) HX-3

Figure 5.6: Plate-fin heat exchanger components specification form in APEA

For the noncatalytic heat exchangers, the calculation of PFHX direct costs can be refined by additionally entering the values of parting sheet thickness, cap sheet thickness, end bar width, side bar width, and core weight from the preliminary design results in Aspen EDR. For

catalytic PFHX, only the core dimensions determine from the simulation of PFHX with kinetic ortho-para conversion are entered to the PFHX specification form. Other parameters followed the default and estimated values given by APEA. Figures 5.6a and 5.6b show the exemplary APEA specification forms of noncatalytic and catalytic PFHX comnponents, respectively. For heat exchanger systems that employ identical PFHXs working in parallel, the total costs can be estimated by specifying the number of PFHXs within the specification form.

5.2.4. Vapor-liquid Separators, Adsorber Columns, and Coldboxes

The hydrogen liquefaction process model in Aspen HYSYS simulation contains unit operation models of two vapor-liquid separators, one liquid hydrogen pump and one mixed refrigerant pump. The vapor-liquid separators are mapped to ICARUS project's Vertical process vessel (VT CYLINDER). Since vapor-liquid separators were not included in the equipment preliminary design in this thesis, the default sizing and design results from APEA mapping are used as the basis of the phase-separator columns capital estimate.

For both pumps from the precooling and liquefaction systems, the simulation models are mapped to the ICARUS project's Centrifugal Pump - Single and multistage (CP CENTRIF). Just like the vapor-liquid separators, the cost estimation of both pumps are based on the quick sizing results of APEA mapping procedure.

In contrast, the feed-hydrogen adsorption system and the coldboxes are not included in the process simulation model. Therefore, like the power-generators, these components need to be manually added to APEA as ICARUS project components. As determined in the preliminary equipment designs, the liquefier plant adsorption system is designed as temperature-swing adsorbers with two adsorption vessels in parallel configuration to allow continuous operation. Thus, the adsorption system is mapped to ICARUS Project's Single Diameter Towers - Dual vessel temperature-swing adsorber (TW TS ADSORB).

Cost estimation can be performed based on the vessel diameter and the tangent-to-tangent height, which were determined during the preliminary design of TSA. To further refine the calculation, parameters such as number of vessel pairs, design gauge pressure, operating temperature, as well as the packing type and height can also be entered in the specification sheet. APEA (ICARUS) does not have a project component specifically for coldbox structure, although the software provides a model for cryogenic double-walled, superinsulated storage tank and cryogenic double-walled, full containment storage tank. In this thesis, the cost estimation of precooling and cryogenic liquefaction coldboxes are estimated with the ICARUS Project's Cryogenic Vertical Tanks - double walled, superinsulated (VT CRYOGENIC) component. Additionally, insulation material from ICARUS Project's Plant's Bulk - Packed Bulk Insulation is also added to the APEA project to refine the cost estimation of both coldbox modules.

The main parameters in the coldbox specification form are the vessel diameter and tangent-to-tangent height, which can be entered based on the preliminary sizing results of coldbox, as described in Chapter 4. The design and operating temperatures of the coldbox can also be defined in the specification form based on the lowest fluid temperature within the coldbox. The design gauge pressure of both coldboxes is assumed to be 5 bar. For the cryogenic liquefaction coldbox, the vacuum and jacket design gauge pressure are assumed to be absolute (-101.33 KPa) and near-absolute vacuum (-100 KPa), respectively. This is used to approximate the cost of vacuum insulation of industrial hydrogen liquefier coldbox.

The packed bulk insulation material of the coldbox is assumed to be Perlite. The required volume of the perlite is based on the insulation volume calculated in the preliminary sizing of coldbox (5% of coldbox volume).

5.3. Results and SLC Calculation

EXECUTIVE SUMMARY		
==========		
PROJECT NAME:	ThesisAnalysis	
CAPACITY:	ERR	
PLANT LOCATION:	Rotterdam	
BRIEF DESCRIPTION:	Claude H2 Liquefier	
SCHEDULE:	----------	
Start Date for Engineering	1APR19	
Duration of EPC Phase	63.00	Weeks
Completion Date for Construction	Friday, June 19, 2020	
Length of Start-up Period	20.00	Weeks
INVESTMENT:	----------	
Currency Conversion Rate	1.00	EUR/EUROPEAN EURO
Total Project Capital Cost	126,770,350.10	EUR
Total Operating Cost	22,910,507.72	EUR/Year
Total Raw Materials Cost	0.00	EUR/Year
Total Utilities Cost	16,833,980.57	EUR/Year
Total Product Sales	0.00	EUR/Year
Desired Rate of Return	20.00	Percent/Year
P.O. Period	0.00	Year

Figure 5.7: APEA executive summary report

Figure 5.7 illustrates an example of the executive summary report that is generated by APEA once the project evaluation has been completed. The primary findings displayed in this summary are the Total Project Capital Cost and Operating Cost. These constitute the key input parameters provided by APEA for computing the SLC of the hydrogen liquefier plant.

Prior to SLC calculation, some adjustments on the total capital cost and operating cost provided by APEA are necessary. To begin with, the total capital cost must be modified to account for the plant's working capital. This is essential since APEA only incorporates this contribution into the plant's cash-flow analysis (at one point in the project schedule, when the project enters the commissioning phase). In this study, a working capital of 10% (of the total project capital cost) is assumed.

In addition, the capital costs are susceptible to cost escalation. As mentioned earlier, the APEA V12 utilized in this thesis has been configured to estimate the plant's expenses based on a 2019 pricing basis. Consequently, the total project capital cost shown in Figure 5.7 represents the projected capital costs of the plant as of 2019. For the purposes of this study, these costs are adjusted to reflect anticipated expenses if computed using the 2022 pricing basis. This can be achieved using Equation (2.27), with the 2019 and 2022 CEPCI Index of 607.5 and 813, respectively.[b]

However, to accurately apply the adjustment using CEPCI, the calculation must be performed in US$. The following equation is used to adapt the capital costs to 2022 pricing in € using CEPCI and the average currency exchange rates in the base year of the capital costs pricing (in

[b]The CEPCI index used here is the CEPCI composite index which is assembled from a set of four sub-indexes: Equipment; Construction Labor; Buildings; and Engineering & Supervision. The values refers to https://personalpages.manchester.ac.uk/staff/tom.rodgers/Interactive_graphs/CEPCI.html?reactors/CEPCI/index.html, accessed on 28 August 2023.

this case 2019) and the year of 2022:[27]

$$f(C)_{€,2022} = f(C)_{€,\text{base}} \cdot \left(\frac{\text{US\$}}{€}\right)_{\text{base}} \cdot \frac{\text{CEPCI}_{2022}}{\text{CEPCI}_{\text{base}}} \cdot \left(\frac{€}{\text{US\$}}\right)_{2022}. \tag{5.1}$$

As shown in Equation (2.17), the calculation of the SLC requires the total project CAPEX to be broken down into its annual cost contribution. Within this study, the overall capital cost of the plant is considered as a fixed annuity payment, representing the annual amount that covers the capital expenditure. The subsequent formula for the capital recovery factor is utilised to determine the CAPEX annual cost contribution:

$$\text{CAPEX}_\text{a} = \text{CAPEX}_\text{tot} \cdot \frac{I_\text{fix} \cdot (1 + I_\text{fix})^{t_p}}{(1 + I_\text{fix})^{t_p} - 1}. \tag{5.2}$$

The fixed annual interest rate, denoted as I_fix, is commonly assumed within the range of 0.07 to 0.11, as stated by Syed et al.[113]. For the purpose of this thesis, a value of 0.09 is adopted. The specified payment duration in this analysis spans 20 years.

Given that the APEA project analysis period is setup for yearly assessments, the Operating Cost resulting from the APEA evaluation (as indicated in Figure 5.7) already equates to the annual operating cost of the liquefaction plant. This value encompasses both variable and fixed operating expenses, including the Operation & Maintenance expenditures. Nonetheless, the financial impact of fluid loss attributed to leaks from the liquefaction plant—primarily anticipated from turbomachinery components—has yet to be considered. This is because the leakage streams have not been taken into account in the process simulation.

This value incorporate the variable and fixed operating costs, including the Operation & Maintenance. However, the cost contribution of the fluid loss due to leaks from the liquefaction plant (expected mainly from turbomachinery components) has not yet considered, as the fluid loss is not included in the process simulations of this thesis.

For the base scenario, with a liquefier capacity of 125 TPD, hydrogen leaks are assumed to constitute 1.5% of the plant's capacity, while the cost of hydrogen itself is presumed to be 3.5€/kgH_2. The makeup flow required to compensate the mixed-refrigerant leaks is assumed to amount to 1.5 kg/h, with specific cost for MR of 5.0 €/kgH_2. These values factor into the final calculation of the total annual operating cost of the plant.

After determining the adjusted total annual CAPEX and OPEX of the plant, the SLC can be calculated using Equation (2.17). The annual capacity of the hydrogen liquefaction plant, denoted as $\dot{m}_{\text{LH}_2,a}$ in Equation (2.17), is calculated as follows:

$$\dot{m}_{\text{LH}_2,\text{a}} = U_\text{a} \cdot 8760 \frac{\text{hour}}{\text{year}} \cdot 3600 \frac{\text{second}}{\text{hour}} \cdot \dot{m}_{\text{LH}_2}. \tag{5.3}$$

The annual plant utilization rate is assumed to be 0.95, corresponding to approximately 8322 operating hours per year. An exemplary summary of liquefier plant SLC calculations based on the inputs of Total Project Capital Cost and Operating Cost obtained from APEA is presented in Figure 5.8.

For the computation of the SLC for a hydrogen liquefaction plant with power recovery (SLC_{recov}), further adjustments to the operating cost are required. First, the electricity costs need to be reduced manually with the amount of power that would be recovered by the turbo-generators. The second adjustment pertains to the operating labor costs. This is necessary because of the APEA evaluation for operating costs includes provisions for operating personnel specifically for the added generators. However, this seems to be unlikely in practise, given that the generators are likely to be installed within the liquefier coldbox. Consequently, the number

	Project Capital Cost	Plant Operating Cost
Values obtained from APEA:	**€ 140,236,953**	**€ 40,748,541**

Parameter	Value	Remarks
Working Capital (10%):	€ 14,023,695	
Total CAPEX (2019)	**€ 154,260,648**	
CEPCI 2019	€ 607.5	CEPCI Composite Index
CEPCI 2022	€ 813	CEPCI Composite Index
Total CAPEX (2022)	**€ 219,391,838**	Equation 5.1
Payment period	20	in years
Fixed annual interest	0.09	
Annual CAPEX	**€ 24,033,602**	Equation 5.2
Total annual OPEX	**€ 40,748,541**	
Hydrogen leaks	1.50%	of plant capacity
Refrigerant leaks	1.5	kg/h
Total annual OPEX with fluid loss	**€ 43,086,503**	
Total annual CAPEX+OPEX	**€ 67,120,106**	
Liquefier capacity	125	tonnes per day
Utilization rate	0.950	
SLC	**€ 1.55**	**per kg of LH_2**

Specific cost details			Remarks
Specific H2 cost	€ 3.5	per kg of H2	Assumption
Specific MR cost	€ 5.0	per kg of MR	Assumption
Electricity price	€ 0.100	per kWh	Base-scenario
Cooling water price	€ 0.000212	per MJh	Assumption

Figure 5.8: Summary of SLC calculations based on cost estimates from APEA

of operating personnel should remain unchanged. Therefore, in this thesis, the operating costs associated with labor, operational charges, plant overhead, and general administrative costs are maintained at the same level in both scenarios, consistent with the values established for the liquefier plant without power recovery.

6

Results & Discussions

In this chapter, the final configuration and stream data of the large-scale hydrogen liquefaction process plant are introduced. This layout is the result of refining the reference process described in Chapter 3 by incorporating insights from the preliminary equipment designs covered in Chapter 4. The chapter proceeds to evaluate the overall efficiency performance of the proposed plant design in terms of its equipment efficiency, overall exergy efficiency, and specific energy consumption. Additionally, the outcomes of the plant cost estimation, following the techno-economic workflow presented in Chapter 5, are presented.

Furthermore, the chapter presents the findings of sensitivity analyses performed on various operational and design parameters of the plant, including the cost of electricity, the hydrogen feed pressure, and the maximum compressor impeller tip velocity. This chapter also includes scale-up analyses aimed at assessing the economies of scale of the hydrogen liquefaction process in this study. Lastly, cost projection studies are conducted to provide insights on the future potential of hydrogen liquefaction technology.

6.1. Baseline Scenario

Figure 6.1 and 6.2 depict the refined process flow diagram compared to the reference process of 125 TPD Claude-liquefier discussed in Section 3.1.1. Noteworthy alterations to this diagram involve the addition of a number of compressor and turbo-expander components. The additional turbomachines become necessary due to the design constraints imposed in the equipment preliminary design, which essentially prevent the desired process compression or expansion ratio from being attained within a single turbomachinery component.

Based on preliminary design for the low-pressure compression equipment, it is determined that three separate compressor units are needed. Each compressor incorporates eight radial compression stages, and together they compress the hydrogen refrigerant from an initial pressure of 1.059 bar to a pressure of 7.402 bar. The isentropic efficiencies for individual LPC units, namely **LPC-1**, **LPC-2**, and **LPC-3**, are assessed at 83.03%, 82.45% and 82.66%, respectively.

Similarly, the design for the high-pressure compression components also calls for three distinct centrifugal compressor units, responsible for compressing the hydrogen coolant from 7.402 bar to 29.80 bar. However, unlike the LPCs, each HPC unit only comprises six compression stages. The calculated isentropic efficiency values for the respective **HPC-1**, **HPC-2**, and **HPC-3** systems are also found to be 83.26%, 82.95% and 82.93%, respectively.

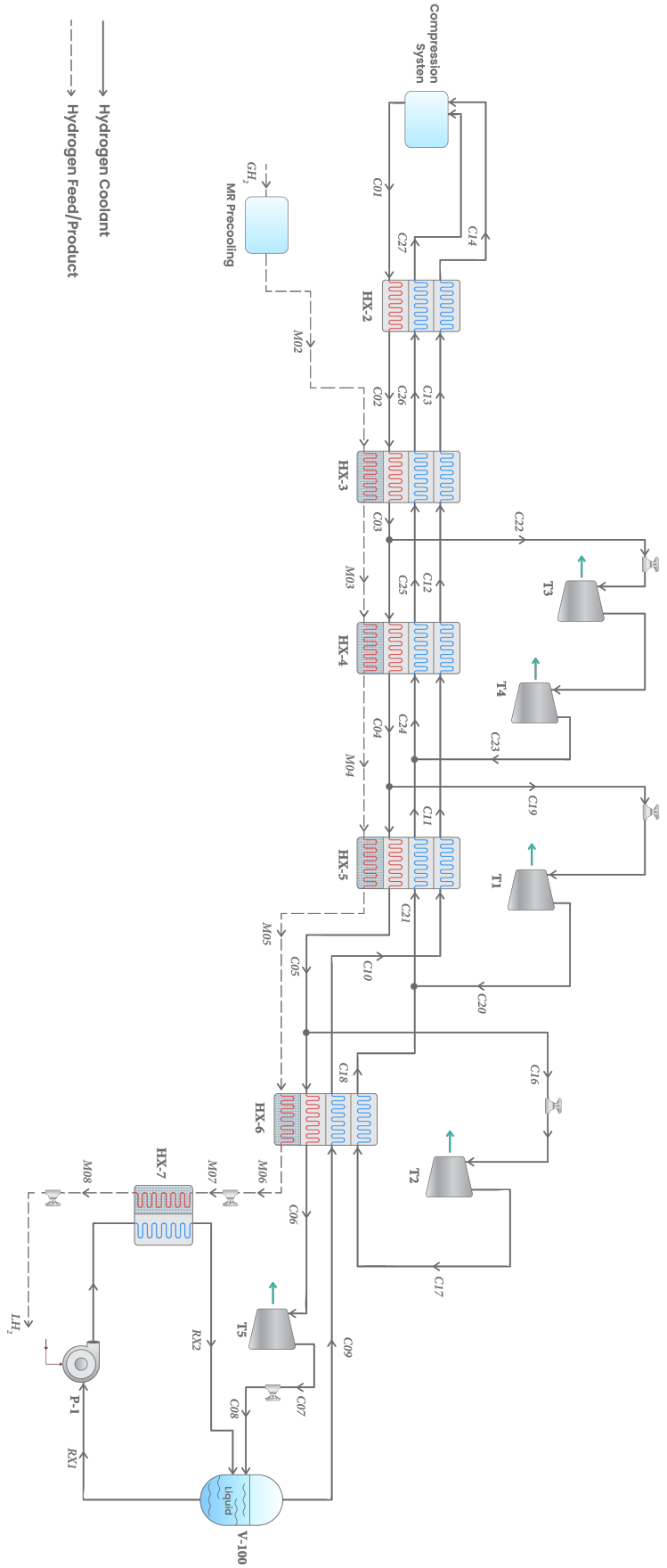

Figure 6.1: Process flow diagram of the baseline scenario (design) of the Claude-cycle H_2 liquefier

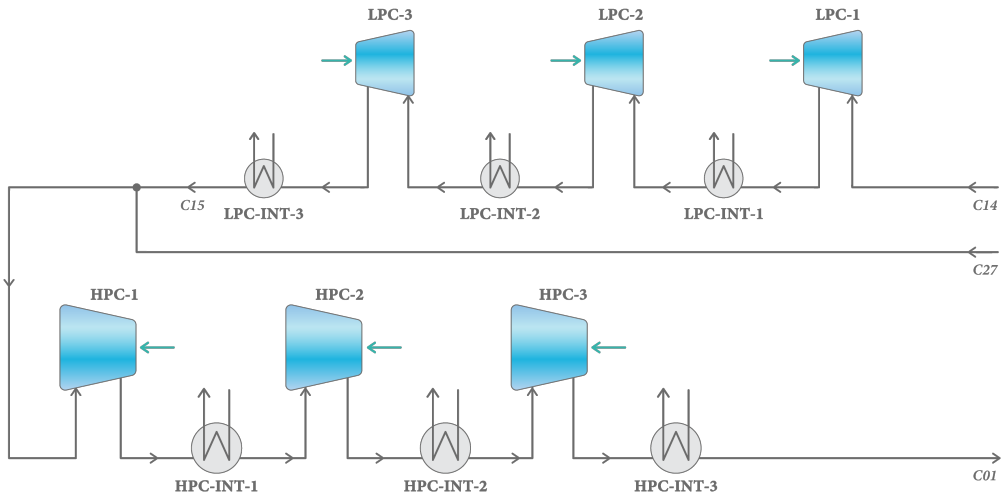

Figure 6.2: Process flow diagram of the baseline scenario (design) of the Claude-cycle compression system

Table 6.1: Stream data of the hydrogen refrigerant streams

Stream*	Temp. [K]	Press. [bar]	Flowrate [kg/s]	Vapour Quality	Stream	Temp. [K]	Press. [bar]	Flowrate [kg/s]	Vapour Quality
C01	298.1	29.80	51,498.8	1	*C16*	47.4	29.44	16,662.1	1
C02	119.4	29.705	51,498.8	1	*C17*	29.89	7.895	16,662.1	0.9942
C03	112.0	29.607	51,498.8	1	*C18*	44.36	7.797	16,662.1	1
C04	74.0	29.522	34,504.2	1	*C19*	74.0	29.522	15,527.0	1
C05	47.4	29.440	18,977.3	1	*C20*	46.0	7.797	15,527.0	1
C06	33.20	29.391	2,315.2	1	*C21*	45.2	7.797	32,189.0	1
C07	25.41	3.500	2,315.2	0.1939	*C22*	112.0	29.606	16,994.6	1
C08	21.1	1.250	2,315.2	0.2936	*C23*	71.2	7.699	16,994.6	1
C09	21.1	1.250	2,315.2	1	*C24*	70.47	7.699	49,183.6	1
C10	25.1	1.244	2,315.2	1	*C25*	102.4	7.599	49,183.6	1
C11	71.9	1.197	2,315.2	1	*C26*	111.3	7.501	49,183.6	1
C12	111.0	1.151	2,315.2	1	*C27*	293.6	7.401	49,183.6	1
C13	118.4	1.107	2,315.2	1	*RX1*	21.10	1.250	1,609.1	0
C14	297.1	1.059	2,315.2	1	*RX2*	21.70	1.250	1,609.1	1
C15	298.1	7.401	2,315.2	1					

**stream names refers to Figure 6.1 & 6.2*

The configuration of the precooling system within the plant remains consistent with the original layout, depicted in Figure 3.2. The MR compressor **MR-1** is designed as a two-stage centrifugal compressor, with an isentropic efficiency of 83.33%. Conversely, **MR-2** is designed as a single-stage centrifugal compressor, characterised by an isentropic efficiency of 83.00%.

As illustrated in the process flow diagram, the Claude-cycle employs a total of five turbo-expander units (due to the design constraints, the number of units equivalent to the number of the expansion stages). Notably, **T-3** and **T-4** are configured in series to deliver the necessary expansion ratio required by the process. For the respective turbo-expanders, namely **T-1**, **T-2**, **T-3**, **T-4**, and **T-5**, the calculated isentropic efficiency values stand at 89.68%, 89.53%, 87.90%, 90.50%, and 89.34%, respectively.

Furthermore, in addition to the incorporation of the calculated efficiencies of the turbomachinery equipment in the simulation, the pressure losses identified during the preliminary designs of the TSA and PFHXs are integrated into the process simulation of the final process configuration. Key stream data concerning the Claude cycle, hydrogen feed, and mixed-refrigerant cycle are summarised in Table 6.1, 6.2 and 6.3, respectively.

In the base scenario, the plant's overall specific energy consumption, SEC_{base}, is determined to be 7.241 kWh/kg_{LH_2}. When the mechanical power from the turbine shafts is recovered using

Table 6.2: Stream data of the hydrogen feed streams

Stream*	Temp. [K]	Press. [bar]	Flowrate [kg/s]	Vapour Quality
GH_2	298.1	20.00	5,208.0	1
M01	114.0	19.923	5,208.0	1
M02	114.0	19.778	5,208.0	1
M03	106.0	19.647	5,208.0	1
M04	73.5	19.618	5,208.0	1
M05	46.0	19.555	5,208.0	1
M06	30.0	19.544	5,208.0	1
M07	22.49	1.850	5,208.0	0.2992
M08	21.60	1.849	5,208.0	0
LH_2	21.63	1.500	5,208.0	0

**stream names refers to Figure 6.1 & 3.2*

Table 6.3: Stream data of the MR streams

Stream*	Temp. [K]	Press. [bar]	Flowrate [kg/s]	Vapour Quality
MR1	292.0	3.451	72,000.1	1
MR2	298.1	12.066	72,000.1	1
MR3	300.0	35.000	11,381.5	0
MR4	298.1	35.000	60,618.6	0.7437
MR5	300.1	35.000	72,000.1	0.6444
MR6	114.0	34.851	72,000.1	0
MR7	111.3	3.600	72,000.1	0.0689

**stream names refers to Figure 3.2*

electric generators, the energy consumption reduces to SEC_{recov} = 6.666 kWh/kg_{LH_2}. Among the three plant systems (compression, cryogenic liquefaction and precooling), the compression system stands out as the largest contributor, accounting for 6.478 kWh/kg_{LH_2} of the total plant SEC. Thus, the MR precooling cycle's energy consumption contributes only for 0.763 kWh/kg_{LH_2}.

By employing Equation (2.1) and incorporating the pseudo-equilibrium properties from Valenti et al.[51] along with the hydrogen spin-isomer models available in REFPROP[50], the theoretical minimum work requirement needed for transforming GH_2 to LH_2 can be determined. The analysis reveals that the ideal specific work for the liquefaction process is 2.218 kWh/kg, or 2.857 kWh/kg when considering the required conversion of ortho- to para-H_2. Based on this result, the exergy efficiency of the base scenario process is determined as 30.63%, or 39.45% when accounting for the conversion to para-H_2 form. The exergy efficiency increases to 33.27% (42.85% when including the conversion to para-H_2) if power recovery is considered.

The evaluation of the plant's CAPEX and OPEX follows the techno-economic methodology described in Chapter 5. The cost estimation for the plant, considering the base scenario, led to the calculation of liquefaction cost of SLC_{base} = 1.55 €/kg_{LH_2} for scenarios without power recovery and SLC_{recov} = 1.51 €/kg_{LH_2} when the power recovery system is incorporated. These SLC computations are conducted in accordance with the assumptions established for the base-scenario, as detailed in preceding chapters. A list of parameter values employed in the base scenario, which will undergo variations and analysis in subsequent sensitivity, scale-up, and projection studies, is provided in Table 6.4 below. Unless explicitly stated otherwise in subsequent analyses, all other parameters will remain consistent with the values specified in the baseline scenario.

Table 6.4: Assumptions of plant, equipment and TEA parameters used in base scenario

Plant and equipment design parameters	Values	Unit	TEA (APEA) parameters	Values	Unit
Hydrogen feed pressure	20	bar	Process description	New process	
Plant liquefaction capacity	125	TPD	Fixed annual interest rate	0.09	
Compressor max. impeller tip velocity	500	m/s	Electricity cost	0.1	€/kWh
			MR leakage rate	1.5	kg/h

Regarding the estimation of capital direct costs, it is determined that the Claude-cycle compression system, which consists of HPC and LPC systems (including the aftercoolers), makes a significant contribution to the overall project capital. This system constitutes a substantial portion of 51 million€ within the total project capital cost of 154 million€ (based on 2019 pricing). This is followed by the direct cost of the cryogenic liquefaction system and lastly, the expense associated with the precooling cycle. The distribution of the total direct equipment costs of the project among the three main systems of the liquefier, for plants with or without power recovery system, are shown in Figure 6.3.

Furthermore, Table 6.5 provides a summary of the total components, main cost-estimation parameters, and direct costs for the primary liquefaction plant's equipment (for liquefier without power recovery). Notably, the plant's most expensive equipment is **HPC-1**, with estimated direct costs reaching a staggering 18 million€, followed closely by the other high-pressure compressors, namely **HPC-2** and **HPC-3**, with costs of approximately 11 and 9 million€, respectively.

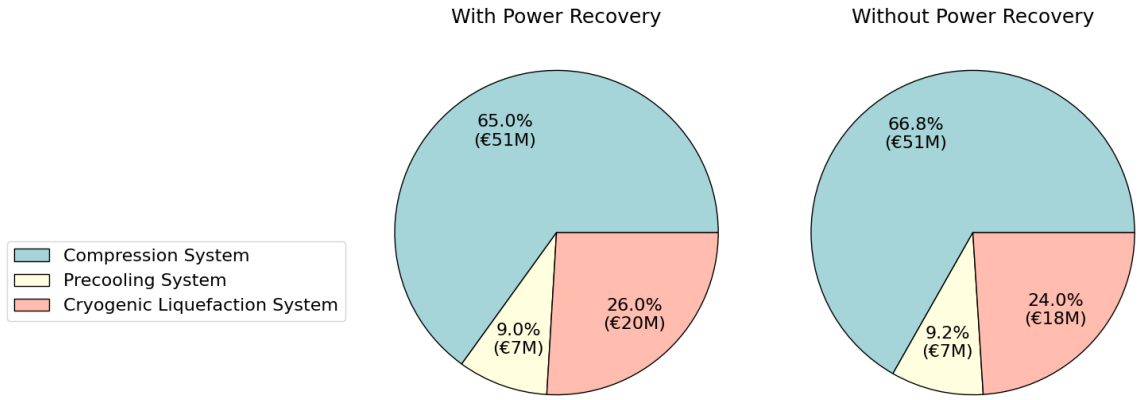

Figure 6.3: Proportion of system's equipment direct costs (estimated using APEA's 2019 pricing basis)

For the same scenario, the operating costs of the liquefier is estimated to be approximately 43 million€/year after accounting for the fluid loss. Within this 43 million€/year, the utility expenses, primarily electricity, make up a significant portion, totaling 33.3 million€ annually, as shown in Figure 6.4. In this particular scenario, the annual CAPEX and OPEX proportions, relative to the total annual costs, are found to be approximately 1.00:1.79. The annual cost ratios for the base scenarios are further depicted in the figures presented in the subsequent sensitivity analyses section.

Table 6.5: Summary of equipment main cost-parameters and direct costs for baseline scenario

Equipment name	Items in parallel	Parameter 1	Parameter 2	Total direct costs*
Compressors**		Inlet flowrate [m^3/h]	Power Input [kW]	
LPC-1	1	29,480.11	676.66	6,057,300 €
LPC-2	1	15,482.84	682.02	3,214,800 €
LPC-3	1	8,107.12	682.42	1,712,400 €
HPC-1	1	93,142.66	10,397.47	18,310,900 €
HPC-2	1	59,564.87	10,622.74	10,771,300 €
HPC-3	1	37,594.57	10,675.71	8,910,700 €
MRC-1	1	16,201.32	2,293.78	2,338,900 €
MRC-2	1	4,006.31	1,663.76	1,574,600 €
Turbines		Inlet flowrate [m^3/h]	Power Output [kW]	
T-1	1	1,689.19	1,127.24	853,900 €
T-2	1	883.74	552.21	563,600 €
T-3	1	2,950.81	1,003.30	942,900 €
T-4	1	4,311.67	1,064.25	822,200 €
T-5	1	44.71	30.84	300,200 €
Plate-fin HXs		Dimensions [m]	Core weight [kg]	
HX-1	1	(6.08 x 1.5 x 1.78)	18,411.50	1,630,300 €
HX-2	2	(4.4 x 1.5 x 2.88)	17,910.70	2,702,500 €
HX-3	1	(4.0 x 1.5 x 3.0)	-	1,675,600 €
HX-4	2	(4.8 x 1.5 x 2.5)	-	3,330,100 €
HX-5	1	(7.7 x 1.5 x 2.9)	-	2,603,400 €
HX-6	1	(6.0 x 1.5 x 3.0)	-	2,381,700 €
HX-7	1	(1.58 x 0.95 x 1.03)	17,910.70	367,700 €
Coldboxes		Diameter [m]	Tan-to-tan height [m]	
Precooling-CB	1	2.37	7.12	547,000 €
Cyogenic-CB	1	4.68	18.22	1,620,300 €

**estimated based on APEA 2019 pricing*

***excluding the costs of the compressors aftercoolers*

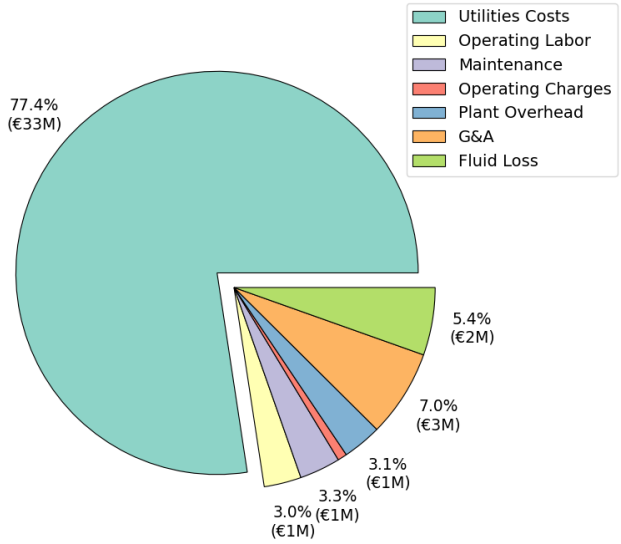

Figure 6.4: Distribution percentage of base scenario annual OPEX

6.1.1. Base Scenario Analysis

In comparison to the SEC values reported by Berstad et al.,[21] the SEC values obtained for the liquefaction plant investigated in this thesis are slightly higher. This difference primarily stems from the temperature adjustment made in Stream *C06*, which were made to maintain hydrogen in its gaseous state as it enters turbo-expander **T-5**. Another contributing factor is the variation in isentropic efficiency values for the turbomachinery units between the two studies, leading to differing results in SEC calculations. Nonetheless, the deviation of SEC observed in this study from the primary reference process remains below 2.2%.

The SEC values of the large-scale liquefaction process presented in this thesis are significantly lower than those of state-of-the-art hydrogen liquefiers, typically falling within the range of 10-12 kWh/kg_{LH_2}. As previously noted, in the baseline scenario, the annual OPEX of the plant contributes about twice as much to the SLC as the annual CAPEX of the plant. Hence, it can be deduced that the relatively modest SEC values of the conceptual plant are the principal driver behind the considerably reduced SLC values when compared to reported figures for existing hydrogen liquefiers, which currently span from 2.37 to 2.85 €/kg_{LH_2}.[a]

Another factor contributing to cost improvement is the economy of scale achieved by the plant. As explained in the literature review, larger liquefaction plants tend to exhibit lower construction costs per unit of liquefied gas. According to Towler & Sinnott[108], gas compressors, pivotal components of the hydrogen liquefaction plant as indicated in the capital cost estimation for the baseline scenario, are characterised with cost-scaling exponents of 0.6 and 0.75 for reciprocating and centrifugal types, respectively. This implies that the specific purchased cost of compressor decreases with increasing compressor capacity. Considering the substantial scale-up in capacity of the conceptual plant in comparison to existing hydrogen liquefiers, it is plausible that the cost curve of compressors significantly contributes to the enhanced SLC outcome.

Furthermore, based on the earlier-discussed SEC and SLC outcomes, an assessment can be made regarding the impact of incorporating turbo-generator assemblies into the hydrogen liquefaction plant. The introduction of a power recovery system leads to a reduction of 7.94% in the plant's SEC, accompanied by a simultaneous increase in CAPEX of around 2.53%. These

[a] Converted from 2.5-3 US$/$kg_{LH_2}$ using average exchange rate in 2022 of 1 € = 1.0530 US$, refers to `https://www.ecb.europa.eu/stats/policy_and_exchange_rates/euro_reference_exchange_rates/html/eurofxref-graph-usd.en.html`, accessed on 28 August 2023.

adjustments result in a modest 2.30% decrease in the plant's SLC, under the assumption of a base-scenario electricity cost of 0.1 €kWh. Consequently, it can be inferred that at this particular electricity price point or lower, the integration of turbo-generators is likely to yield minimal or possibly negligible improvements in the plant's economic performance. The economic assessment of including turbogenerator units under higher electricity price scenarios is elaborated in the following electricity sensitivity analysis section.

6.2. Sensitivity Analyses

6.2.1. Electricity Cost Analysis

The specific liquefaction costs in the baseline scenario are calculated with specific electricity costs of 0.1 €/kWh. In this sensitivity analysis, the 125 TPD conceptual plant's annual total costs and specific liquefaction costs are computed for varying electricity costs between 0.02 and 3.0 €/kWh. These outcomes are presented in the right graph of Figure 6.5. Meanwhile, the left bar chart of the same figure illustrates the estimated overall capital expenses of the 125 TPD plant, both with and without the integration of power recovery systems. Both charts are plotted with the same costs axis (y-axis) for comparison.

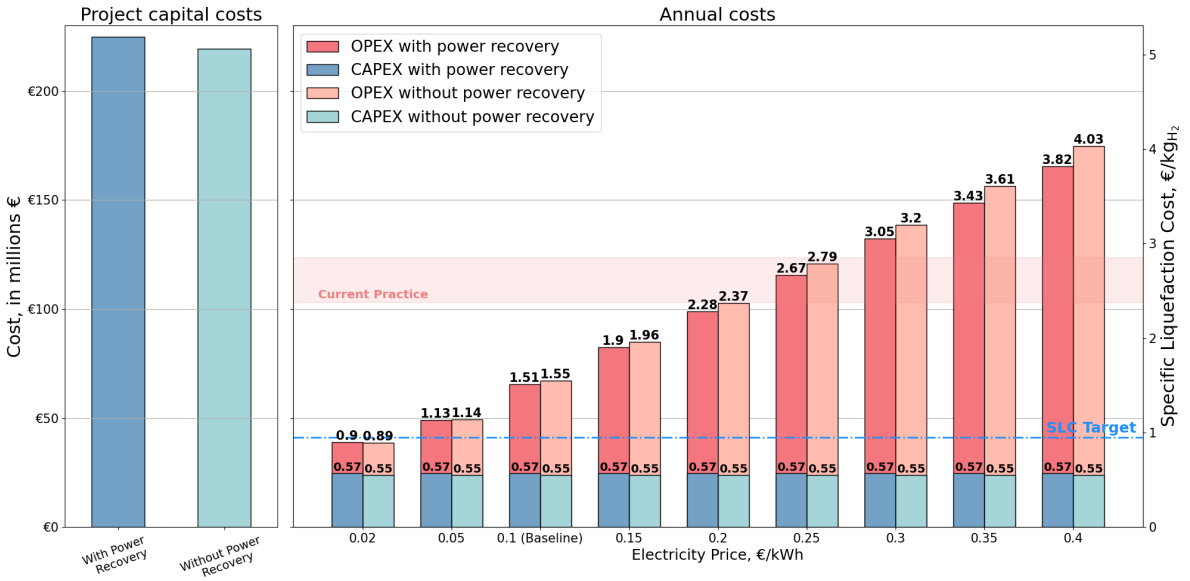

Figure 6.5: SLC of the 125 TPD hydrogen liquefier concept as a function of specific electricity costs

The graphs reveal that the specific liquefaction costs of the hydrogen liquefier are considerably influenced by electricity costs. The SLC values of the large-scale plant increase to the current industrial value of 2.37 to 2.85 €/kgLH_2 when electricity is priced relatively high at 0.20-0.25 €/kWh. With electricity prices of 0.4 €/kWh, the plant's total annual expenses reach essentially 175 million€, a figure which corresponds to 80% of the entire project capital expenses. It is important to note that the range of electricity prices in this analysis is deliberately chosen to exceed the variation of typical electricity costs in the EU. This choice is intentional to assess the potential impact of a sudden surge in energy prices (similar to what the EU has witnessed in recent years), on the overall costs of the hydrogen supply chain.

Conversely, the specific liquefaction costs rapidly decrease to an optimistic value suggested in existing literature, approaching 0.95 €/kg$_{LH_2}$ when the electricity price is 0.05 €/kWh. Some research indicates that certain renewable energy expenses, particularly from sources like wind, could potentially drop to as low as 20 €/kWh. If such renewable energy sources were harnessed

for hydrogen liquefaction, the specific liquefaction costs might even approach as low as 0.88 €/kg_{LH_2}.

Furthermore, it is apparent that the OPEX contribution to the cost of liquefaction becomes very dominant at high electricity price. In fact, when the electricity price is doubled from the baseline scenario, the annual OPEX becomes more than four times the plant's annual CAPEX. Moreover, as the plant's OPEX increases, the economic benefit of incorporating recovery generators becomes more pronounced. However, the improvement is negligible compared to the drawbacks that the plant would face at high electricity price. For instance, the addition of turbo-generators at electricity rate of 0.4 €/kWh results in a mere 5.17% reduction in SLC.

6.2.2. Feed Pressure Analysis

As highlighted in the literature review, the ideal energy input necessary for a hydrogen liquefaction process reduces as the hydrogen feed pressures increase. To evaluate liquefaction plant design with a higher hydrogen feed pressure, readjustment of the state conditions for each stream within the liquefaction process is necessary; since otherwise the process simulation would not be able to achieve convergence results. Consequently, without the implementation of an optimisation strategy, performing a sensitivity analysis on the liquefaction process concerning feed hydrogen pressures higher than the baseline value becomes considerably challenging.

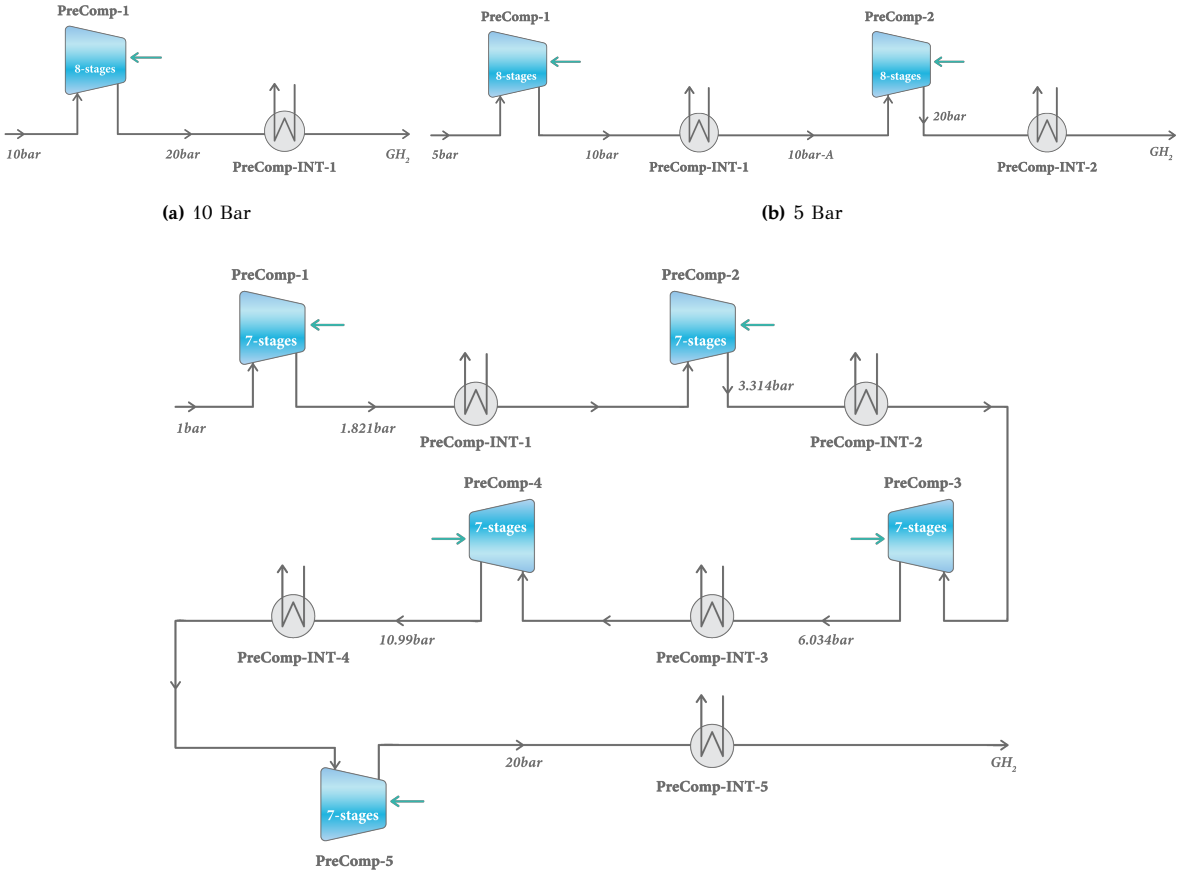

(a) 10 Bar **(b)** 5 Bar

(c) 1 Bar

Figure 6.6: Precompression sytems configuration for different H_2 feed pressure

However, when evaluating the plant with lower feed pressures, this study considers the utilisation of feed pre-compression system. The additional power requirement and capital costs

of the pre-compression system are incorporated to the calculation of SEC and SLC of the plant. In this work, the precompression system is assumed to be constructed using one or multiple centrifugal compressors equipped with aftercoolers. These compressors are designed following the same guidelines and limitations outlined in Section 4.2. The analysis involves varying the feed pressure across 1, 5, and 10 bar. The configuration of the resulting pre-compression system and the outcomes of the SEC and SLC calculations for each feed pressure value are depicted in Figure 6.6 and 6.7, respectively.

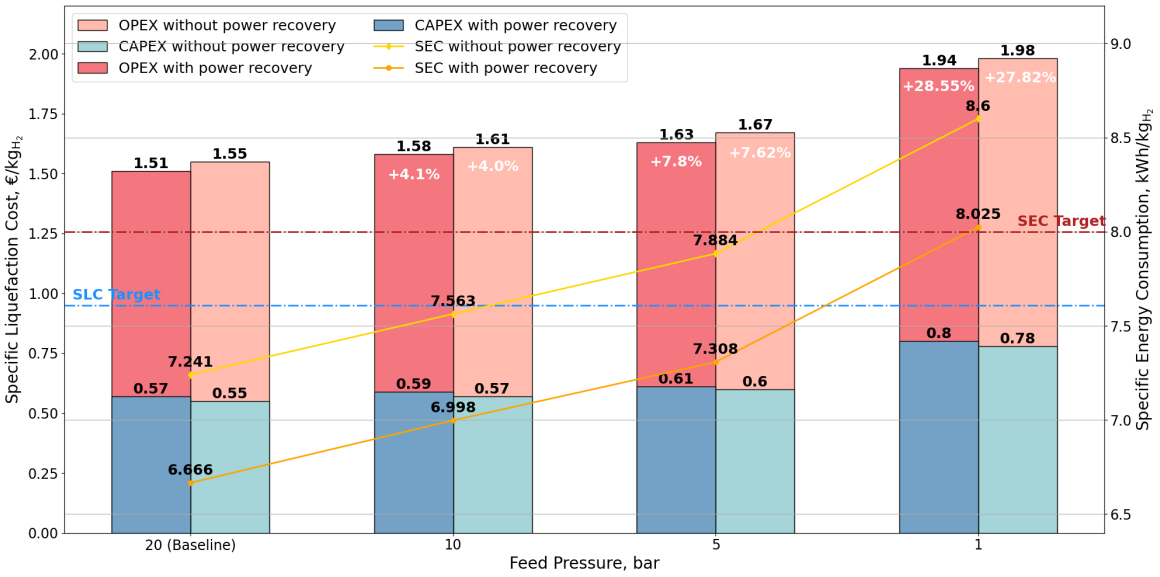

Figure 6.7: SEC and SLC of the 125 TPD hydrogen liquefier concept as functions of feed pressure

As seen in the figures, the SEC and SLC of the plant increase drastically when the feed pressure is lowered to 1 bar. This is because the pressure ratio requirement increases drastically from 4.0 to 20.0 when the feed pressure is reduced from 5 bar to 1 bar. It can also be observed in Figure 6.7, that the increase in CAPEX and OPEX are roughly the same, by 3.5-4.1%, both when the feed pressure is decreased from 20 to 10 bar, and from 10 to 5 bar. However, when the feed pressure is decreased from 5 to 1 bar, the CAPEX increases around 31% while increased in OPEX is only about 12%.

From this analysis, it can be concluded that the efficiency and economic performance of the plant design are fairly sensitive to decreasing feed hydrogen pressure. Although the impact of the feed pressure on the SLC is notable, it is not as profound as the influence stemming from variations in electricity costs.

6.2.3. Compressor's Max. Impeller Tip Velocity Analysis

As mentioned in the literature review, considerable research is currently underway to enable the use of centrifugal compressors for pure-hydrogen compression. A key focus area of this research is the development of a radial compressor capable of operating at a higher impeller tip velocity limit. This objective aims to minimise the number of compression stages required for a given hydrogen application. In this analysis, the maximum tip speed limit in the compressor design constraints is varied from the baseline value of 500 m/s to 600 and 700 m/s.

With an increased maximum tip speed, the design of the plant's compression system becomes more compact, since it reduces the total number of compression stages in both the LPC and HPC units. Since the total number of aftercoolers within the compression system has a significant influence on the performance of the liquefier, to give a more comparable analysis between com-

pression systems, the total number of compressor units, including the aftercoolers, is maintained at three for both low- and high-pressure compression (as shown in Figure 6.2). Therefore, only the number of stages in each compressor is reduced as the tip speed limitation increases.

The design results reveal that with a maximum impeller tip velocity of 600 m/s, both LPCs and HPCs experience a reduction of two stages, resulting in a total of 6 and 4 compression stages for LPC and HPC, respectively. When the maximum tip speed is at 700 m/s, the number of stages in each LPC compressor is reduced by two, leaving each with 4 compression stages. In contrast, the HPC compressors see a reduction of one stage, with each HPC compressor now consisting of 3 compression stages. The corresponding SEC and SLC of the liquefier following these design configurations are displayed in Figure 6.8.

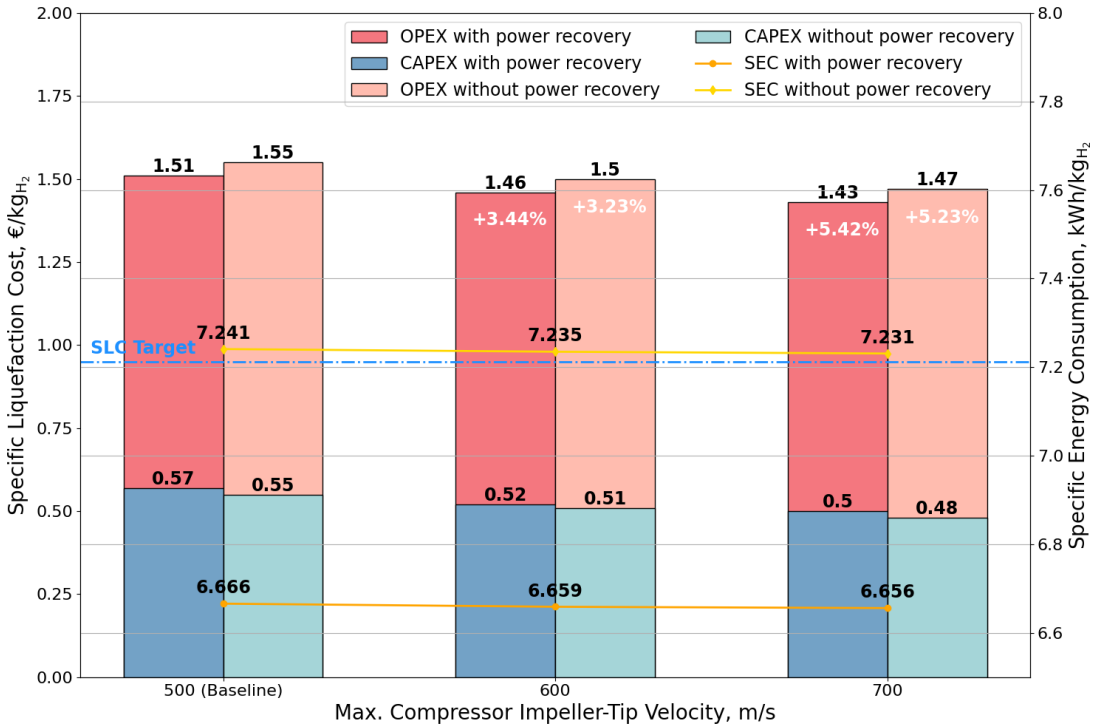

Figure 6.8: SEC and SLC of the 125 TPD hydrogen liquefier using different compressor's max. tip velocity

As observed in the figure, there is not a significant difference in the SEC of the plant when comparing compression systems with varying maximum tip speeds. This similarity arises because the specific speed of the compressors, which is the primary parameter used to estimate the compressors' isentropic efficiency in this study, remains relatively consistent across each design. Thus, as seen in the figure, the improvement in the SLC of the plant is mainly due to the reduction in the contribution of the annual CAPEX.

The similar values of specific speed across several compressors can be attributed to the constraints imposed on their designs (outlined in Section 4.2), which dictate that the specific speed falls within a similar range. However, it is worth noting that the design process was largely conducted through trial and error, without the use of an optimisation scheme. Therefore, it is plausible that higher tip speed velocities could potentially result in higher efficiency through a design optimisation procedure.

According to the compressors direct-costs estimation from APEA, it can be predicted that the introduction of high-speed compressors could improve the SLC of the liquefaction plant by 3.0 to 5.5% depending on how significant the increase in the tip speed limitations is. To provide some perspective, an SLC improvement of 5% in a 125 TPD hydrogen liquefier would correspond to

approximately 3 million€ of annual savings.

Another important aspect to note is that compressors direct-cost estimation provided by APEA only accounts for the differences in cost associated with the reduced number of stages, changes in power requirements, flow rates, and other process parameters. What both the software and this thesis have yet to incorporate are the additional costs associated with the use of high-strength materials and advanced manufacturing techniques required to construct high-speed hydrogen compressors. These factors are likely to increase the equipment's purchase costs significantly beyond the predictions made by APEA. Consequently, there is a possibility that the potential cost reduction resulting from the decreased number of compression stages could be offset by the higher costs associated with materials and manufacturing for high-speed compressors. To comprehensively analyse this, the projected commercial costs of high-speed hydrogen compressors must first be obtained.

6.3. Scale-Up Analyis

In this scale-up scenario, the 125 TPD liquefaction plant from the base scenario is scaled up to 250 and 500 TPD hydrogen liquefier. Within the APEA framework, there is a feature called the *Analyzer Scale-Up Module* which calculates the project cost for various production capacities. APEA achieves this by examining each element of a project, applies a set of scale-up rules unique to that element and recreates the entire plant description according to the new production capacity. However, using this process would ignore the preliminary design steps that are an integral part of the plant's technical and economic assessment in this study. Therefore, in this work, the scale-up analysis is performed by readjusting the plant design starting from the process simulation, equipment design and techno-economic analysis.

6.3.1. Direct Scale-Up vs Modular Cryogenic System

In this thesis, the plant is scaled-up via two distinct cryogenic liquefier system arrangements. The first arrangement follows the baseline scenario 125 TPD plant configuration, shown in Figure 6.1, but adopting more and/or larger equipment for the cryogenic system. However, as will be shown in the following subsections, this might not be applicable for such high-capacity hydrogen liquefiers due to the size limitations of the hydrogen liquefier coldbox, as outlined in Section 4.5. Therefore, this thesis considers another plant configuration that uses multiple (modular) 125 TPD cryogenic liquefier systems for the design of larger-scale liquefaction plants. Figure 6.9 shows the simplified block flow diagrams of 250 and 500 TPD plants to illustrate the contrast between the two system arrangements.

As shown in Figure 6.9b and 6.9c, only the cryogenic liquefier portion of the Claude cycle is split into multiple parallel systems. This is because the two other systems are not bound to size limitations. In contrast to the liquefier coldbox, the precooling coldbox can be constructed directly on-site, thus it's dimensions are not constrained by the transportation weight and size limits. Similarly, the compression system operates at temperatures higher than room temperature, allowing them to be installed in a simple building or even open areas.

Furthermore, there is a significant economic incentive for increasing the size of the compressor units. As mentioned previously, compressors exhibit cost-scaling exponents of 0.6-0.75.[118] Given that the purchased costs of compressors are a major contributor to the capital expenditures of hydrogen liquefaction plants, a substantial reduction in SLC can be anticipated when the capacity of the compressors is doubled.

The comparison of SLC calculation results for the upgraded plants, without power recovery, using the direct scale-up and modular cryogenic system configurations at electricity costs of 0.05

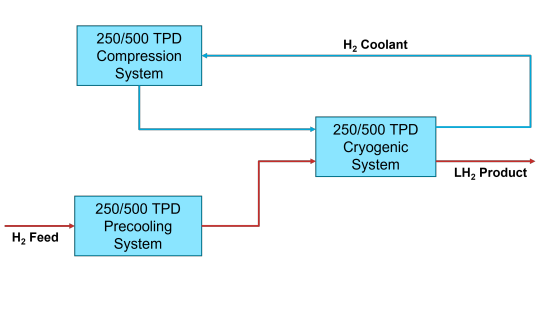

(a) 250 and 500 TPD with direct scale-up

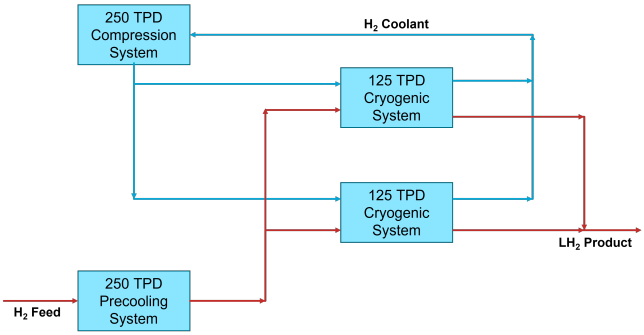

(b) 250 TPD with modular 125 TPD cryogenic liquefier system

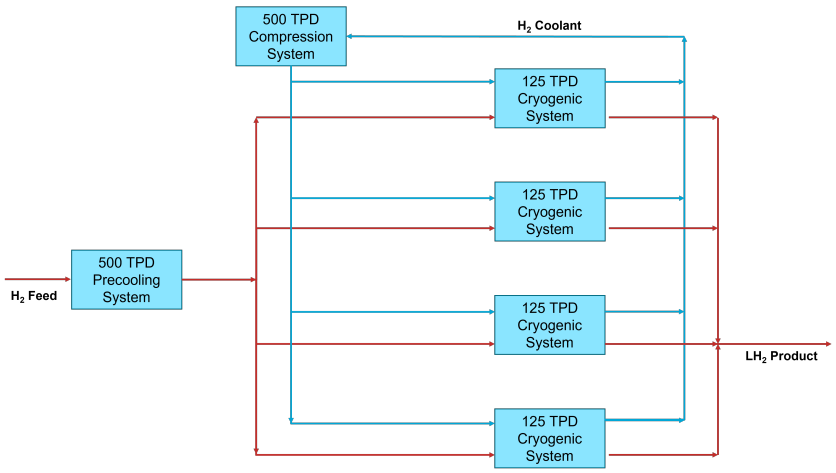

(c) 500 TPD with modular 125 TPD cryogenic liquefier system

Figure 6.9: Simplified block flow diagrams for 250 and 500 TPD scaled-up hydrogen liquefaction plant

and 0.1 €/kWh is illustrated in Figure 6.10a and 6.10b, respectively. The MR leakage losses for the scaled-up plants of 250 and 500 TPD are adjusted from the initial 1.5 kg/h for 125 TPD to 3 kg/h and 6 kg/h, respectively. Conversely, the hydrogen losses of 1.5% of the plant capacities are maintained in all scenarios.

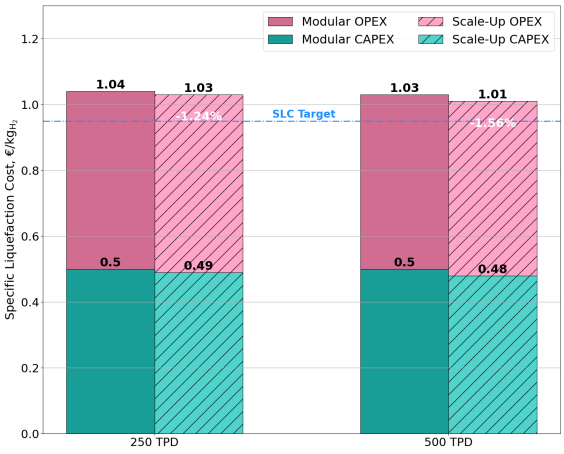

(a) Electricity price of 0.05€/kWh

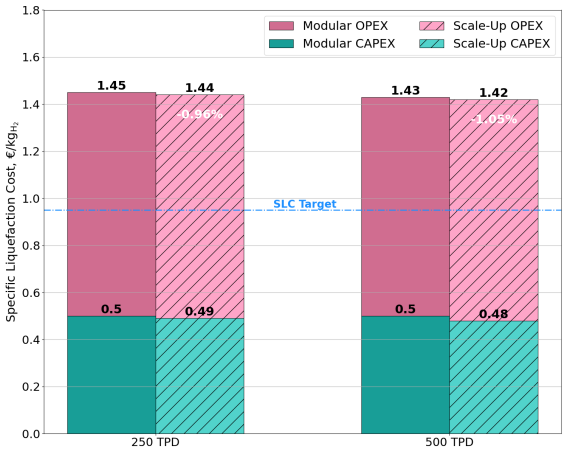

(b) Electricity price of 0.1€/kWh

Figure 6.10: Comparison between the SLC results of 250 and 500 TPD plant using direct scale-up and modular cryogenic liquefaction systems

6.3.2. Scale-up Results and Comparison

As shown in the plots, the difference in the calculated SLC results between scale-up plants with multiple cryogenic coldboxes and those with simply larger liquefier coldbox is not significant. However, as expected, directly upgrading the capacity of the cryogenic system provides a better economic evaluation compared to multiplying the 125 TPD cryogenic systems. Given its cost effectiveness, the subsequent results presented will primarily focus on the direct scale-up approach.

Figure 6.11 presents a comparison of calculated Specific Liquefaction Costs (SLC) for liquefiers operating at 125, 250, and 500 TPD capacities. This comparison is based on the direct cryogenic liquefier scale-up, both with and without the utilisation of a power recovery system.

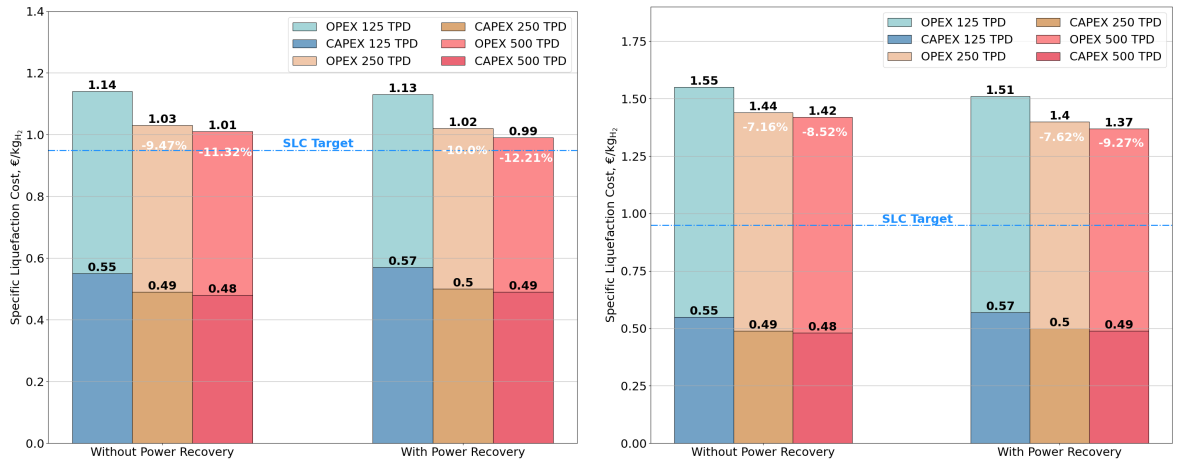

(a) Electricity price of 0.05€/kWh

(b) Electricity price of 0.1€/kWh

Figure 6.11: Comparison between the SLC results of 125, 250 and 500 TPD liquefiers

It is important to note that, in this thesis, the SEC of the plant remains essentially constant as the process capacity increases. Because no adjustments were made to the stream data except for the mass flowrates and slight changes in pressure drops, the total power consumption simply doubles when the hydrogen feed capacity is doubled, thus maintaining the original SEC value for the 125 TPD capacity. The implications of this can be observed in Figure 6.11, where the reduction of SLC due to the increase in plant capacity is slightly higher at lower electricity costs. This is attributed to the fact that, at lower electricity costs, the SLC contribution of CAPEX is more substantial. Additionally, specific CAPEX tends to be lower for larger plants. Consequently, this interplay results in a more noticeable reduction in SLC.

Another noteworthy observation from the graph above is the substantial difference in CAPEX and SLC reductions when scaling up the plant from 125 to 250 TPD as opposed to scaling up from 250 to 500 TPD. To gain insight into the underlying reasons for this discrepancy, it is essential to examine and compare the equipment summary lists for both upscaled plants. The equipment summary lists for liquefaction plants with capacities of 250 and 500 TPD are provided in Table 6.6.

Upon a close examination and comparison between Table 6.5 and Table 6.6, a significant reduction in high-pressure compressosrs specific costs when scaling-up from the 125 TPD to the 250 TPD plant, specifically **HPC-1**, **HPC-2**, and **HPC-3** the three most costly components in the liquefaction plant. This cost advantage arises from the economy of scale applied to the equipment. In the 250 TPD plant, each compressor's capacity is doubled, leading to notable cost savings.

Table 6.6: Summary of equipment main cost-parameters and direct costs for scale-up scenarios

	250 TPD Liquefier				500 TPD Liquefier			
Equipment	Items in parallel	Parameter 1	Parameter 2	Total direct costs*	Items in parallel	Parameter 1	Parameter 2	Total direct costs*
Compressors**		Act. inlet flowrate [m3/h]	Power Input [kW]			Act. inlet flowrate [m3/h]	Power Input [kW]	
LPC-1	1	59,092.48	1,354.79	10,641,900 €	1	118,483.06	2,713.49	25,281,500 €
LPC-2	1	31,010.68	1,369.48	6,250,600 €	1	62,137.81	2,742.58	10,907,800 €
LPC-3	1	16,224.99	1,368.47	3,407,600 €	1	32,489.98	2,740.89	6,526,400 €
HPC-1	1	186,260.64	20,794.57	29,851,100 €	2	186,370.33	20,802.00	59,702,000 €
HPC-2	1	119,115.55	21,242.83	24,850,700 €	2	119,185.58	21,250.41	49,701,000 €
HPC-3	1	75,180.19	21,343.63	17,661,900 €	2	75,224.32	21,351.21	35,324,000 €
MRC-1	1	32,412.54	4,588.87	3,753,600 €	1	64,826.10	9,177.89	8,449,600 €
MRC-2	1	8,013.87	3,328.04	2,088,700 €	1	16,027.99	6,656.19	3,209,900 €
Turbines		Act. inlet flowrate [m3/h]	Power Output [kW]			Act. inlet flowrate [m3/h]	Power Output [kW]	
T-1	2	1,690.77	1,127.27	1,573,200 €	3	2,254.38	1,500.00	3,137,700 €
T-2	1	1,770.91	1,104.70	780,700 €	2	1,770.88	1,104.68	1,701,200 €
T-3	2	2,951.92	1,004.23	1,590,900 €	3	3,935.93	1,338.99	3,246,800 €
T-4	2	4,311.62	1,070.74	1,689,400 €	3	5,748.88	1,427.66	3,438,700 €
T-5	1	89.45	61.65	317,100 €	1	178.89	123.31	349,600 €
Plate-fin HXs		Dimensions [m]	Core weight [kg]			Dimensions [m]	Core weight [kg]	
HX-1	2	(6.08 x 1.49 x 1.78)	18,404.60	3,276,100 €	3	(6.52 x 1.50 x 2.22)	24,814.60	6,795,900 €
HX-2	4	(4.41 x 1.50 x 2.82)	17,778.65	5,401,800 €	8	(4.41 x 1.50 x 2.96)	18,513.68	13,295,600 €
HX-3	2	(4.00 x 1.50 x 3.00)	-	3,351,200 €	3	(7.00 x 1.50 x 3.00)	-	7,639,000 €
HX-4	3	(5.80 x 1.50 x 3.00)	-	5,895,900 €	5	(7.50 x 1.50 x 3.00)	-	13,142,800 €
HX-5	2	(6.00 x 1.50 x 3.00)	-	4,763,500 €	3	(7.50 x 1.50 x 3.00)	-	7,885,700 €
HX-6	2	(7.50 x 1.50 x 2.50)	-	4,846,300 €	3	(8.00 x 1.50 x 3.00)	-	8,132,500 €
HX-7	1	(2.05 x 1.38 x 1.52)	4,120.80	535,600 €	1	(2.32 x 1.50 x 2.87)	9,399.90	801,400 €
Coldboxes		Diameter [m]	Tan-to-tan height [m]			Diameter [m]	Tan-to-tan height [m]	
Precooling-CB	1	2.94	8.83	794,300 €	1	3.87	11.62	956,700 €
Cyogenic-CB	1	5.09	27.01	2,104,900 €	1	5.93***	41.52***	3,248,800 €

**estimated based on APEA 2019 pricing*

***excluding the costs of the compressors aftercoolers*

****exceeding coldbox design constraints*

However, in the 500 TPD plant design, the circumstances are different. Here, the size of these compressors cannot be directly increased to meet the process requirement, due to design constraints associated with centrifugal compressors, as illustrated in Table 4.2. These constraints prevent compressor flowrates and driver power from exceeding 300,000 m^3/h and 37,000 kW, respectively. Consequently, in the 500 TPD liquefier design of this thesis, the number of HPC units is doubled and configured in a parallel arrangement. As a result, the total cost of the HPC units for the 500 TPD plant experience no substantial cost scaling advantage and essentially doubles compared to the HPC costs of the 250 TPD system.

While more cost-effective HPC configurations may exist, a comprehensive cost optimization study is required to identify the most optimal solution, a task beyond the scope of this study. Additionally, it's noteworthy that the inlet flowrates of the HPC compressors in the 500 TPD liquefier fall within the operating range of axial compressors. Exploring the potential of axial compressors in large-scale hydrogen liquefaction plants could open up new avenues for cost efficiencies. However, to the best of the author's knowledge, research on the application of axial compressors in pure-hydrogen compression has been limited to date.

Another important result from the equipment preliminary design is that the cryogenic coldbox dimensions, shown in above Table 6.6, for the 500 TPD liquefier exceeds the size limitations outlined in Section 4.5. Consequently, according to the design constraints, which were proposed based on current technological limitations, direct cryogenic liquefier scale-up is not feasible for scaling up the baseline 125 TPD process to 500 TPD. Instead, the arrangement of multiple 125 TPD cryogenic liquefiers in parallel represents the feasible plant configuration alternative for the 500 TPD capacity.

6.4. Future Scenarios

6.4.1. Design Allowances and Contingencies

In all previous analyses, the estimation of project capital costs has been conducted through APEA, with the selection of "New Process" in the Process Description input under the project's General Specs. This choice results in a 10% design allowance for all equipment, and material costs are derived from the APEA ICARUS engine. Additionally, when combined with the default selections for Project Complexity and Project Type (which are "Typical" and "Grass roots/Clear Field," respectively), it specifies the project contingencies to be as high as 30% of the bare plant cost. The following Table 6.7 shows the changes in the design allowance and contingency percentages employed by APEA when different selections are made for Process Description (while maintaining the selections for Project Complexity and Project Type fields).

Table 6.7: Equipment design allowance and contingency percentages following Process Description

APEA Process Description	Design Allowance %	Contingency %
New & Unproven Process	15	36
New Process	10	30
Redesigned Process	7	26.4
Licensed Process	5	21.6
Proven Process	3	18

In the foreseeable future, with the successful construction of larger hydrogen liquefaction plants, the technology is expected to mature. Companies will likely gain greater confidence in undertaking such projects with reduced design allowances and contingency percentages. This analysis attempts to capture the essence of this progression by varying the selection of the APEA process description input to examine how overall liquefaction costs respond to lower (and higher) project design allowances and contingency percentages. Figure 6.12 displays the SLC calculation

results for 125, 250, and 500 TPD plants without a power recovery system at an electricity cost of 0.1€/kWh, using different selections for Process Description. The different percentages depicted on the bar graphs represent differences in the SLC values relative to the baseline SLC_{base} = 1.55 €/kg_{LH_2}.

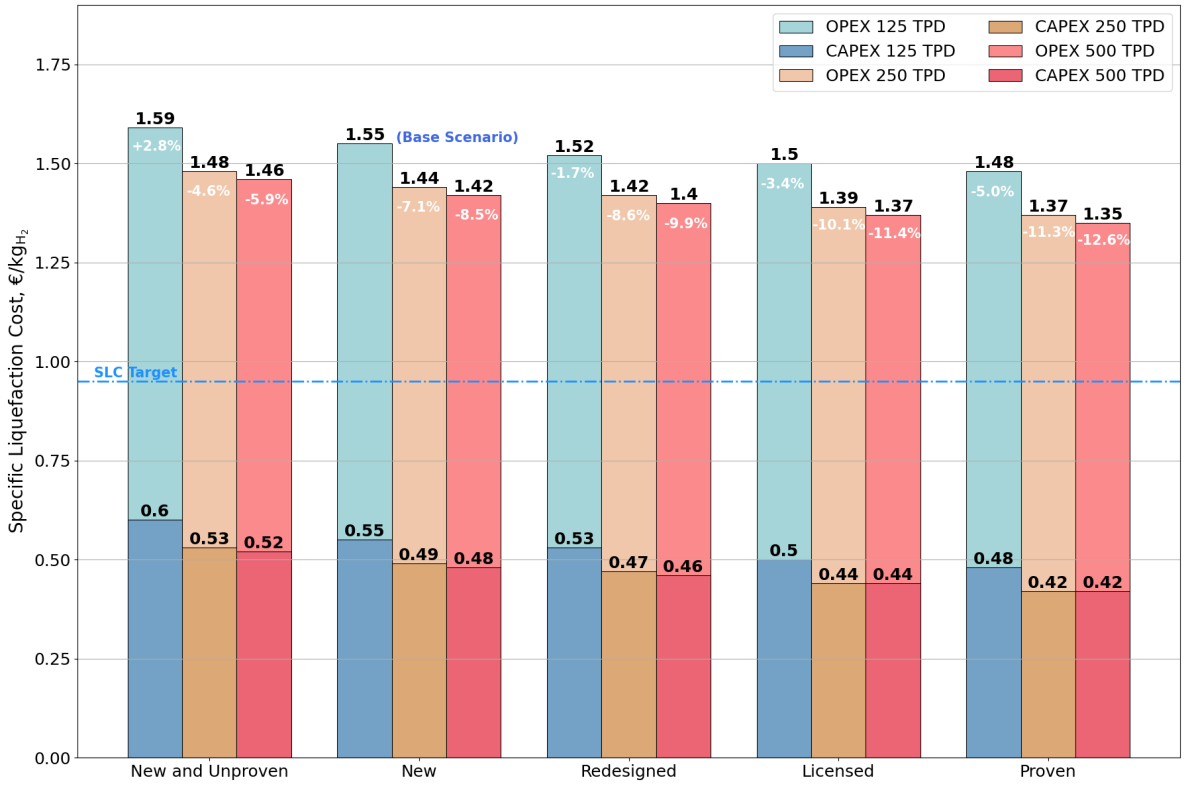

Figure 6.12: SLC results for 125, 250 and 500 TPD hydrogen liquefier using different selection of Process Description at electricity costs of 0.1 €/kWh

As shown in Figure 6.12, the study shows that an improvement of 5% in SLC can be expected for the 125 TPD liquefier as the industry gains more experience in the construction of hydrogen liquefiers. Furthermore, it is evident that the SLC can be further reduced from the initial baseline value of large-scale liquefiers by aligning with the maturation of the technology and increasing the scale of the plants.

Based on the plots, the SLC of the original large-scale concept is expected to decrease by approximately 10.0-12.6% as a result of cumulative company experience, technological advancement, and the upscaling the original large-capacity hydrogen liquefier concept. However, it is important to note that transitioning from a "New and Unproven Process" to a "Licensed" or "Proven Process" status in an industrial context can be a time-consuming process, spanning several years or even decades. Therefore, this transformation may require substantial time and effort involving various stakeholders, including industry, government, and academia, before fully realising these potential cost savings.

6.4.2. Best Case Projection

In addition to potential cost improvements from gaining more industrial experience, there are also expectations on the implementation of green policies and renewable infrastructure, which could potentially boost the development of the overall hydrogen supply chain. This analysis seeks to project the best cost-reduction scenario for liquefaction costs, by assuming the presence

of financial incentives, potentially stemming from governmental sources, and access to low-cost renewable electricity.

Emerging low-carbon policies, such as incentives that offer reduced interest rates for large-scale low-carbon fuel production, could exert a significant influence on hydrogen liquefaction costs. Up to this point in the analysis, the overall capital cost of the conceptual plant has been treated as a fixed annuity payment with a fixed annual interest rate of 0.09. In the following analysis, the fixed annual interest rate for the calculation of the annual CAPEX of the plant is adjusted to a relatively low value of 0.07.

As shown in the previous sensitivity analysis, harnessing low-cost electricity sources can significantly reduce the OPEX of hydrogen liquefaction plants. In this analysis, the specific electricity price is assumed to be at 0.05 €/kWh. Additionally, the liquifier plants are assumed to have incorporated turbine power-recovery systems. The SLC calculation results for liquefaction plants with capacities of 125, 250 and 500 TPD following different selections for Process Description are shown in Figure 6.13.

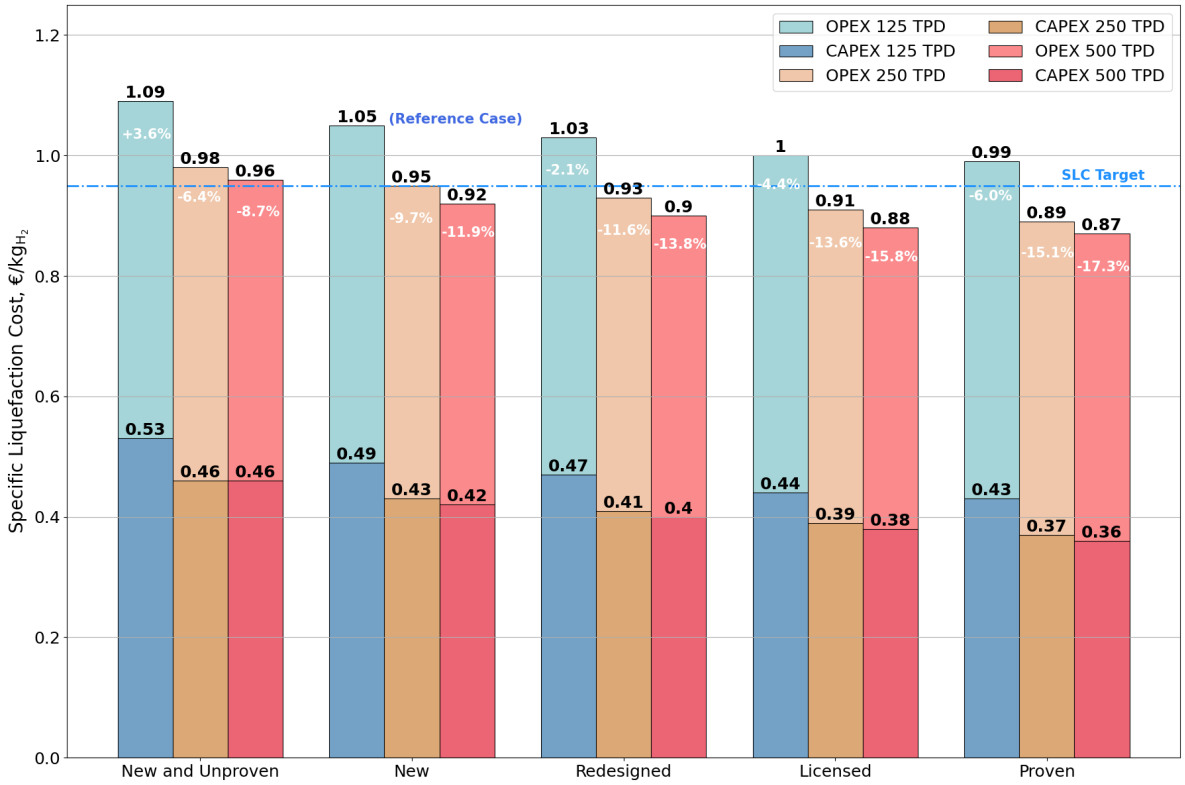

Figure 6.13: SLC results for hydrogen liquefiers employing power recovery, calculated using fixed annual interest rate of 0.07 and electricity costs of 0.05 €/kWh

From the figure, it becomes evident that, with relatively modest project interest rates and electricity costs, the realization of large-scale Claude-cycle hydrogen liquefiers has the potential to significantly reduce the industrial cost of hydrogen to around 1.0 €/kg$_{LH_2}$. This is in accordance with recent cost projection studies as discussed in the literature review. Although the rates considered in this analysis are relatively low, they still fall within the reasonable range based on past industry experience. Furthermore, the calculations indicate that for 250 TPD and 500 TPD capacities, the cost estimations suggest that the SLC could decrease to as low as approximately 0.87 €/kg$_{LH_2}$ as hydrogen liquefaction technology matures within the industry.

6.4.3. Cost and Experience Curves

Cost Curve

As mentioned in the literature review, several cost curve models have been developed and published in the past to estimate the initial investment associated with hydrogen liquefaction plants. In this section, the capital cost estimations obtained in this thesis are utilised to predict a novel cost curve. The capital costs used are from the 125, 250 and 500 TPD concepts using APEA process descriptions "New Process", "Redesigned", and "Licensed", respectively. This cost curve, referred as *Cost Curve 1*, is compared with existing cost curves documented in the literature in Figure 6.14. For better comparison, the various cost models shown in the graph have all been adapted to 2022 pricing in € using Equation 5.1.

Furthermore, within the same figure, *Cost Curve 2* is presented, which is constructed based on combining the capital cost findings from this thesis with reported capital costs of hydrogen liquefaction plants from various published sources.[4,13,19,27,122,137] These capital costs originate from a variety of sources, including actual establishment cost reports, contractor quotations, and cost projections. The accompanying cost data can also be found in Figure 6.14. The various capital cost data shown in the graph have been adapted to 2022 pricing in € using Equation (5.1).

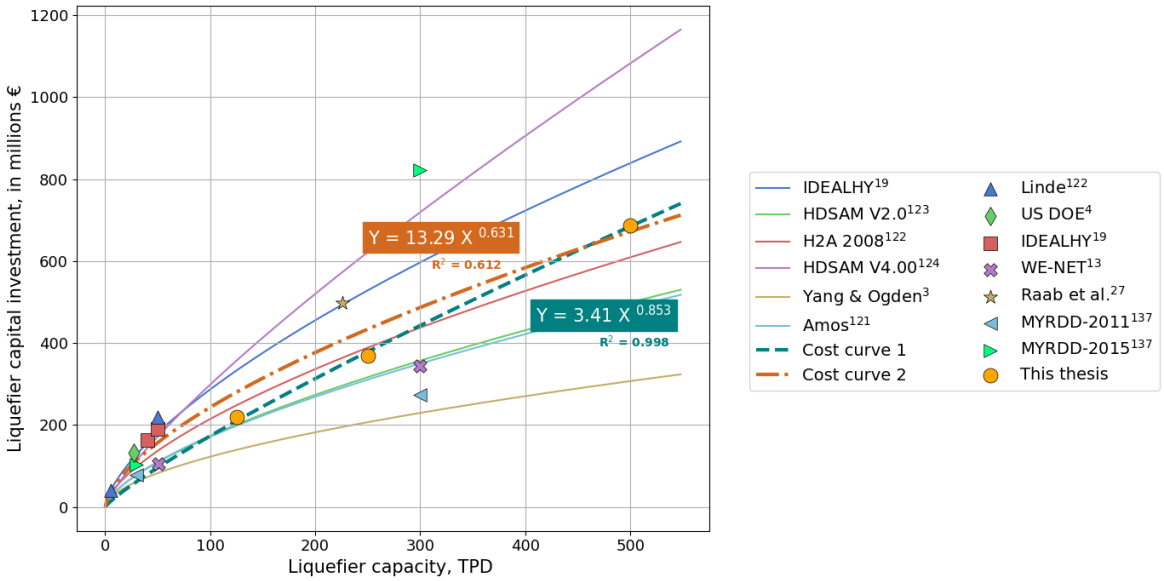

Figure 6.14: The cost curves and capital cost data from this thesis and those found in the literature

Both *Cost Curve 1* and *Cost Curve 2* are formed following Equation (2.29). In the case of *Cost Curve 1*, the constant a and n are found to be 3.41 million€ and 0.853, respectively. Meanwhile, for *Cost Curve 2*, the constant a and n are determined as 13.29 million€ and 0.631, respectively. As depicted in the figure, both curves fall within a range that is intermediate to values derived from other models. In comparison to each other, *Cost Curve 1* estimates a lower capital investment for smaller capacity plants (up to 250 TPD) than *Cost Curve 2*, but estimates a higher value for large-scale plants (larger than 250 TPD).

Compared to other cost curve models, *Cost Curve 1* predicted a higher scaling coefficient. This is possibly because the economy-of-scale potential of high pressure centrifugal compressors has reached their limit in the 500 TPD liquefier design studied in this thesis, as explained in Section 6.3. However, as previously mentioned, the introduction of an optimisation scheme as well as the implementation of high flow-rate axial compressor designs are likely to reduced the specific capital costs of large scale plants and ultimately predict a more moderate value for the scaling

exponent of hydrogen liquefiers. These two points are reserved for future research.

It is also important to note the other cost curve models found in the literature were developed without access to cost data points for extra large plants, with no cost data available for liquefaction plants exceeding 300 TPD. This could also be the reason for the higher value of the scaling coefficient of *Cost Curve 1* compared to the other models. Specifically, for the liquefier capital cost model used in HDSAM V4.0[4,124], it has been explicitly mentioned that this model is only valid for a liquefier with a scale of less than 200 TPD.[4]

Ultimately, as demonstrated in Figure 6.14, it is evident that the capital cost results in this thesis align closely with the estimates generated by existing hydrogen liquefier cost projection models. Therefore, it is reasonable to assert that the methodologies for process modelling, preliminary equipment design, and techno-economic analysis developed and described in this thesis are valuable tools for making sound predictions regarding the economic viability of conceptual large-scale hydrogen liquefaction processes.

Experience Curve

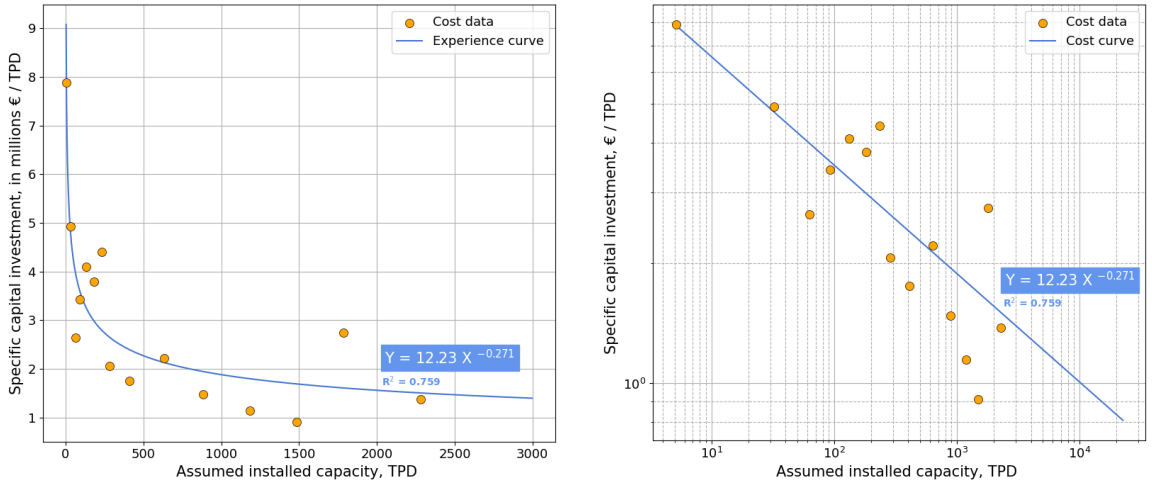

(a) Linear scale

(b) Logarithmic scale

Figure 6.15: Prediction of experience curve of hydrogen liquefaction technology based on cost data from this thesis and those found in the literature

In addition to the cost curves for liquefaction plants, this thesis also aims to provide a prediction regarding the potential learning/experience curve for hydrogen liquefaction technology. This prediction is based on the cost data shown in Figure 6.14, where the capacity is rearranged in a cumulative sum array, starting from the smallest capacity plant and progressing to the largest. Essentially, the assumption is that the liquefier concepts have all been installed in a sequential manner, from the smallest concept to the largest concept. Note also that, for experience curve, the y-axis represents the specific capital costs, which are derived by dividing the capital investment costs by the plant's capacity. The results are depicted in Figure 6.15.

The curve fitting of the manipulated cost data to Equation (2.31), resulted to a constant a of 12.23 million€ per plant capacity in TPD and a learning coefficient b of 0.271. Using Equation (2.32) and (2.33), the progress ratio and learning rate of the above learning curve are determined as 82.87% and 17.13%. These results essentially means that with each doubling of the installed global liquefaction capacity the price of hydrogen liquefiers is predicted to drop on average by 17.13%. This is comparable to solar panels, which have learning rate of around 20.20%, based on the reported reduction in solar panel specific costs from 1976 to 2019.[138]

When extending the learning curve to include higher assumed installed capacity, as depicted in Figure 6.16, it becomes evident that the specific capital investment decreases to 1 million €/TPD when the global capacity reaches 10,000 TPD. Eventually, it drops further to 0.81 million €/TPD at 20,000 TPD. Using the same economic assumptions as in the base scenario, including the 20-year payment period and fixed annual interest rate of 9%, a specific capital cost of 0.81 million €/TPD corresponds to an SLC contribution of 0.28 €/kg_{LH_2}. Incorporating the OPEX contribution from the 125 TPD plant in the base scenario, assuming an electricity price of 0.1 €/kWh, results in an SLC of 1.28 €/kg_{LH_2}. This represents a reduction of approximately 17.66% compared to the original SLC_{base} of 1.55€/kg_{LH_2}.

While these findings appear promising for the advancement of hydrogen technology and infrastructure, it is important to note that this prediction in this thesis relies on extrapolation of preliminary cost estimates for large-scale concepts. There is a high possibility that certain technological constraints could hinder cost improvements at the above anticipated rate.

Furthermore, the capital investment data used in the construction of previous cost and experience curves are based on varying assumptions and levels of comprehensiveness. To provide a more accurate projection of the true potential of hydrogen liquefaction, an experience curve based on actual global liquefaction capacity should be employed. Unfortunately, the technology is still in its early stages of implementation, with a global capacity of only 350 TPD. Therefore, it is highly advisable to continually improving the experience curve as more cost data on hydrogen liquefaction systems become available, which will ultimately enhance our forecasting capabilities for the expanding hydrogen economy.

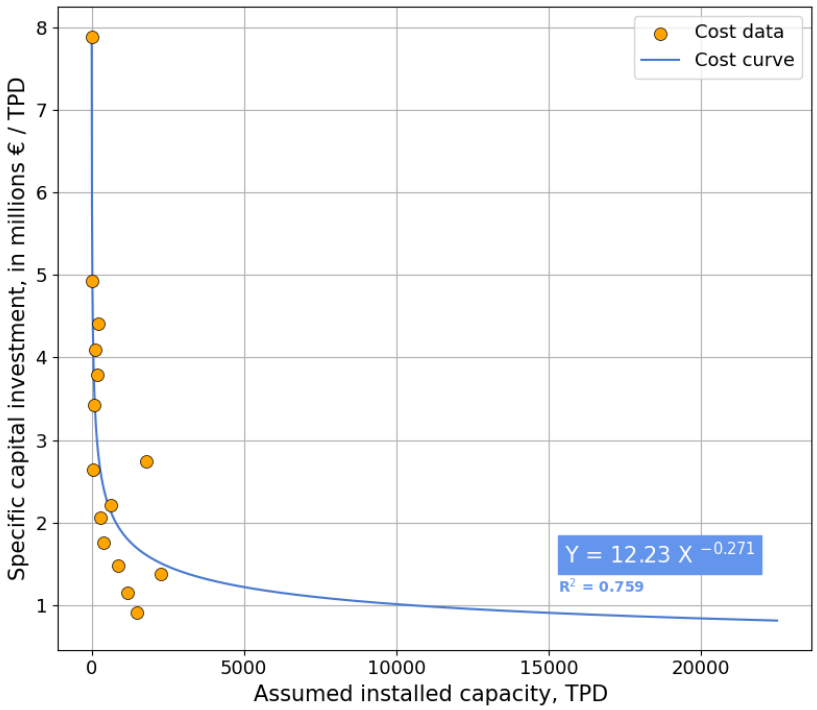

Figure 6.16: Extended experience curve of hydrogen liquefaction technology

7

Conclusion & Recommendation

7.1. Conclusion

In this conclusion, the sub-research questions formulated in the introduction chapter are addressed, drawing from the key insights and implications uncovered in this research.

How can a conceptual high-capacity H_2 liquefaction plant be accurately modelled using a commercial process simulation tool?

In this thesis, a modified version of the high-pressure H_2 Claude-cycle large-scale hydrogen liquefaction concept presented by Berstad et al.[21], is selected for evaluation. The modeling of the process is conducted using Aspen HYSYS process simulation software, making use of its built-in unit operation models to calculate the operation of various components, such as heat exchangers, compressors, and expanders. For the calculation of the multi-stream counter-current PFHX unit operation, the built-in "LNG exchanger" model in Aspen HYSYS is used.

The properties of normal hydrogen, serving as the primary refrigerant in the Claude-cycle, are determined using the state-of-the-art Helmholtz free energy-explicit fundamental EOS for normal hydrogen[49], retrieved from the REFPROP database[50]. Meanwhile, the properties of the mixed-refrigerant fluid in the precooling cycle are computed using the Peng-Robinson cubic EOS available in Aspen HYSYS.

To simulate the hydrogen feed stream that undergoes continuous catalytic ortho- to para-hydrogen conversion in the heat exchangers, an equilibrium-hydrogen assumption is applied. For this purpose, the pseudo-equilibrium-hydrogen heat-capacity model developed by Valenti et al.[51] is employed. Implementation of the pseudo-e-H_2 model by Valenti et al.[51] involves modifying the REFPROP[50] fluid file (.FLD file) for parahydrogen and subsequently calling REFPROP's parahydrogen model from Aspen HYSYS.

Prior to equipment preliminary designs, isentropic efficiency values for the pressure changer components and the pressure drops in the PFHXs are assumed. These assumptions are subject to refinement during subsequent equipment design iterations. Once the final isentropic efficiencies and pressure drops values are obtained, the SEC of the modeled plant is calculated, resulting in a value of SEC_{base} = 7.241 kWh/kg_{LH_2}. When mechanical power is recovered from turbine shafts through electric generators, the energy consumption is reduced to SEC_{recov} = 6.666 kWh/kg_{LH_2}. These SEC values are values exhibit a 2.2% increase compared to the SEC values reported in the original reference by Berstad et al.[21]

What is the technical evaluation procedure for the preliminary designs of the main equipment in a large-scale hydrogen liquefaction process, and how can the findings from these preliminary designs be incorporated into the overall plant design?

This technical evaluation in this thesis primarily focuses on the preliminary design of major process equipment for large-scale liquefaction systems, including compressors, turboexpanders, heat exchangers. A brief discussion on the preliminary sizings of cryogenic adsorbers and coldboxes are also presented. Compatibility with existing technology constraints is ensured.

For noncatalytic PFHXs, Aspen EDR's design mode is utilized, importing input directly from the Aspen HYSYS simulation file. The resulting calculations, particularly the pressure drop estimates, refine Aspen HYSYS simulation pressure values.

For catalytic PFHXs, a pseudo-homogeneous continuum reactor model developed by O'Neil et al.[45] is employed to approximate geometric specifications. This model simulates hydrogen spin-isomer conversion, heat transfer, and pressure loss in a two-stream PFHX with ortho-para catalyst. Due to multi-stream catalytic heat exchanger models in the liquefaction process, the catalytic PFHX preliminary design is split into two stages: noncatalytic HX sizing and catalytic HX sizing, which are then combined for the final size calculation. This approach ensures that the size of PFHXs facilitate the required heat transfer and hydrogen spin-isomer conversion while adhering to dimensional constraints. These geometric parameters are considered to be sufficient for making sound cost estimations.

Centrifugal compressors are suitable for the compression process required in the liquefaction plant under evaluation, with flow rates ranging from 4,000-85,000 m3/h and a maximum discharge pressure of 30 bar. Therefore, only radial-flow turbo-compressors are considered in this thesis. Each design includes an aftercooler to cool outlet gas to 298.15 K with cooling water. While radial-turbo compressors are not yet used in industrial hydrogen liquefiers, this study adheres to design constraints aligned with current turbo-compressor technology limitations.

The centrifugal compressor preliminary designs estimate the isentropic efficiencies of each compression stage and determine the number of modules, stages, and rotational speed for each compressor. The resulting isentropic efficiency values are used to refine the initial assumptions used in the process simulation. The resulting number of units, stages, and rotational speed are used to enhance the accuracy of the cost estimation. The procedure is a simplification of the preliminary design procedure given by Gambini & Vellini.[95].

Radial in-flow turbines, or centrifugal turbines, are considered for turboexpanders. The design process is similar to that of compressors, but with different input and output parameters. The outcomes include the estimation of the isentropic efficiencies, number of turbine modules and acceptable rotational speed for the turboexpander system. These are used to refine the process simulation as well as additional input for cost estimation.

How to effectively estimate the capital and operating costs of a conceptual hydrogen liquefier based on process simulation model and equipment preliminary designs, and what are the key factors influencing the plants economic feasibility?

In the technical enonomic analysis of this thesis, the CAPEX and OPEX associated with the large-scale high-pressure hydrogen Claude cycle concept is estimated. To determine these cost, the Aspen Process Economic Analyzer (APEA) software is utilised for its ability estimate equipment expenses using up-to-date cost data obtained from real engineering, procurement, and construction (EPC) projects and equipment manufacturers In addition to estimating the costs of purchasing equipment, APEA also evaluates the total installed costs, which encompass both direct and indirect field expenses. A notable advantage of choosing APEA over other cost estimation methods is its integration with Aspen HYSYS simulation software, which is employed

for the process modeling in this thesis. The estimation of the primary process equipment costs is based on their design parameters, as established during the preliminary equipment design and sizing. Furthermore, APEA facilitates the calculation of the plant's operating costs, covering both variable and fixed operational expenditures.

In the baseline scenario with an electricity price of 0.1 €/kWh, the techno-economic assessment of the 125 TPD Claude-cycle concept resulted in a low SLC of 1.55 €/kg_{LH_2}, significantly below the current industrial hydrogen liquefaction cost of 2.37 to 2.85 €/kg_{LH_2}.This cost advantage primarily stems from two factors: Firstly, the large-scale liquefaction process presented here has much lower Specific Energy Consumption (SEC) values compared to state-of-the-art hydrogen liquefiers, which typically range from 10-12 kWh/kg_{LH_2}. Secondly, the economy of scale achieved by this plant is noteworthy. Another factor contributing to cost improvement is the economy of scale achieved by the plant. Gas compressors, a critical component of the hydrogen liquefaction plant, exhibit cost reductions with increasing capacity. Given the substantial capacity increase in the conceptual plant compared to existing hydrogen liquefiers, compressor cost scaling likely plays a significant role in the improved SLC.

Sensitivity analyses reveal that changes in electricity prices have a substantial impact on the plant's economic performance. Furthermore, it also shows that the plant's efficiency and economic viability are fairly sensitive to a decrease in the feed hydrogen pressure. While feed pressure impacts the SLC of the plant, it is not as significant as the effect from variations in electricity costs. Moreover, based on the methodology presented in this thesis, the incorporation of high-speed centrifugal compressors in hydrogen liquefaction systems has the potential to reduce the SLC of hydrogen about 5.21%, particularly when electricity costs are lower.

Moreover, when scaling up the 125 TPD concept, there is potential for cost improvements, including a 7% reduction in Specific Liquefaction Cost (SLC) at 250 TPD and a 10% reduction at 500 TPD, assuming a base electricity price of 0.1 €/kWh. Looking ahead, future projections and cost reassessments with reduced design allowances and contingencies suggest the possibility of a 12.3% reduction in SLC as the Claude cycle becomes a "proven" industrial concept. In the best-case scenario, with financial incentives and access to low-cost renewable electricity, liquefaction costs could range from 0.87 to 1.09 €/kg_{LH_2}.

Furthermore, the cost findings from this thesis are used to estimate a cost-scaling curve for hydrogen liquefaction plants. The curve aligns closely with the existing cost curves reported by collaborative efforts between industry and government research projects, thereby validating the methodologies developed in this thesis. The cost data from this research and information gathered from various sources are also used to predict the experience curve of hydrogen liquefaction technology, by assuming that these plants have been installed scatteredly across the globe. The resulting prediction indicates that as the global liquefaction capacity doubles, the expected average reduction in the price of hydrogen liquefiers is approximately 17%.

7.2. Comments & Recommendation

Based on the findings presented in this thesis, it has been demonstrated that the SLC values of the large-scale Claude-cycle hydrogen liquefaction concept can achieve the suggested target cost of 1 US$/$kg_{LH_2}$, with an electricity cost at approximately 0.05 €/kWh. It's important to note that the capital costs for the liquefier estimated in this study are categorized as "Class 4" estimates, which are essentially initial assessments based on preliminary design results and limited cost data (refer to Section 2.4.1). These types of cost estimates have an accuracy range of ± 30%. Consequently, the methodology developed in this thesis is better suited for comparing costs among various design options or process concepts rather than making investment decisions.

Having said that, due to the inherent uncertainty in these estimates, it is possible that the

actual implementation of the large-scale Claude-cycle concept could result in significantly higher or lower liquefaction costs. Nonetheless, the authors argue that the SLC results in this thesis probably still underestimate the true potential of hydrogen liquefaction as a cost-effective solution for hydrogen transportation and storage.

There are several reasons for this assertion. Firstly, the APEA software calculates capital costs for the construction of hydrogen liquefaction facilities as if they were conventional chemical process plants. Consequently, estimates for land acquisition, the number of personnel required for operation, heavy-duty construction equipment, and other factors are all based on the assumption that the facility resembles a conventional chemical plant. In reality, the construction of hydrogen liquefaction facilities differs significantly from chemical plants, as the majority of liquefier equipment must be installed into cryogenic coldboxes, which would mainly be constructed inside a production building. The equipment configuration also results in a considerably smaller land requirement compared to conventional plants with equivalent equipment, as the components are densely packed inside the cold box. Furthermore, due to the encapsulation of equipment within the cryogenic coldbox, except for the compression system, the operation of the coldbox is likely to be centralized. This has the potential to reduce the number of personnel required to operate the plant compared to what would be necessary for conventional plants. These aspects can be taken into account by making certain adjustments in APEA, however, more construction and operation data need to be obtained. Therefore, once this detailed information becomes available, it may be necessary to refine APEA cost estimation.

Secondly, the methodology employed for process modeling and equipment design in this thesis lacks an optimization component. Incorporating optimization steps into this thesis framework would unlock the genuine potential for efficiency and cost-effectiveness in large-scale hydrogen liquefaction. This can be implemented into either the process modeling or equipment design phases, or more interestingly, it could involve optimizing both phases simultaneously, with the objective function focused on either plant efficiency or liquefaction costs. However, optimisation based on liquefaction costs within this thesis framework may present greater challenges, given the capital and operating costs are estimated using APEA. Cardella has previously carried out liquefaction cost optimization by integrating Honeywell UniSim Process Simulation with Matlab,[22] although the cost estimation used in their study is self-developed and relies on adapted cost correlations that have not been fully published.

Considering these factors, the author recommends that future research should explore the integration of optimisation algorithms into the methodologies for process modelling and preliminary equipment design in the context of hydrogen liquefiers. However, prior to the implementation of an optimisation procedure, a more robust equipment preliminary design procedure may be necessary, particularly for the catalytic plate-fin heat exchanger design.

The methodology for the sizing of the catlytic PFHX in this thesis assumes that the non-catalytic and catalytic part of the multi-stream PFHX can be designs separately. It combines the results from Aspen EDR with the pseudo-homogeneous continuum reactor model developed by O'Neil et al.[45] to estimate the necessary sizing for both heat transfer and hydrogen spin-isomer conversion.

This is performed because the model proposed by O'Neil et al.[45] is primarily intended for simulating hydrogen conversion, heat transfer, and pressure loss in a two-stream PFHX with an ortho-para catalyst, which is different from the multi-stream (more than two streams) PFHXs used in the large-scale Claude-cyle liquefier concept studied in this thesis. Since most large-scale hydrogen liquefaction concepts employ a series of three- or four-stream PFHXs, it is strongly recommended to develop a steady-state continuum reactor kinetic model specifically for the three- or four-stream catalyst-filled PFHXs. This would provide a more robust foundation for design optimization and obtaining more accurate sizing for the PFHXs used in large-scale hydrogen liquefiers.

Furthermore, the design process for centrifugal compressors and radial turbo-expanders could also be enhanced by incorporating stage loss calculations into the design flowchart. This enhancement would improve the accuracy of estimating the isentropic efficiencies of these components and provide additional geometric parameters that can be used as inputs for more detailed equipment designs.

It is also worth emphasizing the importance of giving more attention to the design of the adsorption system. The regeneration process of the adsorber columns can have an impact on the power requirements, and thus, overall efficiency of the plant. Moreover, refining the cost estimation for the coldbox vessel is also advisable if cost data for its production becomes available. In this thesis, the cost of the cryogenic coldboxes is estimated using the ICARUS Project's Cryogenic Vertical Tanks - double-walled, superinsulated (VT CRYOGENIC) component. However, this estimation may not be entirely accurate since cryogenic hydrogen liquefiers and their precooling coldboxes tend to be more complex, with a greater number of electrical and instrumentation system connections, as they encapsulate high-tech equipment rather than simply containing cryogenic fluid.

In conclusion, the technical and techno-economic assessment of large-scale hydrogen liquefaction of this thesis shows that the concept of a high-pressure hydrogen Claude cycle could potentially meet the liquefaction cost target of 1 US\$/kg_{LH_2} and become a cost-effective solution for hydrogen transportation and storage. However, the author recognises that there is ample room for improvement in the developed framework, starting by enhancing equipment design methodologies, refining cost estimations, and implementing optimisation techniques. These advancements will contribute to making hydrogen a more accessible and viable energy carrier for the future.

Bibliography

1. International Energy Agency. *The Future of Hydrogen* tech. rep. (2019). https://iea.blob.core.windows.net/assets/9e3a3493-b9a6-4b7d-b499-7ca48e357561/The_Future_of_Hydrogen.pdf.
2. Al Ghafri, S. Z. *et al.* Hydrogen liquefaction: a review of the fundamental physics, engineering practice and future opportunities. *Energy & Environmental Science* **15**, 2690–2731. ISSN: 1754-5692 (2022).
3. YANG, C. & OGDEN, J. Determining the lowest-cost hydrogen delivery mode. *International Journal of Hydrogen Energy* **32**, 268–286. ISSN: 03603199 (Feb. 2007).
4. Connelly, E. *et al. DOE Hydrogen and Fuel Cells Program Record 19001: Current Status of Hydrogen Liquefaction Costs* tech. rep. (US Department of Energy, 2019). https://www.hydrogen.energy.gov/pdfs/19001_hydrogen_liquefaction_costs.pdf.
5. Ohlig, K. & Decker, L. *The latest developments and outlook for hydrogen liquefaction technology* in (2014), 1311–1317.
6. Monterey Gardiner. *DOE Hydrogen and Fuel Cells Program Record 9013: Energy requirements for hydrogen gas compression and liquefaction as related to vehicle storage needs* tech. rep. (US Department of Energy, 2009). http://www.eere.energy.gov/hydrogenandfuelcells/hydrogen_publications.html#h2_storage%20https://www.hydrogen.energy.gov/pdfs/9013_energy_requirements_for_hydrogen_gas_compression.pdf.
7. Hydrogen Council. *A sustainable pathway for the global energy transition* tech. rep. (2017). www.hydrogencouncil.com..
8. Heuser, P.-M., Ryberg, D. S., Grube, T., Robinius, M. & Stolten, D. Techno-economic analysis of a potential energy trading link between Patagonia and Japan based on CO2 free hydrogen. *International Journal of Hydrogen Energy* **44**, 12733–12747. ISSN: 03603199 (May 2019).
9. Wijayanta, A. T., Oda, T., Purnomo, C. W., Kashiwagi, T. & Aziz, M. Liquid hydrogen, methylcyclohexane, and ammonia as potential hydrogen storage: Comparison review. *International Journal of Hydrogen Energy* **44**, 15026–15044. ISSN: 0360-3199 (June 2019).
10. Teichmann, D., Arlt, W. & Wasserscheid, P. Liquid Organic Hydrogen Carriers as an efficient vector for the transport and storage of renewable energy. *International Journal of Hydrogen Energy* **37**, 18118–18132. ISSN: 0360-3199 (Dec. 2012).
11. Ishimoto, Y. *et al.* Large-scale production and transport of hydrogen from Norway to Europe and Japan: Value chain analysis and comparison of liquid hydrogen and ammonia as energy carriers. *International Journal of Hydrogen Energy* **45**, 32865–32883. ISSN: 0360-3199 (Nov. 2020).
12. Bruce S *et al. National Hydrogen Roadmap: Pathways to an economically sustainable hydrogen industry in Australia* tech. rep. (CSIRO, Australia, 2018). www.csiro.au%20https://www.csiro.au/en/work-with-us/services/consultancy-strategic-advice-services/csiro-futures/energy-and-resources/national-hydrogen-roadmap#:~:text=The%20National%20Hydrogen%20Roadmap%20provides,economically%20sustainable%20industry%20in%20Australia..
13. Watanabe, T., Murata, K., Kamiya, S. & Ota, K.-i. *Cost Estimation of Transported Hydrogen, Produced by Overseas Wind Power Generations* in *18th World Hydrogen Energy Conference 2010* (eds Stolten, D. & Grube, T.) (2010). ISBN: 9783893366538.

14. Kamiya, S., Nishimura, M. & Harada, E. Study on Introduction of CO2 Free Energy to Japan with Liquid Hydrogen. *Physics Procedia* **67**, 11–19. ISSN: 1875-3892 (Jan. 2015).
15. APERC. *Perspectives on hydrogen in the APEC region* tech. rep. (Asia Pacific Energy Research Centre, Tokyo, June 2018). https://aperc.or.jp/file/2018/9/12/Perspectives+on+Hydrogen+in+the+APEC+Region.pdf.
16. Ishimoto, Y., Kurosawa, A., Sasakura, M. & Sakata, K. Significance of CO 2 -free hydrogen globally and for Japan using a long-term global energy system analysis. *International Journal of Hydrogen Energy* **42**, 13357–13367. ISSN: 03603199 (May 2017).
17. International Energy Agency. *Energy Technology Perspectives 2020* tech. rep. (2020). www.iea.org/t&c/%20https://iea.blob.core.windows.net/assets/7f8aed40-89af-4348-be19-c8a67df0b9ea/Energy_Technology_Perspectives_2020_PDF.pdf.
18. Alekseev, A. in *Hydrogen Science and Engineering : Materials, Processes, Systems and Technology* 733–762 (Wiley-VCH Verlag GmbH & Co. KGaA, Weinheim, Germany, Apr. 2016).
19. Stolzenburg, K. & Mubbala, R. *Hydrogen Liquefaction Report* tech. rep. (IDEALHY, Dec. 2013).
20. Quack, H. *Conceptual design of a high efficiency large capacity hydrogen liquefier* in (AIP Publishing, Feb. 2003), 255–263.
21. Berstad, D., Skaugen, G. & Wilhelmsen, Ø. Dissecting the exergy balance of a hydrogen liquefier: Analysis of a scaled-up claude hydrogen liquefier with mixed refrigerant precooling. *International Journal of Hydrogen Energy* **46**, 8014–8029. ISSN: 03603199 (Feb. 2021).
22. Cardella, U. F. *Large-scale hydrogen liquefaction under the aspect of economic viability* en. 2018. https://mediatum.ub.tum.de/604993?query=hydrogen+liquefaction&show_id=1442078&sortfield1=&srcnodeid=604993&sortfield0=author.fullname_comma%20https://mediatum.ub.tum.de/doc/1442078/1442078.pdf.
23. Krasae-In, S. Optimal operation of a large-scale liquid hydrogen plant utilizing mixed fluid refrigeration system. *International Journal of Hydrogen Energy* **39**, 7015–7029. ISSN: 03603199 (Apr. 2014).
24. Kuendig, A., Loehlein, K., Kramer, G. J. & Huijsmans, J. *Large scale hydrogen liquefaction in combination with LNG re-gasification* tech. rep. (Proceedings of the 16th world hydrogen energy conference, 2006), 3326–3333. https://www.cder.dz/A2H2/Medias/Download/Proc%20PDF/POSTERS/%5BGIV%5D%20Liquid%20&%20gaseous%20storage,%20delidevy,%20safety,%20RCS/713.pdf.
25. Valenti, G. & Macchi, E. Proposal of an innovative, high-efficiency, large-scale hydrogen liquefier. *International Journal of Hydrogen Energy* **33**, 3116–3121. ISSN: 03603199 (June 2008).
26. Ohira, K. *A Summary of Liquid Hydrogen and Cryogenic Technologies in Japans WE-NET Project* in *AIP Conference Proceedings* (AIP, 2004), 27–34.
27. Raab, M., Maier, S. & Dietrich, R.-U. Comparative techno-economic assessment of a large-scale hydrogen transport via liquid transport media. *International Journal of Hydrogen Energy* **46**, 11956–11968. ISSN: 03603199 (Mar. 2021).
28. Reu, M. *et al.* Seasonal storage and alternative carriers: A flexible hydrogen supply chain model. *Applied Energy* **200**, 290–302. ISSN: 0306-2619 (Aug. 2017).
29. Timmerhaus, K. D. & Flynn, T. M. in *Cryogenic Process Engineering* 103–188 (Springer US, Boston, MA, 1989).
30. Flynn, T. *Cryogenic Engineering, Revised and Expanded* ISBN: 9780429216411 (CRC Press, Nov. 2004).
31. Chang, H.-M., Ryu, K. N. & Baik, J. H. Thermodynamic design of hydrogen liquefaction systems with helium or neon Brayton refrigerator. *Cryogenics* **91**, 68–76. ISSN: 00112275 (Apr. 2018).

32. Randall F. Barron. in *Cryogenic Systems* (ed Scurlock, R. G.) 2nd, 60–143 (Oxford University Press, New York, June 1985).
33. Barron, R. F. & Windmeier, C. in *Ullmann's Encyclopedia of Industrial Chemistry* (Wiley-VCH Verlag GmbH & Co. KGaA, Weinheim, Germany, June 2000).
34. Aasadnia, M. & Mehrpooya, M. Large-scale liquid hydrogen production methods and approaches: A review. *Applied Energy* **212**, 57–83. ISSN: 03062619 (Feb. 2018).
35. Maytal, B.-Z. & Pfotenhauer, J. M. in *Miniature Joule-Thomson Cryocooling* 39–72 (Springer New York, New York, NY, 2013).
36. Moran, M. J. & Shapiro, H. N. *Fundamental of Engineering Thermodynamics* 6th (Hoboken : Wiley, 2008., 2008).
37. NANDI, T. & SARANGI, S. Performance and optimization of hydrogen liquefaction cycles. *International Journal of Hydrogen Energy* **18**, 131–139. ISSN: 03603199 (Feb. 1993).
38. Maytal, B.-Z. & Pfotenhauer, J. M. in *Miniature Joule-Thomson Cryocooling* 73–118 (Springer New York, New York, NY, 2013).
39. Valenti, G. in *Compendium of Hydrogen Energy* 27–51 (Elsevier, 2016).
40. Chang, H.-M., Kim, S. G., Weisend Ii, J. G. & Quack, H. Modified Brayton Refrigeration Cycles for Liquid Hydrogen in Spallation Neutron Source Moderator. *Cryocoolers* **19**, 463–470 (June 2016).
41. Grochala, W. First there was hydrogen. *Nature Chemistry* **7**, 264–264. ISSN: 1755-4330 (Mar. 2015).
42. Sherif, S. A., Zeytinoglu, N. & Veziroglug, T. N. *LIQUID HYDROGEN : POTENTIAL, PROBLEMS, AND A PROPOSED RESEARCH PROGRAM* tech. rep. 7 (1997), 683–688.
43. Donaubauer, P. J., Cardella, U., Decker, L. & Klein, H. Kinetics and Heat Exchanger Design for Catalytic Ortho-Para Hydrogen Conversion during Liquefaction. *Chemical Engineering and Technology* **42**, 669–679. ISSN: 15214125 (Mar. 2019).
44. Ohlig, K. & Decker, L. in *Ullmann's Encyclopedia of Industrial Chemistry* 1–6 (Wiley-VCH Verlag GmbH & Co. KGaA, Weinheim, Germany, Sept. 2013).
45. O'Neill, K. T. *et al*. Hydrogen ortho-para conversion: process sensitivities and optimisation. *Chemical Engineering and Processing - Process Intensification* **184**. ISSN: 02552701 (Feb. 2023).
46. Weitzel, D. H., Blake, J. H. & Konecnik, M. in *Advances in Cryogenic Engineering* 286–295 (Springer US, Boston, MA, 1960).
47. Weitzel, D. H., Valin, C. C. & Draper, J. W. in *Advances in Cryogenic Engineering* 73–84 (Springer US, Boston, MA, 1960).
48. Hutchinson, H. L., Barrick, P. L. & Brown, L. F. in *Advances in Cryogenic Engineering* 190–196 (Springer US, Boston, MA, 1965).
49. Leachman, J. W., Jacobsen, R. T., Penoncello, S. G. & Lemmon, E. W. Fundamental Equations of State for Parahydrogen, Normal Hydrogen, and Orthohydrogen. *Journal of Physical and Chemical Reference Data* **38**, 721–748. ISSN: 0047-2689 (Sept. 2009).
50. Lemmon, E. W., Bell, I. H., Huber, M. L. & McLinden, M. O. *NIST Standard Reference Database 23: Reference Fluid Thermodynamic and Transport Properties-REFPROP, Version 10.0, National Institute of Standards and Technology* 2018. `https://www.nist.gov/srd/refprop`.
51. Valenti, G., Macchi, E. & Brioschi, S. The influence of the thermodynamic model of equilibrium-hydrogen on the simulation of its liquefaction. *International Journal of Hydrogen Energy* **37**, 10779–10788. ISSN: 03603199 (July 2012).
52. Le Roy, R. J., Chapman, S. G. & Mccourt, F. R. W. *Accurate Thermodynamic Properties of the Six Isotopomers of Diatomic Hydrogen* tech. rep. (1990).
53. Lasala, S., Privat, R., Arpentinier, P. & Jaubert, J.-N. Note on the inconsistent definition assigned in the literature to the heat capacity of the so-called equilibrium hydrogen mixture. *Fluid Phase Equilibria* **504**, 112325. ISSN: 03783812 (Jan. 2020).

54. Krasae-in, S., Stang, J. H. & Neksa, P. *Development of large-scale hydrogen liquefaction processes from 1898 to 2009* May 2010.
55. Chart Industries. *Hydrogen Liquefiers* 2023. https://files.chartindustries.com/21757382_Hydrogen_Liquefiers_brochure.pdf%20https://www.chartindustries.com/Products/Hydrogen-Liquefiers.
56. Kariya, D. & Komiya, T. Accomodating the Energy Supply Needs of the Next Era: Kawasaki's Hydrogen Liquefaction System. *Scope Winter 2018 no. 114.* https://global.kawasaki.com/en/scope/pdf_e/scope114.pdf (2018).
57. GLOBUC. *Air Products plans second hydrogen liquefaction plant in Rotterdam* Oct. 2022. https://globuc.com/news/air-products-plans-second-hydrogen-liquefaction-plant-in-rotterdam/.
58. Ellis, D. & Gas World. *Air Products plans second hydrogen liquefaction plant in Rotterdam* Sept. 2022. https://www.gasworld.com/story/air-products-plans-second-hydrogen-liquefaction-plant-in-rotterdam/2095313.article/?red=1.
59. Essler, J. *et al. Report on Technology Overview and Barriers to Energy- and Cost-Efficient Large Scale Hydrogen Liquefaction* tech. rep. (2012).
60. Decker, L. *Making our world more productive Latest Global Trend in Liquid Hydrogen Production* tech. rep. (HYPER Closing Seminar, Brussels, Dec. 2019).
61. Yin, L. & Ju, Y. Review on the design and optimization of hydrogen liquefaction processes. *Frontiers in Energy* **14**, 530–544. ISSN: 2095-1701 (Sept. 2020).
62. Faramarzi, S., Nainiyan, S. M. M., Mafi, M. & Ghasemiasl, R. A novel hydrogen liquefaction process based on LNG cold energy and mixed refrigerant cycle. *International Journal of Refrigeration* **131**, 263–274. ISSN: 01407007 (Nov. 2021).
63. Cardella, U., Decker, L., Sundberg, J. & Klein, H. Process optimization for large-scale hydrogen liquefaction. *International Journal of Hydrogen Energy* **42**, 12339–12354. ISSN: 03603199 (Apr. 2017).
64. Cardella, U., Decker, L. & Klein, H. Roadmap to economically viable hydrogen liquefaction. *International Journal of Hydrogen Energy* **42**, 13329–13338. ISSN: 03603199 (May 2017).
65. Cardella, U., Decker, L. & Klein, H. *Economically viable large-scale hydrogen liquefaction* in *IOP Conference Series: Materials Science and Engineering* **171** (Institute of Physics Publishing, Mar. 2017).
66. Stolzenburg, K. *et al. Efficient Liquefaction of Hydrogen: Results of the IDEALHY Project* tech. rep. (IDEALHY, Energie Symposium, Stralsund, Nov. 2013). https://www.idealhy.eu/uploads/documents/IDEALHY_XX_Energie-Symposium_2013_web.pdf.
67. Berstad, D. O., Stang, J. H. & Nekså, P. Large-scale hydrogen liquefier utilising mixed-refrigerant pre-cooling. *International Journal of Hydrogen Energy* **35**, 4512–4523. ISSN: 03603199 (May 2010).
68. Berstad, D. O., Stang, J. H. & Nekså, P. Comparison criteria for large-scale hydrogen liquefaction processes. *International Journal of Hydrogen Energy* **34**, 1560–1568. ISSN: 03603199 (Feb. 2009).
69. Krasae-In, S., Stang, J. H. & Neksa, P. Simulation on a proposed large-scale liquid hydrogen plant using a multi-component refrigerant refrigeration system. *International Journal of Hydrogen Energy* **35**, 12531–12544. ISSN: 03603199 (Nov. 2010).
70. Skaugen, G., Berstad, D. & Wilhelmsen, Ø. Comparing exergy losses and evaluating the potential of catalyst-filled plate-fin and spiral-wound heat exchangers in a large-scale Claude hydrogen liquefaction process. *International Journal of Hydrogen Energy* **45**, 6663–6679. ISSN: 03603199 (Feb. 2020).
71. Towler, G. & Sinnott, R. in *Chemical Engineering Design* 1047–1205 (Elsevier, 2013).
72. Häring, H.-W. *Industrial Gases Processing* (ed Häring, H.-W.) ISBN: 9783527316854 (Wiley, Dec. 2007).

73. ALPEMA. *The Standards of the Brazed Aluminium Plate-Fin Heat Exchanger Manufacturers' Association*. May 2012.
74. Walnum, H. T. *et al*. *Principles for the liquefaction of hydrogen with emphasis on precooling processes* in *12th Cryogenics 2012 - IIR Conference* (Dresden, Sept. 2012).
75. Towler, G. & Sinnott, R. Transport and Storage of Fluids. *Chemical Engineering Design*, 1207–1265 (Jan. 2013).
76. Elliott, H. & Bloch, H. *Compressor Technology Advances* ISBN: 9783110678765 (De Gruyter, Feb. 2021).
77. Bahadori, A. in *Natural Gas Processing* 223–273 (Elsevier, 2014).
78. Khan, M. A., Young, C., Mackinnon, C. B. & Layzell, D. B. *The Techno-Economics of Hydrogen Compression* 2021. www.transitionaccelerator.ca.
79. Tahan, M. R. *Recent advances in hydrogen compressors for use in large-scale renewable energy integration* Oct. 2022.
80. Van Lier, L., Tumer, C., Tedesco, M. & Buijs, L. *Hydrogen Compression Boosting The Hydrogen Economy* tech. rep. (European Forum for Reciprocating Compressors, Nov. 2022).
81. Brun, K. *Technology Options for Hydrogen Compression* tech. rep. (Elliott Group).
82. Brun, K. & Simons, S. Compression Options for The Hydrogen Economy. *Gas Compression Magazine* (May 2021).
83. Barton, M., Soriano, L., Stahley, J., Talakar, A. & Siemens Energy. Under Pressure: The Challenge of Hydrogen Compression. *Hydrocarbon Engineering* (Aug. 2021).
84. Adam, P., Bode, R. & Groissboeck, M. Hydrogen Turbomachinery. *Turbomachinery International Magazine Vol. 61 No. 6*. www.turbohandbook.com (Dec. 2020).
85. Brun, K. & Kurz, R. Myth: Centrifugal Compressors are Terrible for Compressing Light Gases. *Turbomachinery International Magazine Vol. 61 No. 6* (Dec. 2020).
86. Brun, K., Ross, S., Scavo-Fulk, S. & Hermann, A. Hydrogen Compression. *Turbomachinery International Magazine Vol. 61 No. 6* (Dec. 2020).
87. Ablondi, T. & Barton, M. Compressors are hydrogen 'colour blind'. *Compressor Tech2 Magazine*. https://assets.siemens-energy.com/siemens/assets/api/uuid:0aa6df14-ed53-4f63-9407-9bcec22d8e7e/comptech2-article-h2compressor-selection-oct2022.pdf (Oct. 2022).
88. Francis A. Di Bella. *Development of a Centrifugal Hydrogen Pipeline Gas Compressor* Apr. 2015.
89. Heshmat, H., Sutherland, E. & Randolph, K. *Oil-Free Centrifugal Hydrogen Compression Technology Demonstration - DOE Hydrogen and Fuel Cells Program FY 2014 Annual Progress Report* tech. rep. (Mohawk Innovative Tachnology Inc., US DOE, Albany, NY, Aug. 2014).
90. Heshmat, H. *Oil-Free Centrifugal Hydrogen Compression Technology Demonstration Hydrogen and Fuel Cells Program Annual Merit Review and Peer Evaluation Meeting* tech. rep. (US DOE, Mohawk Innovative Technology Inc, Arlington, VA, May 2013).
91. Heshmat, H. *Oil-Free Centrifugal Hydrogen Compression Technology Demonstration, Hydrogen and Fuel Cells Program Annual Merit Review and Peer Evaluation Meeting* tech. rep. (US DOE, Mohawk Innovative Technology, Inc., Arlington, VA, June 2014).
92. Heshmat, H. *Oil-Free Centrifugal Hydrogen Compression Technology Demonstration Final Report Prepared for Department of Energy Hydrogen and Fuel Cells Program Principal Investigator* tech. rep. (Mohawk Innovative Technology, Inc, Albany, NY, May 2014). www.miti.cc.
93. Dixon, S. L. & Hall, C. A. *Fluid Mechanics and Thermodynamics of Turbomachinery* 7th. ISBN: 9780124159549 (Elsevier, 2014).
94. Gambini, M. & Vellini, M. in, 89–107 (2021).
95. Gambini, M. & Vellini, M. in, 255–308 (2021).

96. Baljet, O. E. A Study on Design Criteria and Matching of Turbomachines: Part ASimilarity Relations and Design Criteria of Turbines. *Journal of Engineering for Power* **84**, 83–102. ISSN: 0022-0825 (Jan. 1962).
97. Baljet, O. E. A Study on Design Criteria and Matching of Turbomachines: Part BCompressor and Pump Performance and Matching of Turbocomponents. *Journal of Engineering for Power* **84**, 103–114. ISSN: 0022-0825 (Jan. 1962).
98. Kerry, F. G. *Industrial Gas Handbook: Gas Separation and Purification* (2007).
99. Bloch, H. P. & Soares, C. *Turboexpanders and Process Applications* ISBN: 9780884155096 (Elsevier, 2001).
100. Bischoff, S. & Decker, L. *First operating results of a dynamic gas bearing turbine in an industrial hydrogen liquefier* in *AIP Conference Proceedings* **1218** (2010), 887–894. ISBN: 9780735407619.
101. Ohlig, K. & Bischoff, S. *Dynamic gas bearing turbine technology in hydrogen plants* in *AIP Conference Proceedings* **1434** (2012), 814–819. ISBN: 9780735410206.
102. Timmerhaus, K. D. & Flynn, T. M. in *Cryogenic Process Engineering* 189–285 (Springer US, Boston, MA, 1989).
103. Jumonville, J. *Tutorial On Cryogenic Turboexpanders* in *Proceedings of the 39th Turbomachinery Symposium* (Texas A&M University. Turbomachinery Laboratories, 2010), 147–154.
104. Gambini, M. & Vellini, M. in, 199–253 (2021).
105. Häussinger, P., Lohmüller, R. & Watson, A. M. in *Ullmann's Encyclopedia of Industrial Chemistry* (Wiley-VCH Verlag GmbH & Co. KGaA, Weinheim, Germany, Oct. 2011).
106. Campbell, J. M., Lilly, L. L. & Maddox, R. N. *Gas Conditioning and Processing : Volume 2 : The Equipment Modules* 8th (Norman, Okla : Campbell, cop. 2000., 2000).
107. Air Liquide Advanced Technologies. *HYLIAL: Range of automatic hydrogen liquefiers* 2023. https://advancedtech.airliquide.com/markets-solutions/space/hydrogen-liquefaction%20https://advancedtech.airliquide.com/sites/alat/files/2021/09/14/hylial_brochure_en_04.21_sd.pdf.
108. Towler, G. & Sinnott, R. in *Chemical Engineering Design* 239–278 (Elsevier, 2022).
109. Couper, J. R. *Process Engineering Economics* ISBN: 9781135528034 (CRC Press, Aug. 2003).
110. Brennan, D. & Golonka, K. New Factors for Capital Cost Estimation in Evolving Process Designs. *Chemical Engineering Research and Design* **80**, 579–586. ISSN: 02638762 (Sept. 2002).
111. Peters, M. & Timmerhaus, K. *Plant Design and Economics for Chemical Engineers* 4th. ISBN: 9780070496132 (New York : McGraw-Hill, l̃1991, 1991).
112. Walas, S. M. in *Chemical Process Equipment* 663–669 (Elsevier, 1990).
113. Syed, M. T., Sherif, S. A., Veziroglu, T. N. & Sheffield, J. W. An economic analysis of three hydrogen liquefaction systems. *International Journal of Hydrogen Energy* **23**, 565–576. ISSN: 0360-3199 (July 1998).
114. Towler, G. & Sinnott, R. Capital Cost Estimating. *Chemical Engineering Design*, 307–354. https://linkinghub.elsevier.com/retrieve/pii/B9780080966595000079 (Jan. 2013).
115. Aspen Technology. *Aspen Icarus V12 Reference Guide - APEA* Jan. 2021. https://esupport.aspentech.com/S_Article?id=000098074.
116. Haydary, J. in *Chemical Process Design and Simulation - Aspen Plus and Aspen Hysys Applications* 263–278 (John Wiley & Sons, 2019). ISBN: 978-1-119-08911-7. https://app.knovel.com/hotlink/khtml/id:kt012XR6W2/chemical-process-design/economic-evaluation.
117. Al-Malah, K. I. M. in *Aspen Pluső - Chemical Engineering Applications* 523–564 (John Wiley & Sons, 2017). ISBN: 978-1-119-13123-6. https://app.knovel.com/hotlink/khtml/id:kt011HOGL2/aspen-plus-chemical-engineering/aspen-process-economic.
118. Towler, G. & Sinnott, R. in *Chemical Engineering Design* 279–304 (Elsevier, 2022).

119. Servet Yanatma. *Energy crisis in Europe: Which countries have the cheapest and most expensive electricity and gas?* Mar. 2023. https://www.euronews.com/next/2023/03/29/energy-crisis-in-europe-which-countries-have-the-cheapest-and-most-expensive-electricity-a.

120. O'Sullivan, A. & Sheffrin, S. M. *Economics Principles in Action* 157. ISBN: 0134373294, 9780134373294 (Prentice-Hall, Inc., 2000).

121. Amos, W. A. *Costs of Storing and Transporting Hydrogen* tech. rep. (National Renewable Energy Laboratory (NREL), Golden, CO (United States), Jan. 1999).

122. Chen, T.-P. *et al. Hydrogen Delivery Infrastructure Options Analysis* tech. rep. (US Department of Energy). https://www.osti.gov/servlets/purl/982359.

123. Elgowainy, A., Mintz, M., Gillette, J., Ringer, M. (& Brown, D. (*Hydrogen Delivery Scenario Analysis Model (HDSAM) V2.0* 2006. https://www.hydrogen.energy.gov/docs/12022c_hdsam2-31_2020_case.xls.

124. Elgowainy, A. *et al. Hydrogen Delivery Scenario Analysis Model (HDSAM) V4.0* 2022. https://hdsam.es.anl.gov/.

125. Wright, T. P. & Curtiss-Wright Corperation. Factors Affecting the Cost of Airplanes. *Journal of the Aeronautical Sciences* **3**, 122–128. ISSN: 1936-9956 (Feb. 1936).

126. Samadi, S. The experience curve theory and its application in the field of electricity generation technologies A literature review. *Renewable and Sustainable Energy Reviews* **82**, 2346–2364. ISSN: 1364-0321 (Feb. 2018).

127. Nemet, G. F. Beyond the learning curve: factors influencing cost reductions in photovoltaics. *Energy Policy* **34**, 3218–3232. ISSN: 0301-4215 (Nov. 2006).

128. Henderson, B. & The Boston Consulting Group. *The Experience Curve* Jan. 1968. https://www.bcg.com/publications/1968/business-unit-strategy-growth-experience-curve.

129. Ritchie, H. & Roser, M. *Why did renewables become so cheap so fast?* 2021. https://ourworldindata.org/cheap-renewables-growth%20ourworldindata.org/energy.

130. Van Hoecke, L. *et al.* Challenges in the use of hydrogen for maritime applications. *Energy & Environmental Science* **14**, 815–843. ISSN: 1754-5692 (2021).

131. Casey, M., Zwyssig, C. & Robinson, C. *The Cordier Line for Mixed Flow Compressors* in *Volume 7: Turbomachinery, Parts A, B, and C* (ASMEDC, Oct. 2010), 1859–1869. ISBN: 978-0-7918-4402-1.

132. Hazby, H., Casey, M., Robinson, C., Spataro, R. & Lunacek, O. *The Design of a Family of Process Compressor Stages* in *12th European Conference on Turbomachinery Fluid dynamics & Thermodynamics* (2017).

133. Aungier, R. H. *Centrifugal Compressors: A Strategy for Aerodynamic Design and Analysis* ISBN: 9780791800935 (ASME Press, 2000).

134. Bommes, L., Fricke, J. & Grundmann, R. *Ventilatoren* 2nd. ISBN: 978-3802732003 (Dec. 2002).

135. Aungier, R. H. *Turbine Aerodynamics: Axial-Flow and Radial-Flow Turbine Design and Analysis* ISBN: 0791802418 (ASME Press, 2006).

136. Kandasamy, S. *Techno economic analysis of salt cavern hydrogen storage* PhD thesis (Delft University of Technology, Delft, Aug. 2023). https://repository.tudelft.nl/islandora/object/uuid:5ce57804-357c-4651-b184-1b701d79825c?collection=education.

137. EERE. *Multiyear Research, Development and Demonstration Plan - Section 3.2 Hydrogen Delivery* tech. rep. (EERE Publication and Product Library, Mar. 2012).

138. Roser, M. *Learning curves: What does it mean for a technology to follow Wrights Law?* Apr. 2023. https://ourworldindata.org/learning-curve.